Design, Applications, and Processing of Synthetic Protein Nanoparticles

by

Daniel F. Quevedo

A dissertation submitted in partial fulfillment
of the requirements for the degree of
Doctor of Philosophy
(Biomedical Engineering)
in the University of Michigan
2020

Doctoral Committee:

Professor Joerg Lahann, Chair
Professor Lola Eniola-Adefeso
Assistant Professor Colin F. Greineder
Professor Blanca H. Lapizco-Encinas, Rochester Institute of Technology
Professor Peter Tessier

Daniel F. Quevedo

danqueve@umich.edu

ORCID iD: 0000-0001-5892-364X

To Ma, Pa, and Miguel for their love and support
and
To Shannon, who is my everything, and without whom this thesis would not exist

Acknowledgements

First and foremost, I would like to convey my deepest thanks and gratitude to my advisor, Professor Joerg Lahann, for guidance, kindness, patience, and support, and without whom nothing contained in this dissertation would be possible. His keen scientific insight, gentle guiding hand, and uncanny ability to calm and reassure any student as soon as they enter his office, no matter what the problem is, got me through the last 5 years. I am honored and proud to have joined his lab and worked with him, from my time at the Karlsruhe Institute of Technology, all the way to being locked up in my apartment for the last few months of my PhD. I would also like to thank my committee members, Professor Lola Eniola-Adefeso, Professor Peter Tessier, Professor Colin F. Greineder, and Professor Blanca H. Lapizco-Encinas, for their help and guidance over the years. Whether it was classes, constantly asking for a meeting to check up on my progress, working with me to design experiments, or even having insightful conversations while driving me to the airport, their contributions have shaped me, my thoughts, and the contents of this dissertation.

I would like to express my thanks to the many people that I had the pleasure to work with, and without whom many of the results here would not be possible. I would like to thank Boya Zhang for her help with cell culture and experimentation for ROS protection and Cody Lentz for his friendship and expertise in electrokinetic microfluidics. In particular, I would like to thank Jason Gregory and Nahal Habibi for their scientific advice and help, their companionship throughout the long years, and many laughs. Jason and Nahal both were instrumental and deserve all credit due for our development of SPNPs, and in working with me to write reviews, develop

techniques and technologies, and all the exciting things we have found along the way. Dr. Brad Plummer was my first office mate at Michigan, and his thoughts and mentorship had a major hand in not just the scientific results presented here, such as showing how SPNPs could be made out of many proteins and his work alongside me in gene delivery carriers and shape shifting, but also in how I have grown over the years, and where I will be going next.

I would like to thank every lab member that I have had the pleasure to work with and alongside during my time in graduate school. The number of people that have come through our lab as students, post docs, and visiting scholars are almost too many to count, but I appreciated each and every one of them. I'd like to specifically thank Ayse Muniz for her insightful conversations and lively game nights full of laughs, delicious food, and friendship, Dylan Neale for being a kind and caring person who I am proud to have known and worked alongside, and current lab mates Anthony Berardi, Ava Mauser, Laura Saunders, Albert Chang, Zane Zhang, Xiaoyang Zhong, John Kim, and, Chris Kim. Many alumni have also left during my time in the lab, and I would like to thank Dr. Sahar Rahmani, Dr. Kathleen McEnnis. Dr. Stephie Christau, Dr. Ramya Kumar, Dr. Kenneth Cheng and many others. The lab members of the Lahann Lab at KIT were the ones who started it all for me, and I would like to thank Anke Steier, Marvin Klaiber, Dr. Christoph Hussal, Dr. Meike Koenig, Dr. Artak Shahnas, Dr. Amit Sitt, Dr. Denise Cunha, Dr. Domenic Kratzer, Fabrice Laye, and Gowthamy Venkidasubramonian. In particular, I am deeply grateful to have had the opportunity to teach, mentor and meet all of the different undergraduate students that I had the pleasure to work with, most importantly Yazmin Hernandez, Rikako Miki, Hamza Turkistani, Bryan Liu, and David Bonhard. Finally, I would like to thank the staff members from the Biointerfaces Institute, Biomedical Engineering Department, and Chemical Engineering

Department. In particular, I would like to thank Lisa Moran, Dr. Nadine Wong, Maria Steele, Mary Beth Westin, and Laura Charlick for all their help over the years.

On a more personal note, graduate school has been a time of troubles and tribulation, alongside success and triumph, and I am glad to have spent my time alongside close and dear friends. In particular, Hans Zander, for all the laughs over the years, and my friends Bobby, Melissa, Phil, Lacie, Elissa, Tiff, Boomie, Erika, Katy, Claire, Sam, Steve, Ashley , and many others. Additionally, my big and loving family, with all the aunts, uncles and cousins, of whom there are over 50 by my latest count and are too many to list here, made this all worth it, with their love, laughs and happiness, especially my Tias and Tios Rosa and Alvaro, Carlos and Gloria, Maxi and Pacho, Patricia, Clara, Blanca and Nena, and my cousins Lina, Camilo, Carlos Andres, Oscar Mauricio, Joel, Denny, and Alejandro. My deepest thanks go to my soon to be wife, Shannon Wetzler. We met in class here in Michigan, and her constant, unyielding love, patience, and support made my time as a PhD student not just bearable, but enjoyable. Most importantly, I would like to thank my parents Luz Becerra and Miguel Quevedo, and brother, Miguel Angel Quevedo, for all their love, guidance, and care, and who should be given all the real credit for what follows.

Table of Contents

List of Figures

List of Appendices

Abstract

Nanomedicine- where a therapeutic is loaded into nanoparticles to increase therapeutic efficiency and improve patient outcomes- has long had the potential to revolutionize medicine. With all of their promise, nanoparticle carrier technologies have yet to make a significant clinical impact, emphasizing the need for new technologies and approaches. In this dissertation, electrohydrodynamic (EHD) co-jetting was used to develop various methods to create novel Synthetic Protein Nanoparticles (SPNPs), which were then applied to the delivery of therapeutic enzymes, and characterized using a microfluidic technique. It was found that SPNPs can be made from various proteins, such as Human Transferrin, Hemoglobin, and others, and that various macromers can be selected, such as a stimuli responsive NHS-Ester based macromer that can detect oxidative environments and show signs of degradation after being taken up by HeLa cells. SPNPs were then loaded with medically relevant enzymes, such as the antioxidant enzyme catalase. The enzymes showed high activity retention rates, with catalase SPNPs maintaining up to 82% of their original enzymatic activity. Additionally, antibody-targeted catalase SPNPs were able to protect REN cells in an inflammatory disease model. Next, an electrokinetic microfluidic system was adapted for the characterization of SPNPs based on their protein composition and anisotropy. The method was able to differentiate bicompartmental particles made from two different proteins from single compartment SPNPs made of an equivalent isotropic mixture of the same two proteins, with a significant voltage difference between the two particle types. Finally, preliminary work was conducted on using a small targeting molecule, meta-acetylenbenzylguanidine (MABG), for the treatment of neuroblastoma, and a system for validating MABG targeting in SK-N-BE(2) cells (a neuroblastoma cell line) was developed. Work done in this dissertation presents the development of multifunctional protein nanocarriers and lays the groundwork for the targeted delivery of active therapeutics using these particles.

Chapter 1

Introduction

Part of the material for this chapter has been adapted with modifications from the following publication:

1. N. Habibi*, D. F. Quevedo*, J. V. Gregory*, J. Lahann, "Emerging Methods in Therapeutics Using Multifunctional Nanoparticles" *WIREs Nanomedicine & Nanobiotechnology* **2020**, 12(4):e1625
   *equal contribution

1.1 Background on Nanotechnology in Medicine and its Shortcomings

Nanoparticles, synthetic material with at least one dimension in the nanoscale (**Figure 1.1**), have become a thriving area of science along a broad range of disciplines over the last 40 years. The conception of the idea of nanotechnology is widely attributed to the prolific Richard Feynman in 1959[1–3] as a way to make smaller machines which could eventually allow the manipulation of matter at the atomic level. Nanotechnology has now become a reality, revolutionizing fields as

varied as electronics,[4,5] automobiles,[6] space technologies,[7–9] architecture,[10] and even in the analysis and conservation of works of art.[11–13]

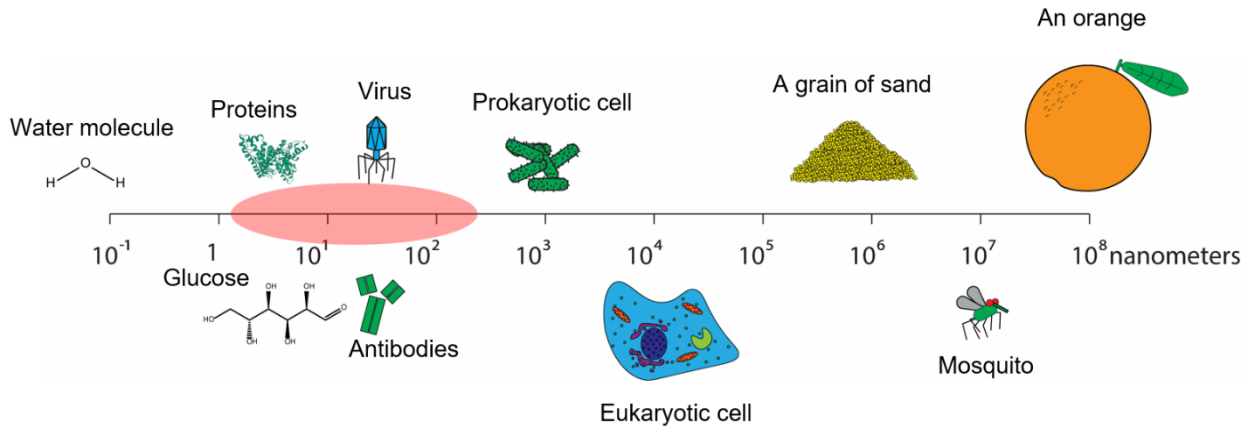

Figure 1.1 Nanoparticles are materials that have at least one dimension in the nanoscale, a size range signified by the red oval.

In the medical space, nanotechnology promises to leave its small-scale, but largely impactful, footprints in various ways. Nanoparticle-based drug delivery has emerged as an application of nanotechnology, whose aim is to improve shortcomings in traditional small molecule-based therapeutics by loading active therapeutic ingredients in nanoparticles.[14,15] The goal is to use the nanoparticles to specifically deliver a therapeutic to the diseased site. This delivery can be done in a variety of ways: passive accumulation using the theorized but much debated Enhanced Permeability and Retention (EPR) effect,[16] attaching targeting molecules that are specific to biomarkers expressed on target cell surfaces,[17,18] incorporating groups, such as magnetic nanoparticles, that allow for non-invasive control of particle location,[19,20] or even using the body's own delivery network and carriers, the cardiovascular system and blood cells, to carry nanoparticles to their desired locations, as is done with hitchhiking nanoparticles.[21–24] By having nanoparticles specifically target diseased parts of the body, along with other advancements, such as high loading ratios of therapeutics[18] and stimuli responsive site specific release,[25] the field of nanomedicine aims to make ineffective therapies viable, reduce side effects of high morbidity

treatments such as chemo- and radiotherapy, improve the performance of existing therapies, and overall improve patient outcomes.[26,27] Nanomedical applications in cancer hold particular promise and are a highly active area of research.[28]

Nanoparticles in medicine have been developed from a wide variety of materials, both organic and inorganic, using a large number of techniques. These methods range from liposomal forms of drugs, such as Doxil, a PEGylated liposomal formulation of doxorubicin,[29] which in 1995 became the first nanotherapeutic approved by the FDA, to taking inspiration from applications in *in vitro* and *in vivo* fluorescent imaging,[30–33] dual use therapeutic/diagnostic (theragnostic) systems,[34–37] stimuli responsive materials,[26,38–43] and all the way to self-assembling materials made from proteins,[44] DNA,[45] small organic molecules,[46] and even inspired by viruses.[47] However, the promise of nanomedicine, the tremendous advance of the techniques and technologies, and the large amount of research time that has been invested, does not seem to reflect the real-world outcomes. For example, in the years between 2016-2019, only 3 new nanoformulations were approved by the FDA,[48] compared to the 153 formulations that were approved overall.[49] This number is contextually even more depressing in light of the fact that in the 25 years since the approval of Doxil, only around 30 nanotherapeutics have been approved, of which only 10 were cancer nanomedicines.[50] Compared to the approximately 35-40 new formulations (a number which includes drugs, biologics, and vaccines) approved *per year*,[51] there is a general disappointment in the field about the lack of translation of nanomedicine from the bench to the bedside. This lack of translation was highlighted in the seminal work by Wilhelm et al in 2016, whose extensive literature review and metanalysis found that only a median of 0.7% of administered nanoparticles are delivered to solid tumors.[52]

This disappointment has led to an avalanche of questions about why nanomedicine, and cancer nanomedicine in particular, has had limited clinical success.[53–58] New research has indicated that this may be due, in parts, to the limitations of the principle behind the EPR effect.[59] The EPR effect is a theory established in 1986, when evidence suggested that the vasculature in solid tumors is "leaky", containing large (2000 nm) gaps.[60,61] The theory postulates that these gaps lead to enhanced permeability of particles to tumors, and low blood flow rates along with incomplete lymphatic clearance lead to enhanced retention of particulates once inside the tumor (thus, Enhanced Permeability and Retention, or EPR).[16] Thus, nanoparticles have been developed with the aim for the delivery carriers to be small enough to enter these fenestrations but not so small as to be cleared by the other mechanisms in the body.[62,63] New research by Sindhwani et al. has found, in a variety of tumor models and patient samples, that these fenestrations are actually quite rare. Additionally, they found that the main method for tumor uptake of nanoparticles is actually through active extravasation, or the uptake of particles by endothelial cells that line blood vessels and their subsequent expulsion into solid tumors.[59] As this evidence contradicts one of the main design principles in nanomedicine, it may explain their disappointing translation to the clinic. Perhaps, the reason why nanomedicines have been ineffective is that they have been designed to take advantage of a quality of solid tumors that never existed in the first place.

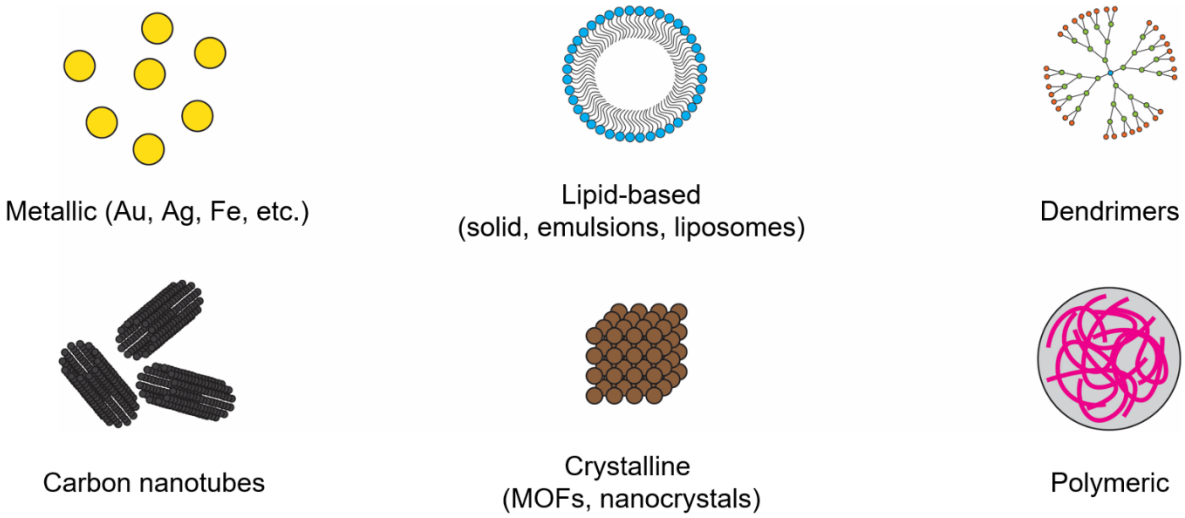

Figure 1.2 Examples of the materials commonly used in nanomedicine.

This new evidence points to a new way forward for nanomedicine. The inherent ability of materials currently popular in nanomedicine (polymers, liposomes, inorganics, etc., **Figure 1.2**) to actively extravasate has generally not been studied well, but the lack of translation suggests that these materials are not ideal. This leads to the thought: why not explore new materials that are built to take advantage of this new discovery, potentially even taking inspiration from nature? A prime example of this methodology is Abraxane, one of the few approved nanomedicines, a nanoparticle built out of physically linked proteins (Human Serum Albumin to be specific) and loaded with paclitaxel.[64] Abraxane demonstrates decreased morbidity compared to the free drug formulation of paclitaxel, whose organic solvent Cremphor EL causes a variety of side effects.[65] Abraxane also has shown improvements in patient outcomes, and a popular argument for the improvements in patient outcomes is the fact that albumin interacts with the glycoprotein gp60, which induces extravasation of the drug-protein complex.[66,67] This has led to a recent development in the field of nanoparticle-based drug delivery, where synthetic polymers and inorganics are replaced by proteins as the primary building blocks of nanoparticles.

1.2 Proteins in Medicine and Nanomedicine

1.2.1 Background on Proteins and their Applications in Medicine

As a material, proteins show great promise for clinical application due to their variety, function, design flexibility through genetic engineering, and potential lack of immunogenicity. Proteins are made from chains of amino acids, which can be characterized as having two main components: the group that becomes the carbon-amide backbone, and the side group (-R) (**Figure 1.3**A). The genetic code of organisms is made up of nucleic acids, every three of which make up a codon, and encode for 20 different α-amino acids (identical backbones, different -R groups). This genetic code, made up of DNA, is transcribed into RNA, and subsequently "translated" into proteins through biochemical processes. RNA is used as a template from which the proteins are "printed" by ribosomes. This printing occurs by reacting amines from one amino acid with the carboxylic acid of the next amino acid, one at a time, resulting in a process much like adding beads to the end of a string (**Figure 1.3B**).

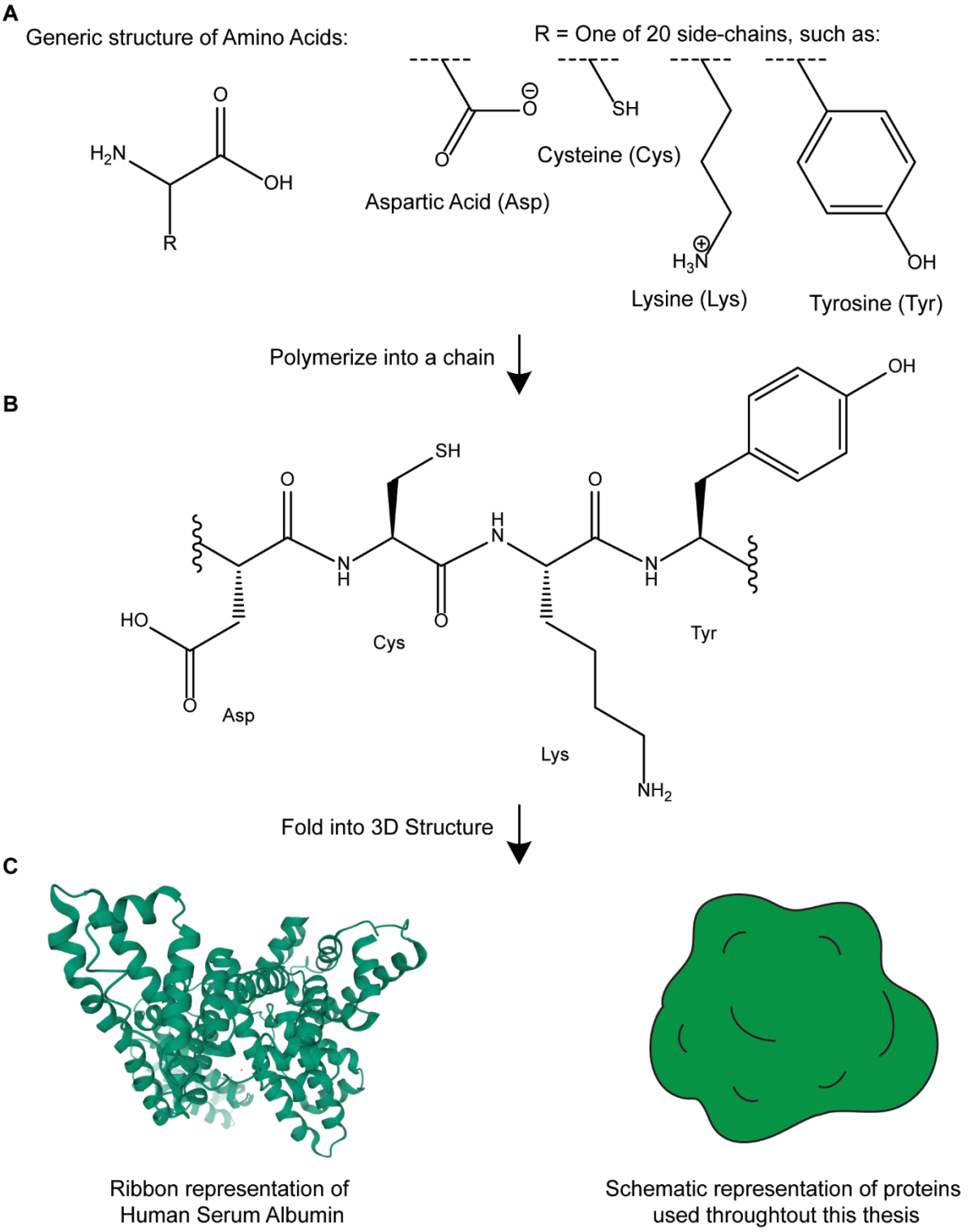

Figure 1.3 Proteins are complex biomolecules. (A) They are made up of amino acids that (B) Polymerize into chains, whose intermolecular interactions, and other outside factors, (C) cause them to fold into complex 3D structures. Ribbon representation of Human Serum Albumin from PDB 1A06.[68]

A variety of mechanisms cause the resulting polypeptide chain to fold into the complex three-dimensional shape distinctive of proteins (**Figure 1.3C**). For example, the hydrophobic or hydrophilic nature of each -R group on an amino acid will cause it to prefer the inside of outside of the structure when it is in water (hydrophobic groups will "hide" inside the structure, and vice versa). Other -R groups will have chemical interactions with each other, such as van der Waals interactions, hydrogen bonds, or ionic bonds. Additionally, the different environments within cells that that proteins go through as they are being made will chemically modify certain -R groups and make them form covalent bonds with each other. For example, cysteines, which contain a thiols (-SH) in their -R group, can lose their H atoms in reducing environments within the cells, and subsequently react with other reduced cysteines to result in disulfide bridges.[69,70]

All these interactions that result in three dimensional structures give rise to what is arguably the main key concept in biochemistry: structure gives rise to function. Evolutionary processes have resulted in a broad range of proteins that can interact with their environments in a variety of ways. For example, they can specifically capture small molecules in enzymatic pockets. Once captured, the small molecule causes a small change in the local forces in the protein, and the resulting change in 3D structure can catalyze reactions of the small molecule, such as hydrolysis reactions to "split" the molecule in tow and consume a water molecule in the process (as performed by penicillin amylase).[71] The opposite is also possible, where a protein captures two molecules, and combines the two through a condensation reaction, producing a water molecule in the process (as happens with citrate synthase).[72] Many other chemical reactions are possible through enzymatic catalysis. Proteins are also able to produce physical actuation forces, such as the interactions between actin and myosin, whose attachment and movement result in muscle contractions.[73,74]

The functionality of proteins means that they have roles in almost all biological functions: from the translation of DNA and RNA to proteins (various RNA synthetases, individual ribosome components), to cellular processes (respiration, membrane channel transport), to cell to cell signaling (Human Growth Hormone, insulin), to digestion (lipases, proteases, amylases) and many more. Proteins are also key in the immune system, where antibodies serve as protein markers that signal foreign or harmful object to immune cells. By having highly specific interactions with their target molecules, antibodies bind to molecules and signal to other systems that said molecules must be cleared from the body. These interactions occur not just with antibodies, but also with proteins such as Human Serum Albumin, which as discussed earlier, interacts with gp60 in endothelial cells,[66,67] or Human Transferrin, which interacts with transferrin receptors overexpressed in a variety of cancer cells.[75]

Many of the above-listed proteins have become therapeutic agents. For example, insulin has been used as a treatment to treat diabetes for the last 70 years, and hormone replacement therapies are common treatments for glandular pathophysiologies.[76] More recent trends in the biopharmaceutical industry have focused on the use of antibodies to treat diseases. By using natural antibodies, modifying them through genetic engineering methods, or producing *de novo* antibodies, antibodies can be used to direct the immune system to attack cancerous cells, deliver conjugated therapeutics, or affect cellular pathways.[77,78] Additionally, there is strong interest in using delivery enzymes to treat either generalized deficiencies, or for specific functions, such as in reactive oxygen species clearance.[79–81]

1.2.2 Protein Nanoparticles

Both due to the perceived problems with the EPR effect and proteins' numerous clinical advantages, exploring protein nanoparticles (PNPs) as potential therapeutics seems a sensible next step for biomedical research. Traditionally, synthesizing protein nanoparticles occur in one of three synthetic methods: *nab* technology, self-assembly and coacervation.

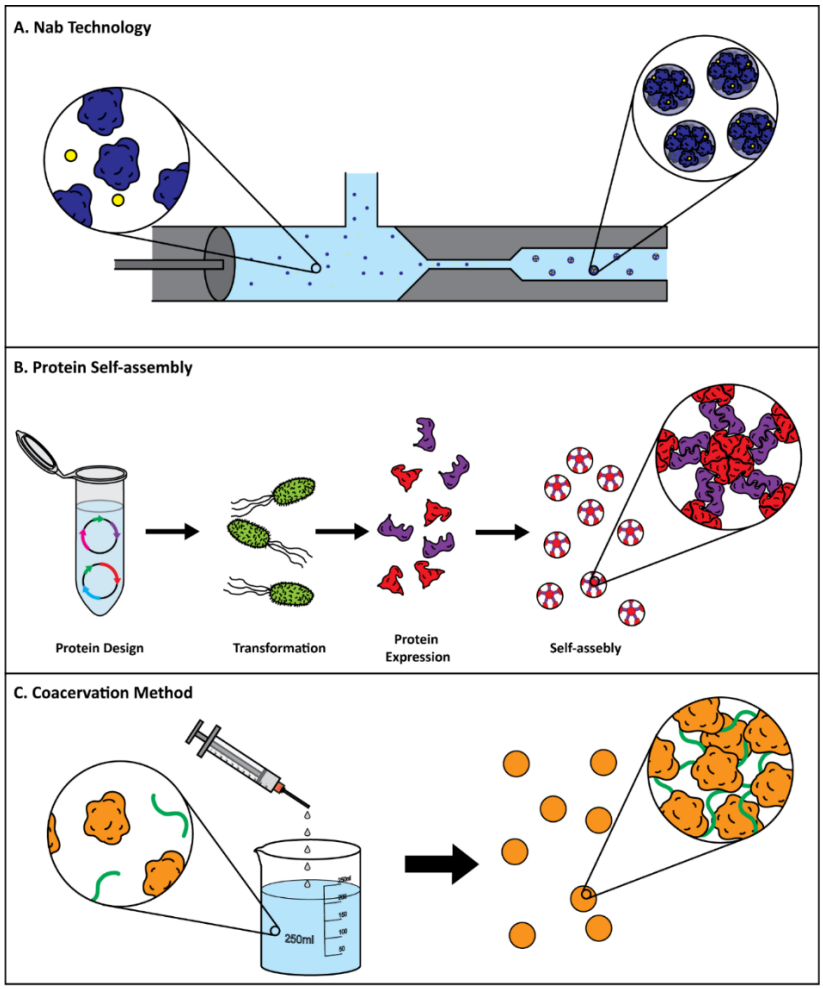

Figure 1.4 Protein Nanoparticles hold great promise in medicine due to their variety and inherent functionalities. Three main methods exist to synthesize these particles. (A) *Nab* technology works by using a sheer mediated process to force hydrophobic drugs within proteins and subsequently cause the proteins to aggregate into nanoscale particles. (B) Self-assembly techniques use the expression of specially designed proteins by microorganisms that subsequently self-assemble into structures that can be used for broad variety of therapeutic applications. (C) Coacervation functions by the addition of an organic solvent or reagent to a protein solution, which causes the formation of particles that are subsequently crosslinked using bifunctional crosslinkers.

1.2.2.1 Nanoparticle Albumin Bound (nab) technology

Nab technology is one of the oldest and most developed methods for making PNPs. Developed by Abraxis Bioscience (now a part of Celgene) to create a way of delivering paclitaxel, *nab*-technology forces highly hydrophobic drugs into the internal hydrophobic pockets of human serum albumin (HSA) using a high-pressure manufacturing process. Paclitaxel is normally administered using harsh organic solvents.[82] By packaging the drug in albumin, a common protein in human blood that is not only water soluble but also has a naturally long circulation time, the drug can be delivered with reduced side effects.[65] The first FDA approved *nab* product was Abraxane, which has been approved for use as a first line therapy for non-small cell lung cancer, metastatic adenocarcinoma, and as treatment for metastatic breast cancer. Additionally, Abraxane is in Japanese clinical trials by Celgene for use in metastatic pancreatic cancer and gastric metastatic cancer.[83]

In addition to the success of Abraxane, multiple other *nab* technologies are under investigation at both the industrial and academic level. ABI-008 through ABI-011 are a family of *nab* based drugs that are undergoing clinical trials. For example, ABI-009 (*nab*-rapamycin/sirolimus, brand name Tarzifix™) is under investigation by Aadi Bioscience (licensed from Celgene) in a variety of phase 1 and 2 trials ranging from Metastatic Colorectal Cancer to Pulmonary Arterial Hypertension (see Table 2). In addition to multiple clinical trials, next generation *nab* technologies are actively being investigated. For example, actively targeted variants of *nab* particles have been made. Thao *et al.* developed *nab* particles made from lactosylated albumin loaded with a mixture of paclitaxel and doxorubicin. The particles were designed to take advantage of the high affinity of lactose to asialoglycoprotein receptors, which are overexpressed in hepatocellular carcinomas. The particles were shown through *in vitro* and *in*

vivo experiments to have increased accumulation in liver vs control (Pac/dox loaded into naïve albumin *nab* particles).[84] In addition to applying targeting moieties to *nab* particles, there has been work done on the use of adjuvants in potential therapies. An interesting case was the work performed by Kinoshita *et al*, where Abraxane was delivered with S-nitrosated HSA dimers.[85] By modifying the HSA dimer through a vasodilator. This effect increased the delivery and efficacy of Abraxane in colon cancer and melanoma murine models, and reduced metastases. Creative combinations of therapies such as this show potential translatability in that they follow the pharmaceutical industry model of expanding the potential of a therapy through combination studies.

While showing great potential, *nab* technologies have potential downsides. Early work has shown that Abraxane is associated with more rapid plasma clearance compared to the traditional liposomal formulation of paclitaxel (Taxol).[64] Abraxane nanoparticles are stable in *ex vivo* saline solutions, but the particles quickly break down into albumin-paclitaxel complexes following administration.[65] This poor colloidal stability has been suggested as the reason behind the rapid clearance of the nanoparticles.[86] Work has been done to improve the colloidal stability of *nab* particles,[86,87] but these works have used albumin bound paclitaxel particles made through coacervation techniques, not high pressure homogenization as Abraxane and other *nab* particles are. Further studies are therefore needed to substantiate claims of improved stability. This problem of using coacervation synthesized particles as a stand-in for Abraxane has also been seen in other studies with potentially impactful advances.[88,89] In addition to poor clearance profiles, *nab* technology has the inherent downside of harsh synthetic conditions.[90] This potentially limits the use of *nab* technology to deliver active proteins, such as enzymes, in ways that other synthetic routes that are able to.[91] Excellent reviews of *nab* technologies have been written by Hawkins *et*

al. and Tan *et al.*, among others, which we recommend for further reading.[92,93] *Nab* technology has shown the clinical potential of proteins as nanocarriers in medicine.

1.2.2.2 Self-assembled protein nanoparticles

Self-assembled nanoparticles are nanoscale structures made of protein complexes that can self-assemble to form PNPs. These structures are designed by creating recombinant proteins that contain oligomerization-domains that create structure, and then a variety of other domains that can result in specific activity.[94] The synthetic methods and design strategies for nanoscale protein structures have been excellently summarized in recent reviews.[94,95]

An interesting application of self-assembled PNPs in the medical space is the use of caged protein nanoparticles.[96] These particles are made up of protein units that self-assemble under specific conditions into hollow cage-like structures. Inside these structures it is then possible to load a variety of therapeutic molecules such as enzymes[97] and small molecules.[98] In a recent study, Kawakami *et al.* designed a 60-mer protein cage with a defined structure. Notably, they were able to design the particle so that specific residues faced either the exterior or interior of the cage, and subsequently were able to covalently modify these particles.[99] These covalent modifications were done using disulfide bonds, and thus this system could be designed to carry a drug in the inside of the cage, and then be released in a reducing environment.

These self-assembled nanoparticle technologies are elegant, sophisticated, and complicated. However, these very characteristics call into question their potential for translation to the clinic in the near future. Most of the proteins used in these nanoparticles are not only novel recombinant proteins, but are also expressed in non-mammalian organisms such as *Escherichia coli*.[99] Expression in non-human organisms of recombinant proteins presents many regulatory

problems and costs, as has been shown though the past 30 years with the rise of recombinant antibody and antibody fragment (Fab) technology.[100] Yet, with careful development, the rise of the multibillion-dollar biological therapeutics field shows the potential for progressively more sophisticated therapies to eventually enter the market.

1.2.2.3 Coacervation-synthesized protein nanoparticles

During coacervation, a "coacervation agent", usually an organic solvent such as acetone or ethanol, is added to a concentrated aqueous solution of a protein of interest. The coacervating agent dehydrates the proteins and causes the precipitation of nanoparticles from the solution. The particles can then be crosslinked, rendering them water insoluble. By controlling a variety of conditions, including the protein type, the rate of addition of the coacervating agent, the temperature of the procedure, the salt content of the solution, and the crosslinking agent and time, the resulting nanoparticle size, mechanical properties, and functionalities can be tailored to fit the needs of the application.[101,102] In addition, the process is highly reproducible, and the particles can be surface functionalized and loaded with a variety of therapeutics.[103–105]

Initial work using coacervation focused on albumin proteins, but the field is now expanding to a variety of different proteins and applications. A wide variety of different proteins have been formulated into nanoparticles, as detailed in a recent review.[106] These proteins have been used in applications such as the packaging of small molecules and micro-nutrients for the food industry. Guo *et al.* produced whey protein nanoparticles loaded with zinc and showed that particle size could be controlled by modulating the amount of zinc added and the synthesis conditions. Additionally, they showed through *in vitro* experiments that site specific delivery of zinc was possible by pH dependent release of the micronutrient from the PNPs to its nutritionally relevant site, the intestinal track, as opposed to the stomach.[107]

Through coacervation techniques, PNPs have been prepared from a wide variety of polypeptides and proteins for therapeutic purposes.[91,108,109] A recent publication that used the PNP technologies developed by the Champion lab demonstrated a proof of concept of a universal influenza virus.[110] Nanoparticles were comprised of a core of a tetramer of M2e epitopes from four influenza subtypes, and surface modified with one of two different recombinant mutants of the highly conserved hemagglutinin (HA) stalks from various subclasses of influenza. By creating a cocktail of two nanoparticles, each modified with different recombinant HA variants, Deng *et al.* elicited universal protection to a wide variety of influenza subtypes. While the use of the highly conserved M2e epitopes has been attempted before in vaccines, these vaccines were constructed from virus-like particles (VLP) loaded with epitopes and resulted in off target immune responses due to the carrier proteins in the VLP.[111,112] PNPs made almost entirely of proteins of interest, as was demonstrated in the work by Deng *et al.*, can avoid off target effect problems. Additionally, coacervation-manufactured PNPs, as opposed to the self-assembled or VLP counterparts, have greater stability over a large range of physiological environments, and studies have shown that they can potentially create cold chain-independent therapies.[113] A clear downside of coacervation particles is inherent in the simplicity of their synthetic method, in that it creates homogeneous distributions of proteins throughout each particle. Only radial complexity through surface modifications methods are able to provide any kind of anisotropy to the particles, as opposed to technologies that will be presented in this thesis.

Knowledge of protein folding and biochemistry has advanced to the point where novel structures and functions can be built *de novo* through either first principles engineering, as demonstrated in a variety of self-assembled nanoparticles previously described, or through directed evolution, as has been seminally shown by the work of Frances Arnold and colleagues.[114]

However, the use of novel proteins does raise questions of translatability of technologies that are based on almost entirely recombinant proteins and have no analogues in the clinic or even the human body. Additionally, new proteins offer the ability to potentially use the function-follows-form principles of proteins to build complex, compartmentalized nanomachines from protein nanoparticles, though this possibility has yet to be fully explored. The large number of different synthetic routes, functionalities and applications of nanoparticles based on proteins as their building blocks that have been recently developed and commercialized shows the bright potential for PNPs as a revolutionary form of nanoparticles in medicine However, more generalizable synthesis techniques will be needed to allow mass production of PNPs, potentially if they are multi-functional and thus require more control over anisotropy during production.

1.3 Electrohydrodynamic Co-jetting

1.3.1 Synthesis of NPs Using Electrohydrodynamic Co-jetting

The Lahann group has developed over the last 10+ years a technique for synthesizing multicompartmental NPs.[115–117] Electrohydrodynamic (EHD) co-jetting functions by dissolving a polymer in an appropriate solvent and then pressure driving said polymer at a low flow rate through a syringe, creating a droplet on the tip of a needle attached to the syringe. A high voltage is placed between this syringe and a collecting surface, causing an electromagnetic pulling effect on the droplet. A Taylor cone is formed at the end of the droplet, breaking the surface tension at a focused point (**Figure 1.5**). This breaks apart the droplet, sending either small particles or fibers (micron to nanometer range) to the grounded collecting surface. The creation of particles (**Figure 1.5A**) or fibers (**Figure 1.5B**), and their respective characteristics, is dependent on a wide range of parameters, namely applied voltage, dielectric constant and volatility of the solvents, total viscosity of the solution, the length of the polymer chains, distance between the needle and collector, type

of collector used, flow rate, and needle gauge. While in midair transit, the small size of the created structures causes near instantaneous solvent evaporation, leaving dry product on the collecting surface.[118]

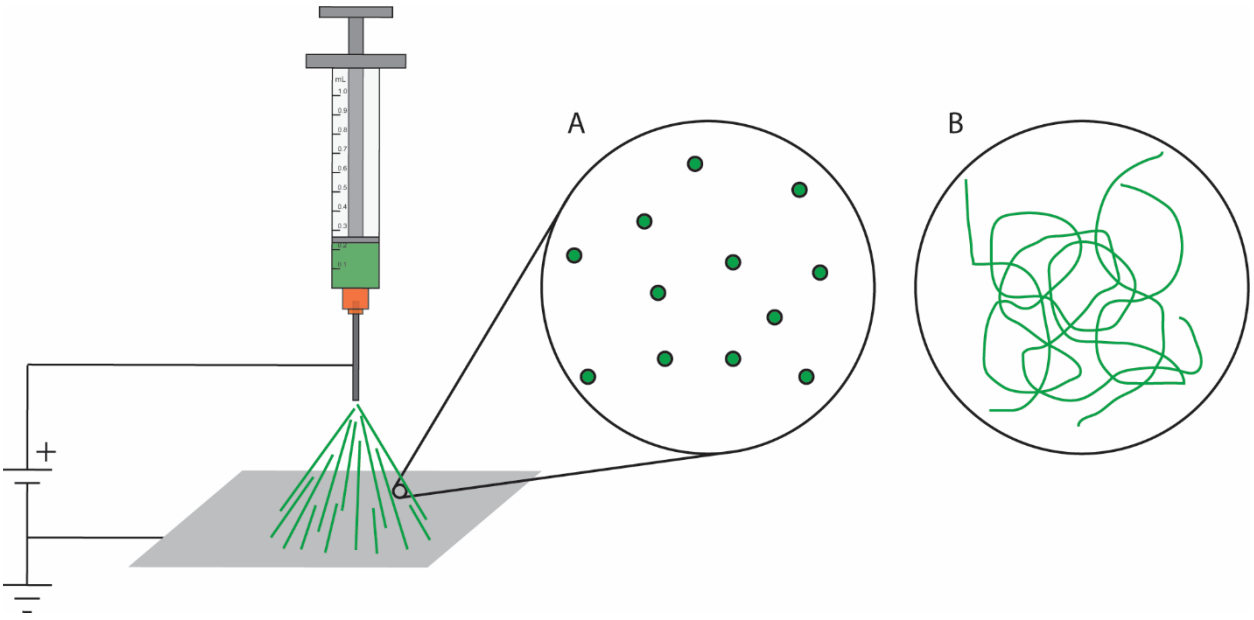

Figure 1.5 Electrohydrodynamic jetting can synthesize micro and nanoscale (A) particles or (B) fibers out of a variety of different materials.

Through the use of a parallel, laminar flow needle setup, it is then possible to create multicompartmental particles that are made of distinct volumes, each of which can be composed of different base polymers (synthetic and natural), and loaded with various small molecules (therapeutics, contrast agents), inorganic, and biological compounds (RNA, peptides) (**Figure 1.6**).[119]

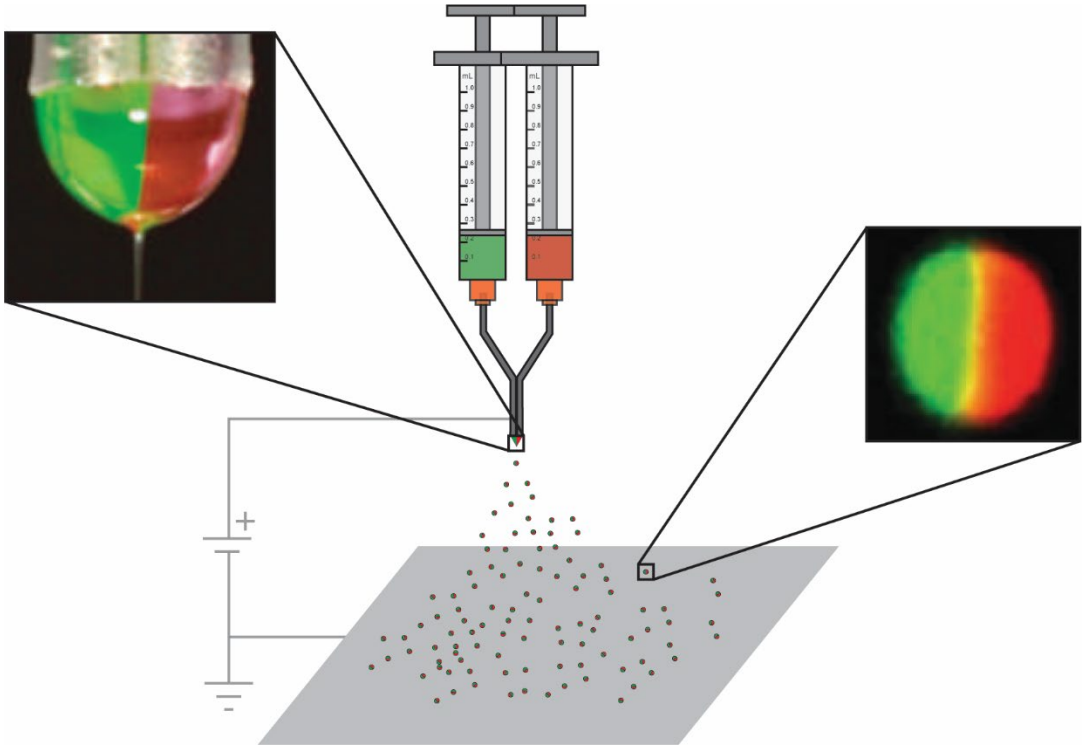

Figure 1.6 EHD co-jetting can make anisotropic micro and nanostructures by using parallel capillaries. Adapted from refs.[115,119]

1.3.2 Applications of EHD Co-jetting

First developed in 2004 as a method to synthesize polymer-based particles with distinct phases,[115] EHD co-jetting has evolved into a robust method to produce micro and nanostructures for various biomedical applications. Beyond microparticles, it is now possible to create micro-fibers, rods and cylinders, disks, and nanoparticles, all with anisotropic features and controllable sizes.[117,119] Improvements in controlling the electric fields have made it so that complex scaffolds made of precisely placed microfibers can be made at large scale.[120] The process has also been scaled up for large scale manufacturing of fibers and particles.[121]

Methods have also been developed for transforming the structures from inert to functional. By including polymers with different functional groups in each compartment, orthogonal chemistries can be used to place different chemical entities, such as proteins, targeting ligands, and

polymer brushes on the surfaces of said compartments (**Figure 1.7**).[122–124] For example, these orthogonal chemistries were used to attach Plexiafor, a targeting molecule that specifically homes to the cell surface receptor CXCR4, which is overexpressed in triple negative breast cancer, onto the surface of one compartment of nanoparticles. These particles were then selectively taken up by CXCR4 cells.[125]

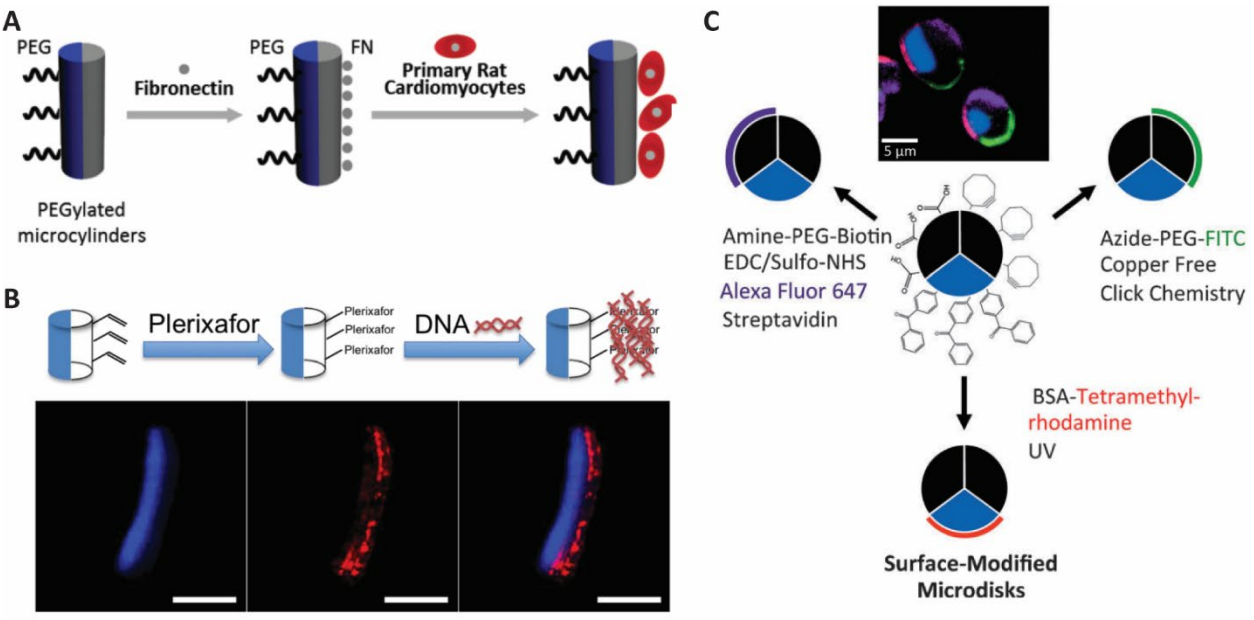

Figure 1.7 EHD co-jetting has been used for a variety of applications. (A) Microcylinders that use cardiomyocytes to self-actuate. (B) Triple-negative breast cancer targeting microcylinders. (C) Multicompartmental microparticles with chemically orthogonal surface modifications. Adapted from refs.[122,123,125]

In addition to surface modification, medically relevant molecules can be independently loaded into each compartment of the structures to allow for the loading of incompatible entities into single particles. This allows for applications such as in theragnostics, where single particles are used both for therapeutic and diagnostic purposes, such as in work by Misra *et al.*, where particles were constructed to deliver both si-RNA and an imaging agent.[126] Since particles can be made of different base polymers, this also allows for the control of release dynamics of therapeutics from each compartment. Rahmani *et al.* demonstrated this ability by constructing a microparticle

system where the chemotherapeutic drug irinotecan was loaded in a two compartment nanoparticle, where one compartment would detect low pHs, such as those inside cells or in cancer environments, and quickly release its irinotecan payload over a period of 10 hours, while the other compartment would slowly release the irinotecan load over a 5 day period.[127]

1.4 Aims of this Work

In this dissertation, electrohydrodynamic (EHD) co-jetting is used to develop a new flexible methodology to create protein based nanocarriers. Synthetic Protein Nanoparticles (SPNPs) are composed of i) a protein or proteins of choice and ii) a macromer that reacts with proteins to hold them together. The work herein builds upon the groundwork protein-based nanoparticles developed previously and expands a technology that was based on a single protein and inert macromer into a design space that allows for a wide variety of proteins and functional macromers. To show how SPNPs could be used not just as inert carriers, a method to load active enzymes into the particles was developed. Additionally, as SPNPs are still in the pre-clinical stage, a microfluidic method to characterize the particles based on material composition was developed to facilitate future scale up. Lastly, preliminary work was conducted on developing additional applications of SPNP technology for neuroblastoma targeting and gene delivery.

Aim 1: To develop SPNPs into a modular system that allows for a choice of protein, macromer, and geometric composition. Here, the design space of current SPNP technologies in terms of protein and macromer choice is expanded. The biological behavior effects of SPNP material choices is explored, and SPNPs made of two compartments are characterized.

Aim 2: To apply SPNPs to active enzyme delivery. Enzymes are some of the most medically useful types of proteins. A method to load active enzymes into SPNPs was developed. Loading, processing, and storage effects of activity in enzyme loaded SPNPs were then characterized. A

method to target SPNPs to specific tissues was developed and their use in an *in vitro* disease model demonstrated. Last, the behavior of bicompartmental SPNPs loaded with complimentary enzymes in each compartment was explored.

Aim 3: To apply Electrokinetic microfluidic devices to characterize multi-protein SPNPs. If SPNPs are eventually developed for clinical used, high throughput characterization methods will be needed for effective manufacturing. Here, we first design and synthesize a multiprotein SPNP system for characterization in electrokinetic microfluidics. With these particles, we were able to characterize and differentiate between single protein, single compartment protein blend, and two compartment SPNPs using electrokinetic microdevices.

Specific Aim 4: To explore further applications for nanomedicine for cancer therapeutics. SPNPs also show promise for in targeted delivery using small molecule targeting ligands. For this purpose, the use of meta-iodobenzylguanidine (MIBG) as a targeting moiety in neuroblastoma was developed, using poly(lactic-co-glycolic acid) as the material for nanoparticles, and key information about the chemical behavior of MIBG for targeting purposes was discovered.

Chapter 2

Preparation of Synthetic Protein Nanoparticles

Part of the material for this chapter has been adapted with modifications from the following publication:

1. D. F. Quevedo*, N. Habibi*, J. V. Gregory, Y. Hernandez, T. D. Brown, R. Miki, B. N. Plummer, S. Rahmani, S. Mitragotri, and J. Lahann, "Multifunctional Synthetic Protein Nanoparticles" *In Preparation*. *equal contribution

2.1 Background and Motivation

Nanoparticle-based drug delivery systems provide improved drug stability, reduced drug toxicity and improved biodistribution compared to free drugs.[128–130] There are a number of nanoparticle therapeutic platforms such as PEGylated liposomal doxorubicin (Doxil) and liposomal vincristine (Marqibo) that have been approved for cancer treatment.[48,131]. Despite the progress made in the field of nanoparticle-based drug delivery, there are still unmet challenges, like poor circulation times due to immunogenicity and a lack for adequate functional materials.[132,133] Solutions to these challenges often conflict with each other, leading to the development of multifunctional, multicompartmental nanoparticles.[117] Multifunctional nanoparticles have traditionally been made of synthetic polymers, such as polyethylene glycol

(PEG),[134] poly(lacticde-co-glycolide) (PLGA),[135] or block copolymer systems.[136] Using proteins as the primary building block of nanocarriers could be an appealing alternative, because of their chemical diversity, inherent biological functions, and a potentially reduced risk for immunogenicity.[137]

Protein nanoparticles (PNP)[132,137] have been pursued for drug delivery applications including the clinically approved drug Abraxane[64] and other preclinically studied candidates.[138–140] Common PNP fabrication methods include, among others, nab technologies,[84,88] coacervation,[91,101] and self-assembly.[99,141] Despite undoubtable progress in recent years, PNP technologies are still hampered by a range of drawbacks. While PNPs prepared via nab technologies have been implicated with decreased morbidity,[142] the processing conditions during particle preparation have been showed to cause protein denaturation.[143] Coacervation can create large quantities of PNPs,[103] but generally lacks sufficient control to prepare multifunctional nanoparticles. Self-assembly can provide more structural diversity,[95] but requires *ab initio* design of new protein building blocks that has to be done separately for each application. Except for the more involved self-assembly route, none of these techniques has so far resulted in architecturally controlled protein nanocarriers, such as bi- or multicompartmental nanoparticles.

Electrohydrodynamic (EHD) co-jetting has previously been shown to be effective at creating multicompartmental particles with nanoscale anisotropy.[144] EHD co-jetting relies on laminar co-flow of two or more polymer solutions prior to the jet ejection to pre-template compartmentalized nanoparticles and nanofibers, with fine control over size, shape, composition, and spatial distribution of matter at the surface and bulk level.[145,146] EHD co-jetting has been used to fabricate multicompartmental polymer particles that incorporate various functionalities, such as stealth

modalities,[147] targeting/tracing,[148] and encapsulation of different cargos such as siRNA,[149] imaging agents,[150] and small molecule cancer drugs.[151]

As traditional protein nanoparticle synthesis methods lack control over anisotropy, we have developed reactive electrojetting as a method for making anisotropic Synthetic Protein Nanoparticles (SPNPs). Reactive electrojetting takes advantage of the anisotropic control afforded by EHD co-jetting to create protein nanoparticles, and then introduces a second chemical step that converts the particles into nanogels through a sol-gel transition using a variety of macromers.

2.2 Methods

2.2.1 Materials

Recombinant Human Serum Album (Cellastim S) was purchased from InVitria. Human Transferrin, Human Hemoglobin, Lysozyme, Horseradish Peroxidase, Human Recombinant Insulin, 2KDa O,O′-Bis[2-(N-Succinimidyl-succinylamino)ethyl]polyethylene glycol (PEG-NHS) or 4,7,10,13,16,19,22,25,32,35,38,41,44,47,50,53-Hexadecaoxa-28,29-dithiahexapentacontanedioic acid di-N-succinimidyl ester (PEG-NHS-S) were acquired from Sigma Aldrich. All buffers, purchased in solution form, and all other reagents used were of lab grade and acquired from Sigma Aldrich or Thermo Fisher.

2.2.2 Electrohydrodynamic Co-jetting

All SPNP types were synthesized using EHD jetting, with differences in the protein solution used and subsequent processing resulting in different copolymer SPNPs. In general, the EHD jetting method was done as previously described,[122,123,152,153] here a protein solution is pressure driven through a 25G blunt tip needle at a flow rate of 0.1 mL hr^{-1}, and a sufficient voltage applied between the needle and a collecting surface to produce a stable Taylor cone. The voltage causes the droplet to be pulled towards the collecting substrate, and the stream subsequently breaks

up into nanometer sized spheres. In mid-flight, the solvents rapidly evaporate to form solid nanoparticles. For fluorescent tagging, BSA-Alexa Fluor dyes were incorporated into the protein solution at a concentration of 0.8% (w/w) of the total mass of protein unless otherwise noted.

2.2.3 SPNP Synthesis Using PEG-NHS and PEG-NHS-S

For SPNPs made with ester-based macromers, a protein solution was made by fully dissolving a protein of interest at 10% w/v in a 90:10 (Ultra-Pure H_2O:EtOH) solution. Depending on the method, PEG-NHS or PEG-NHS-S was added at 10% (w/w of protein mass) to the solution. After EHD jetting, the nanoparticles were placed in a dry 37 °C oven for 7 days, and subsequently collected by scraping them off the collection surface using a solution of DPBS supplemented with 0.01% Tween 20.

2.2.4 SPNP Synthesis Using GA

To synthesize SPNPs polymerized with vapor-phase Glutaraldehyde (GA), a protein solution was made by fully dissolving a protein of interest at 10% w/v in a 90:10 (Ultra-Pure H_2O:EtOH) solution, without macromer included in the jetting solution. After EHD co-jetting the resulting particles were incubated at room temperature in a closed container, which contained 2.5mL of 20% Glutaraldehyde in a plastic reservoir, for 30 minutes. The unreacted glutaraldehyde was quenched by collecting the particles by scraping them off the collecting surface using Ultra-Pure H_2O supplemented with glycine (100 mM) and 0.01% Tween 20.

2.2.5 SPNP Synthesis Using S-S

SPNPs synthesized through oligomer-free disulfide bonds (S-S) were made by dissolving the protein of interest at 2.5% w/v in a 90:10 (2,2,2-Trifluoroethanol: Ultra-pure H_2O) solution, and the protein allowed to denature for 2 hours in order to fully break all disulfide bonds. 2-Mercaptoethanol was then added at a 10x molar excess to the number of disulfide bonds in the

protein and allowed to incubate for 30 minutes at room temperature. The solution was then jetted, and the resulting particles collected as previously described.

2.2.6 Nanoparticle Collection

After collection, the collected solution was sonicated on ice, run through a 40 μm cell filter, and then centrifuged at 3,200 rcf for 5 minutes to remove large particles. The resulting supernatant was then centrifuged at 21,130 rcf for 40 minutes to collect the desired particles. The final particles were washed at least 5 times through centrifugation using DPBS supplemented with 0.01% Tween 20.

2.2.7 Nanoparticle Characterization

Particles, prior to collection, were imaged using Scanning Electron Microscopy (Thermo Fisher Nova 200 Nanolab Dualbeam FIB). Particle diameters were measured using an automated MATLAB macro based on the function 'imfindcircles', and the resulting diameters converted to frequency histograms using GraphPad. To determine their hydrodynamic size distribution after isolation, the particles were suspended in 0.22 μm filtered DPBS supplemented with 0.01% Tween 20, sonicated on ice, and measured using dynamic light scattering (Malvern ZSP ZEN-5600). Standard settings were used and an average of three measurements are reported. Particle zeta potential was measured on the same instrument using a disposable folded capillary cell (DTS1070, Malvern) and using standard settings. Particle concentration was measured using a BCA assay, using a BSA standard for a standard curve. Particle number concentrations were measured using Nanoparticle Tracking Analysis on a Malvern Nanosight.

2.2.8 CD Spectroscopy

Circular Dichroism (CD) Spectroscopy was used to study the effects of EHD jetting on the proteins that compose SPNPs prior to polymerization. Fully synthesized SPNPs were not studied using CD spectroscopy due to the method's inability to obtain measurements that can be analyzed with deconvolution based secondary structure analysis from aggregated protein complexes.[154] The different methods used to polymerize the SPNPs were carried out, without the corresponding macromers, for the NHS-PEG, NHS-PEG-S and GA macromers. As S-S crosslinking occurs during immediately during the jetting process, it was not possible to quantitatively study the effect of jetting on the proteins, but since the process for S-S includes purposeful denaturation of the proteins with a strong organic solvent and a reducing agent, it stands to reason that little to one of the original secondary structure would be maintained after the jetting process.

Particles were jetted, but no macromers were included in the jetting formulations or post-jetting. The particles were then treated identically as if they would have been had macromers were included, with incubation at 37°C for 7 days for PEG-NHS based macromers, and storage at 4°C overnight for GA treated SPNPs. After treatment, the particles were collected and treated following protocols for secondary structure analysis based on deconvolution of CD signals.[155] Briefly, the particles were collected using a 10 mM Potassium Phosphate, 100 mM potassium fluoride (pH: 7.4) buffer. The collected solution was filtered using a 0.22 μm syringe filter, and the protein concentration measured using a Nanodrop 2000c Spectrophotometer (Thermo Fisher Scientific), with the absorption at 280 nm measured and converted to mass concentration using an extinction coefficient of 85.1 $M^{-1}cm^{-1}$.[156]

The samples were then diluted to a concentration of 0.15 mg/mL in the same buffer described previously and measured in a 0.1 cm pathlength Hellma quartz cuvette in a Jasco J-815

CD Spectrometer. Temperatures were controlled using a Peltier stage. Spectra were acquired at a stage temperature of 20 °C from 185-260 nm, using a data pitch of 0.2 nm, a digital integration time of 1 sec, bandwidth of 1 nm, and a scan speed of 50 nm/min. Each sample was measured for a total of 10 accumulations and was smoothed using Savitzky-Golay algorithm (Convolution Width of 21) and normalized to the buffer. Native and denatured proteins were measured by dissolving protein in the same buffer as the nanoparticle samples. A thin layer of mineral oil was placed atop the sample to reduce evaporation, and the sample was measured at 20 °C for the native protein control measurement. The sample was then heated to 90 °C and subsequently allowed to equilibrate for 5 min prior to measurement for the denatured sample. The smoothed signals were analyzed for secondary structure using DichroWeb.[157–161]

2.2.9 Cell Culture

HeLa cells (ATCC) were grown at 37 °C in a humidified environment at 5% CO_2. Cells were cultured in DMEM media supplemented with 10% fetal bovine serum (FBS), 1% Non-essential Amino Acids (NEAA), D-glucose (25 mM), and Sodium Pyruvate (1 mM). Cells were passaged at 70-80% confluence and media changed as needed.

2.2.10 Confocal Microscopy

HeLa cells were seeded in 8 well chamber slides at a concentration of 50,000 cells per well and allowed to adhere overnight. SPNPs were sonicated in ice, and immediately added at a concentration of 10 μg mL^{-1} to cell media supplemented with penicillin (100 Units mL^{-1}), streptomycin (100 μg mL^{-1}), and Amphotericin B (250 ng mL^{-1}). Cells were incubated with the particles for 1 hr. Particle media was removed following incubation, and the cells thoroughly washed with DPBS. Cells were fixed with 4% paraformaldehyde, washed with DPBS, and then stained with Alexa Fluor 488 Phalloidin following manufacturer recommendations. The samples

were then air dried, mounted using ProLong Diamond Antifade Mountant with DAPI, and allowed to cure for 24 hr prior to imaging. Confocal micrographs were obtained using a Nikon A1si inverted confocal microscope. A 60X water objective with excitation at 401, 488, and 641 nm for the cell nuclei, actin fibers, and SPNPs, respectively, was used for image acquisition. NIS-Elements and ImageJ software was used for image acquisition and processing.

2.2.11 Flow Cytometry

HeLa cells were seeded in a 96-well plate at a density of 30,000 cells per well. After overnight incubation at 37 °C and 5% CO_2, the media was then removed from the wells, and fresh media containing each SPNP group at 10 μg mL^{-1} was added to the wells. The cells were incubated with SPNPs for 24 hr. The cells were washed with DPBS three times and then trypsinized. The cells were washed two more times and stained with DAPI before analyzing them with Cytoflex (Beckman Coulter) cell analyzer located at the Flow Cytometry Core of the University of Michigan. FlowJo software was used for data analysis. Statistical analysis was conducted using a one-way ANOVA, followed by Tukey's post-test, using GraphPad software. A P-value of <0.05 was considered statistically significant (*$P<0.05$, **$P<0.01$, ***$P<0.001$; ****$P<0.0001$).

2.2.12 Blood Brain Barrier Transwell Assay

For particle transport studies, 5E10 NP/mL Human Transferrin (hTf)- and Human Serum Albumin (HSA)-SPNPs were prepared in complete cell culture media and added to the apical compartment. The companion plate in the basolateral compartment contained only complete culture media. At each hour timepoint for 6 hr, a 100 μL aliquot was sampled from the basolateral compartment and pipetted into a 96-well plate. Fresh complete cell culture media (100 μL) was immediately added to the basolateral compartment upon removal. Fluorescence intensities of samples obtained from the basolateral medium upon 1 hr, 2 hr, 3 hr, 4 hr, 5 hr and 6 hr intervals

were measured in triplicate using the BioTek Synergy H1 Hybrid Multi-Mode Microplate Reader. Solute concentration was determined based on calibration curves of standard fluorescence intensities created in triplicate. Percent (%) transport of SPNPs were then calculated.

2.2.13 Bicompartmental SPNP Synthesis

Bicompartmental SPNPs were synthesized using GA as a macromer but using a parallel capillary EHD co-jetting setup previously described.[122,123,152,153]

2.2.14 Structured Illumination Microscopy

Anisotropic SPNPs (ASPNPs) with two compartments were synthesized as described above using HSA and hTf. To facilitate imaging of the resulting particles, BSA Alexa 488 and hTf Alexa 647 were incorporated, at 0.08% (w/w) of the total protein mass, into the albumin and transferrin protein jetting solutions, respectively. GA was used to crosslink the resulting ASPNPs. Albumin-transferrin ASPNPs were collected and purified as previously described and finally suspended directly in Prolong Diamond before being deposited onto glass slides. Samples were allowed to cure for at least 24 hr prior to imaging. Structured Illumination Microscopy (SIM) imaging was conducted using a Nikon N-SIM +A1R confocal microscope equipped with a 100X oil objective. Excitation using the 488 and 647 nm lasers were used for image acquisition. Three-dimensional z-stacks of multiple regions were collected and deconvoluted using the Nikon Elements software. The resulting z-stacks were analyzed to confirm bicompartmental particle architecture.

2.3 Results and Discussion

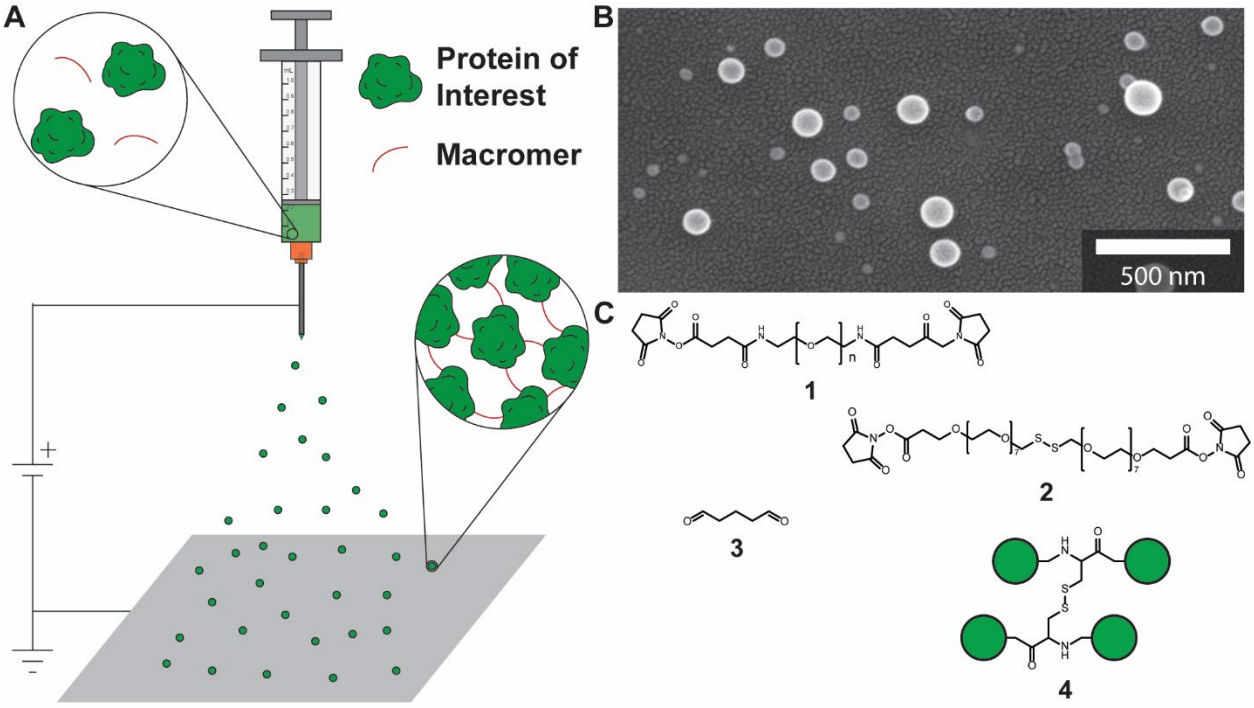

Figure 2.1 (A) Preparation of Synthetic Protein Nanoparticles (SPNPs) using Electrohydrodynamic jetting. (B) SEM images of particles made using EHD jetting. Particles are jetted, and subsequently (C) polymerized using a variety of different macromers.

To prepare SPNPs using reactive electrojetting, particles are first made using EHD jetting. Protein was dissolved in an aqueous solvent system with 10% ethanol. The addition of an organic solvent increases the volatility and decreases the surface tension of the solution.[162] Solid nanoparticles are then prepared by accelerating the jetting solution in an electrical field created between the tip of the jetting needle and a collection plate (**Figure 2.1A**). Once the electrical potential is applied, a Taylor cone is spontaneously formed,[163] and the jet is ejected from the Taylor cone towards the collection plate. In EHD jetting, conditions (i.e. surface tension, flow rate, solute concentration, applied electric field) can be controlled to result in either particle formation or fibral formation. The protein concentrations in all jetting solutions were maintained 10% (w/v) or lower to ensure that only particles were formed. After EHD jetting, particles were examined for

uniformity and sphericity using Scanning Electron Microscopy (SEM) (**Figure 2.1B**). Circular Dichroism (CD) spectroscopy demonstrated that component proteins had unchanged secondary structures compared to their native confirmations (**Figure 2.2**, **Table 2.1**).

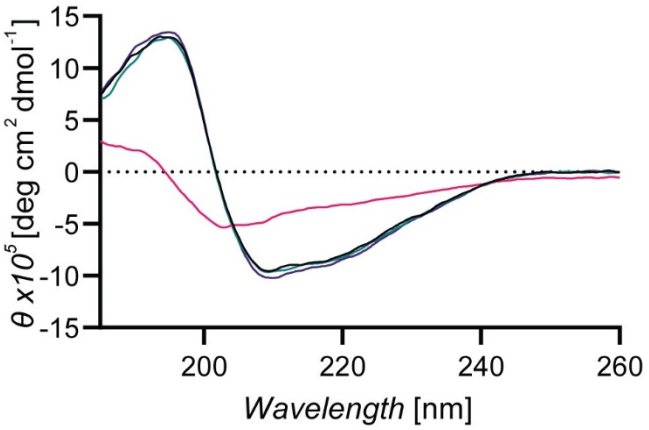

Figure 2.2 The effect of EHD jetting on proteins was analyzed using Circular Dichroism (CD) Spectroscopy. Transferrin was jetted and treated as described in the text but did not include macromer for NHS-PEG and NHS-PEG-S (purple) or GA (green). Native (black) and heat denatured transferrin (pink) were measured as controls.

Table 2.1 measured CD spectra for free transferrin controls and analogues for methods 1-3 were deconvoluted using the different algorithms and neural networks available in Dichroweb. For all but the denatured transferrin, most of the algorithms were able to fit the measured signals within high degrees of certainty, and the ratios of secondary structures were similar to those found using X-Ray crystallography (from PDB). Additionally, the ratios found for all algorithms matched almost identically for the different polymerization methods studied.

Sample	Sample Treatment	Structure	X-Ray	Selcon3	Contin-LL	CDSSTR	K2d
Free Transferrin	Native	α-Helix	0.34	0.29	0.25	0.24	0.29
		β-Sheet	0.19	0.24	0.27	0.30	0.27
		Turn	0.22	0.23	0.23	0.22	ND
		Unordered	0.25	0.28	0.26	0.26	0.43
	Denatured	α-Helix	NA	0.07	0.15	0.06	0.09
		β-Sheet		0.32	0.32	0.33	0.39
		Turn		0.19	0.23	0.27	ND
		Unordered		0.30	0.30	0.33	0.52
Jetted Transferrin	Methods 1 and 2	α-Helix	NA	0.25	0.25	0.24	0.29
		β-Sheet		0.24	0.27	0.28	0.30
		Turn		0.23	0.22	0.22	ND
		Unordered		0.28	0.26	0.26	0.41
	Method 3	α-Helix	NA	0.25	0.25	0.24	0.29
		β-Sheet		0.24	0.27	0.28	0.30
		Turn		0.23	0.22	0.22	ND
		Unordered		0.28	0.26	0.26	0.41

The second step of reactive electrojetting is the reaction of the proteins in the nanoparticles with a variety of reactive macromers, such as short NHS-ester functionalized polyethylene glycol (PEG) chains (**Figure 2.1C**). The reaction occurs during or immediately after the EHD jetting process, rendering the SPNPs stable in aqueous environments and locks in their geometry. A small library of commercially available macromers was selected to investigate different sol/gel transitions. The first two macromers, PEG-NHS and PEG-NHS-S, react the macromers' ester functional groups with the proteins' amine groups. This reaction completes after SPNPs are

deposited by EHD jetting onto the collecting surface and then placed at 37 °C for 7 days. The third macromer, GA binds proteins together by reacting aldehyde groups with a variety of protein residues.[164] GA crosslinking is conducted immediately after EHD jetting, when dried protein particles are placed in a sealed container containing 20% glutaraldehyde, which vaporizes and reacts at room temperature. The last crosslinking method does not rely on a macromer but instead takes advantage of native disulfide bonds within proteins (S-S). Prior to EHD jetting, proteins are treated by Trifluoroethanol (TFE) to break intra-protein disulfide bonds, and with β-mercaptoethanol (BME) to inhibit spontaneous reformation of disulfide bridges from resulting free thiols. The solution is then jetted as described previously. While droplets are traveling to the collecting surface, TFE and BME evaporate allowing the disulfide bonds to reform between proteins, resulting in insoluble SPNPs on the collecting surface.

PEG-NHS was selected as a biocompatible and biodegradable macromer that can be imparted with functional groups. PEG-NHS-S showcases the flexibility of macromers based on PEG-NHS. By incorporating stimuli responsive groups into the PEG chain, such as the disulfide in the PEG-NHS-S, particles can be made to react differently to different environments. GA vapor treatment was developed as a faster alternative to PEG-NHS macromers, as the vapor-phase reaction occurs in as little as 30 minutes to form fully water insoluble SPNPs. Thus, GA allows for the incorporation of time sensitive agents into SPNPs, such as radiotherapeutics. S-S was developed to have a method which does not use any available functional groups on the protein residues, unlike the three other macromers. Additionally, S-S takes place in an organic solvent system, as opposed to the aqueous system used for the other macromers. This different solvent system introduces the ability for SPNPs to be loaded with hydrophobic drugs, opening up a large number of potential therapeutics for drug delivery with SPNPs.

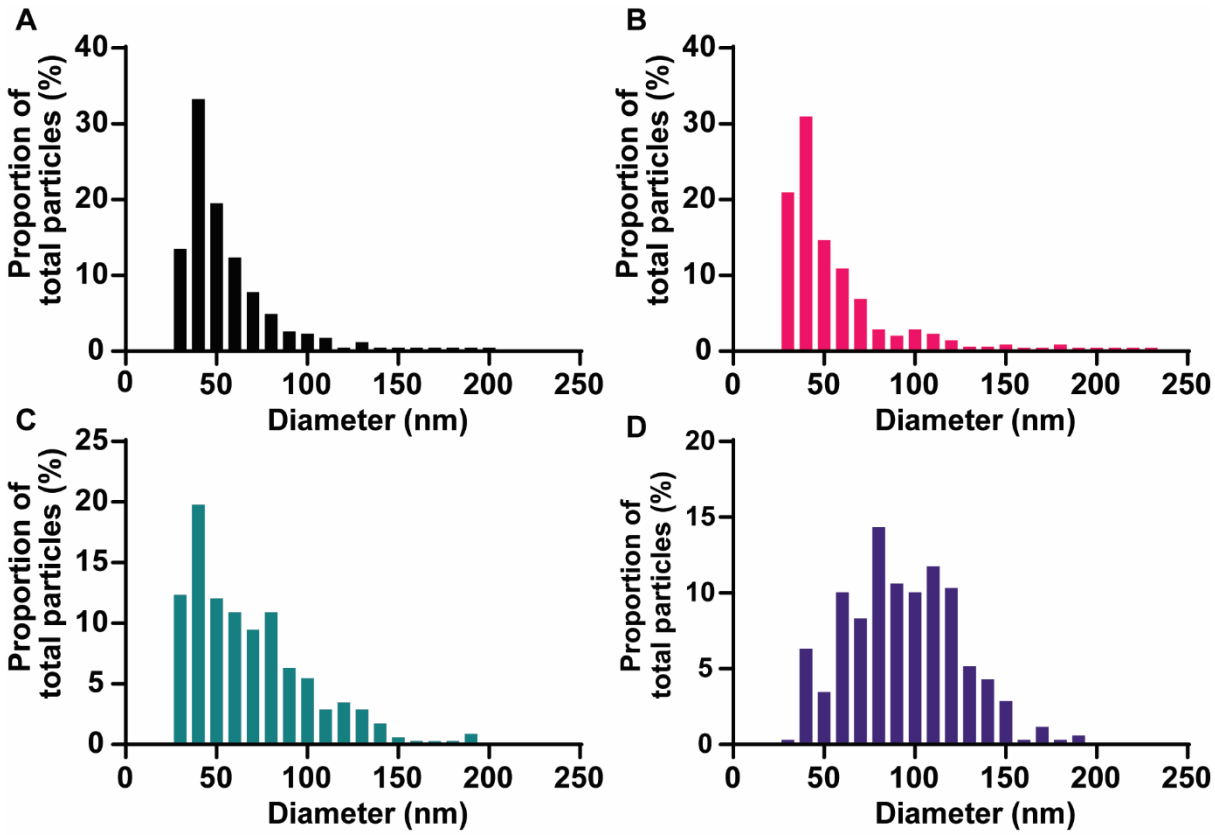

Figure 2.3 Histograms of diameters measured by SEM. SEM micrographs of SPNPs made using (A) Insulin, (B) Hemoglobin, (C) Lysozyme, and (D) Transferrin were measured using an automated MATLAB program.

After the reactive electrojetting process, the resulting particles have a broad size distribution as seen by SEM (**Figure 2.3**). To further narrow particle size distribution, particles were first collected, then sonicated to cause disaggregation, and were size purified using a previously established serial centrifugation technique.[150] After hydration, particles made with hTf and each of the different macromers were measured using Dynamic and Electrophoretic Light Scattering (DLS and ELS), and found to have similar size distributions and zeta potentials (**Figure 2.4**).

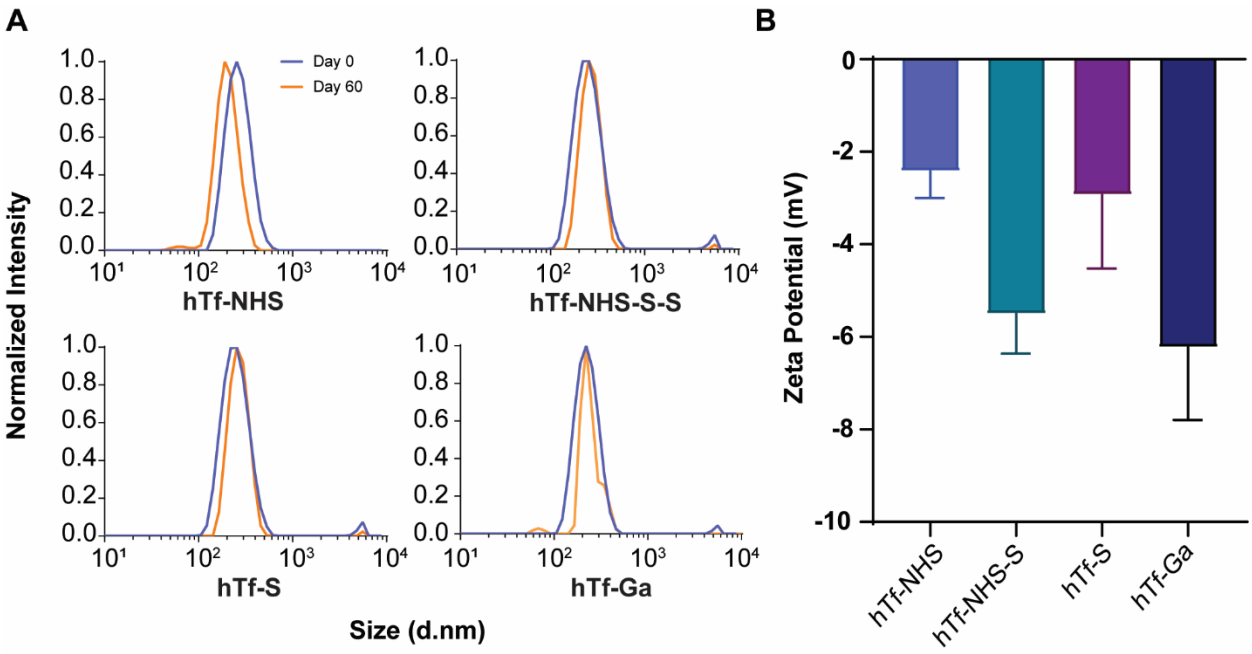

Figure 2.4 Different macromers do not significantly change size or zeta potential, and are stable over a 1 month period. hTf SPNPs were made with all 4 different macromers, and (A) their sizes after synthesis and 60 days later were measured using DLS. Macromers were found to not affect particle size, and the particles maintained stability over the time period. (B) The same SPNPs were measured using ELS and found to not have significantly different zeta potentials.

To show how macromer conditions can be used to tailor SPNPs hydrodynamic size, HSA particles were made with PEG-NHS. The hydrodynamic size was tuned by changing the macromer to protein ratio. Increasing the ratio of macromer to protein does not change the size of particles in their dry state, but as the amount of macromer is increased, SPNPs swell less, going from a hydrodynamic diameter of 200 nm to 120 nm, when the crosslinker ratio is increased from 10% (w/w) to 30% (w/w) (**Figure 2.5**).

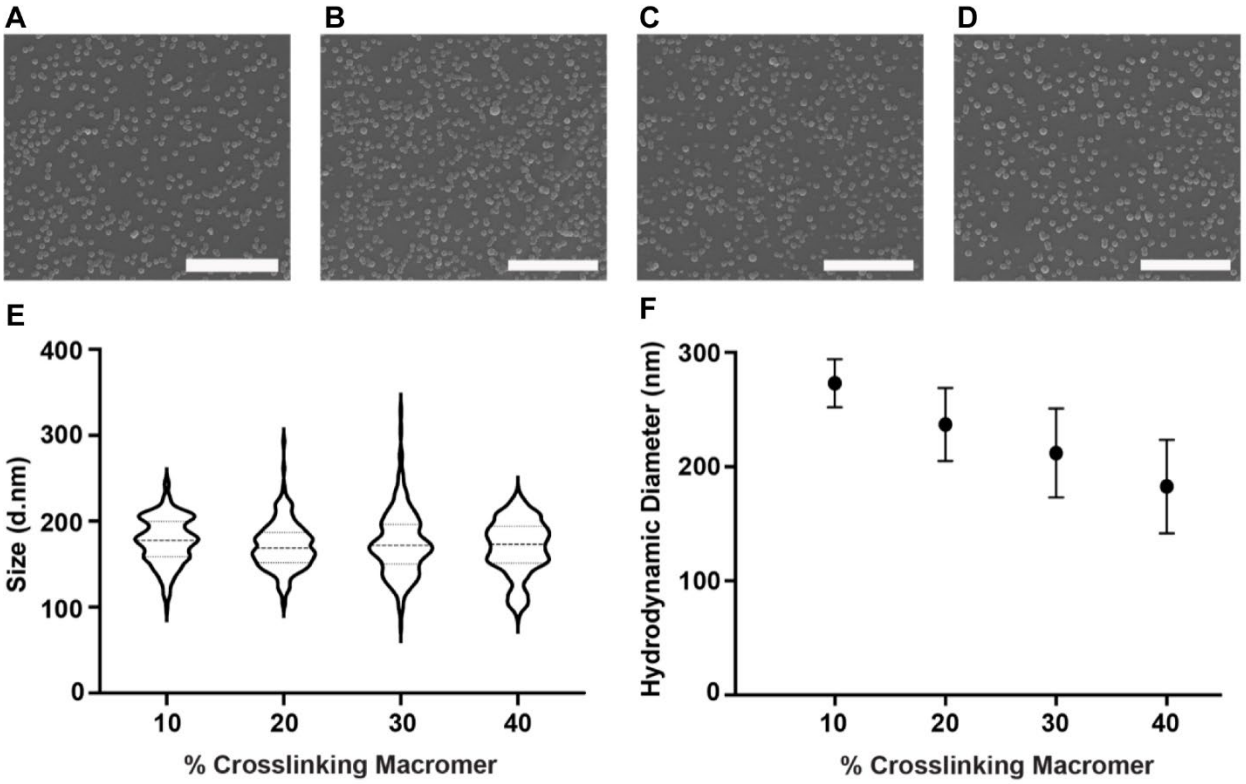

Figure 2.5 Effect of crosslinking macromer on particle size. (A-D) SEM images of SPNPs synthesized with various amounts (A) 10, (B) 20, (C) 30, and (D) 40 w/w% of crosslinking macromer relative to Human Serum Albumin. (E) Size distribution of SPNPs in their dry state. Individual SPNPs (n = 200) measured using ImageJ. No significant difference observed between the various formulations. ANOVA, multiple comparisons. (F) Hydrodynamic diameters of the resulting SPNPs in PBS measured by DLS, median ± SD. Scale bars = 4 μm

We also explored how reactive electrojetting can make SPNPs from a variety of proteins. A small library of proteins was selected to synthesize SPNPs, each with potential biomedical applications: Human Transferrin, [165] Insulin (Ins),[166] Hemoglobin (Hem), [167] and Lysozyme (Lys).[168] For these experiments, each protein was used to fabricate stable SPNPs with PEG-NHS. Proteins were dissolved as previously described, with the exception of Ins which was dissolved by adding 10% acetic acid to the solvent mixture, due to poor solubility. SEM images of SPNPs as sampled from the collecting surface demonstrated that different proteins did not affect the morphology of the resulting particles (**Figure 2.6A-D**) . To evaluate the stability of the particles,

SPNPs were collected, size purified, and stored at 4 °C for seven days. Their size distributions after a week were similar, confirming particle stability after storage (**Figure 2.6E**).

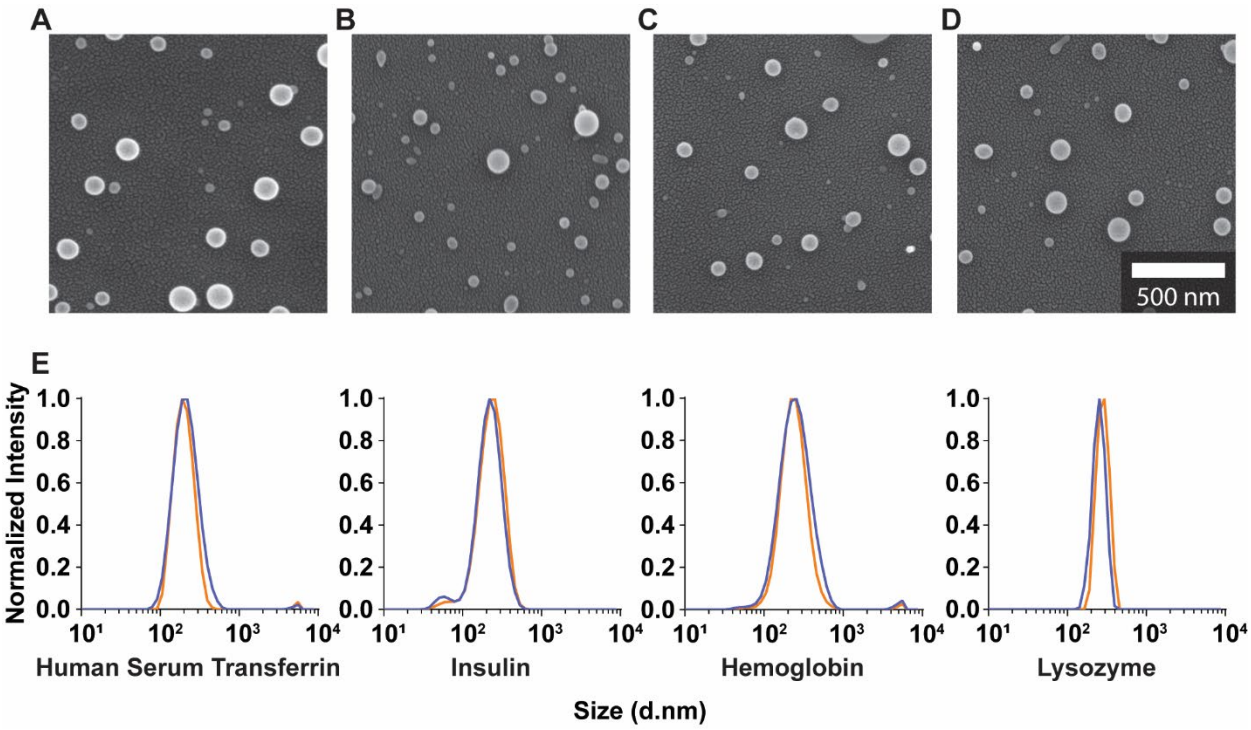

Figure 2.6 Stable synthetic PNPs can be made using a variety of proteins. SEM images of SPNPs made from (A) hTf-PEG-NHS, (B) Ins-PEG-NHS, (C) Hem-PEG-NHS, and (D) Lys-PEG-NHS. (E) The stability of particles in PBS over a 1-week period was characterized by measuring the particles using DLS 1 day (blue trace) and 7 days (red trace) after synthesis and size purification.

Various experiments were conducted to explore how protein and macromer choice affects SPNP behavior in biological systems. To investigate the effects of different macromers on the *in vitro* behavior of SPNPs, hTf SPNPs were synthesized with each of the different macromers and loaded with fluorescently labeled Bovine Serum Albumin. SPNPs were then incubated with HeLa cells. SPNPs behaved differently depending on their macromer. hTf-PEG-NHS and hTf-GA SPNPs remained punctate when observed using confocal microscopy (**Figure 2.7A and Figure 2.7B**). In contrast, hTf-PEG-NHS-S and hTf-S-S SPNPs, which rely on disulfides-bonds for structure, were more diffuse (**Figure 2.7C and Figure 2.7D**). It is likely that these particles

degraded due to disulfide bonds breaking in the cellular oxidizing environment. These effects have been observed with other particles made with similar chemical principles.[91]

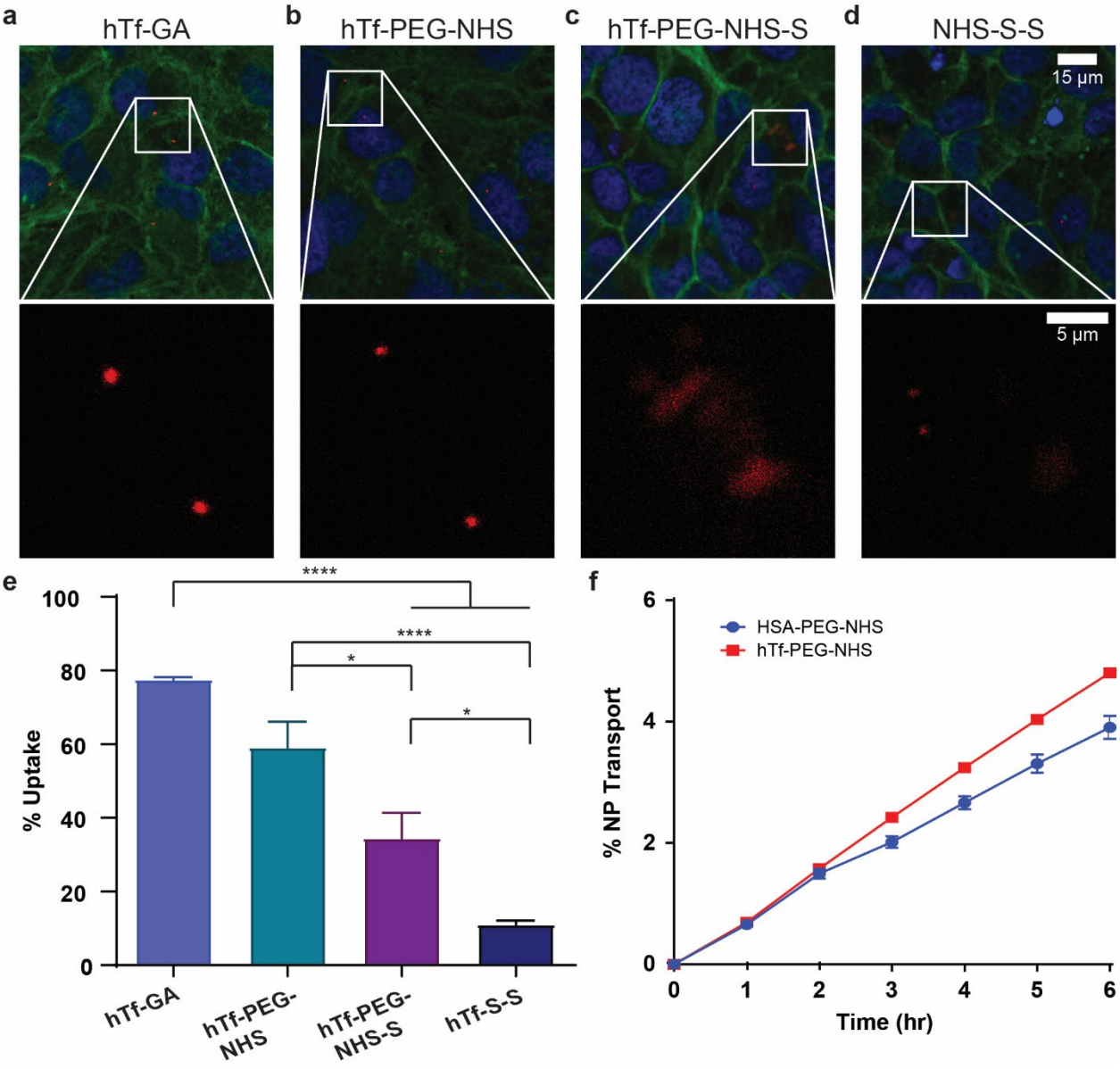

Figure 2.7 SPNPs can be made using different methods that have a distinct effect on the *in vitro* uptake and behavior of the particles. (A-D) Fluorescent SPNPs made with macromers were added to HeLa cells for 1 hr, and their behavior studied using confocal microscopy. (E) Uptake was quantified using confocal microscopy using HeLa cells cultured at equivalent conditions and with SPNPs added for 24 hr. (One-way ANOVA). (F) SPNP BBB transport. Percentage transport of HSA and hTf SPNS across hCMEC/D3 monolayers in Transwell inserts. (*P<0.05, **P<0.01, ***P<0.001; ****P<0.0001

The uptake of SPNPs was evaluated quantitatively by flow cytometry (**Figure 2.7E**). There was an observed difference in the uptake level for SPNPs based on macromer. Cells incubated with hTf-GA showed a 7-fold greater uptake percentage than those exposed to hTf-S-S ($P<0.0001$), and a 2-fold increase compared with hTf-S-S ($P<0.0001$). Uptake values for cells incubated with hTf-GA and hTf-PEG-NHS were not statistically different. As the particles made using different macromers had no significant differences in size distributions or zeta potentials, the reasons for these observed differences are yet unknown. We hypothesize that these effects may be caused by differences in the secondary structures of the proteins after they undergo polymerization after jetting, or in the mechanical properties of the SPNPs, and this will be explored in future studies.

To demonstrate the potential of SPNPs' variable protein composition biologically, we compared the blood brain barrier (BBB) permeability of hTf-PEG-NHS SPNPs to Human Serum Albumin SPNPs (HSA-PEG-NHS), which have been previously developed.[169] A static *in vitro* BBB model was constructed using a Transwell® migration assay which analyzes cellular transport across an analogue of the BBB, where hCMEC and D3 cells are placed in the apical compartment .[170] SPNPs were fluorescently tagged, and particles that were able to go from the apical to the basolateral compartments of the assay were measured using fluorometry. hTf-PEG-NHS SPNPs exhibited higher percentage transport across the BBB model, as compared to HSA-PEG-NHS SPNPs (**Figure 2.7F**) as expected, due to the overexpression of transferrin receptors on brain endothelium.

Finally, we sought to demonstrate how reactive electrojetting can synthesize anisotropic SPNPs (ASPNPs). Co-jetting is a well-established method where a parallel capillary system is used to create laminar flow in EHD jetting.[145] To demonstrate that this technology can be applied

to SPNPs, particles were made that had one compartment containing fluorescent BSA, and the other fluorescent hTf. These particles were processed as previously described and then imaged using Structured Illumination Microscopy (SIM). As can be seen in **Figure 2.8**, the resulting particles are clearly composed of two separate compartments that are easily resolved.

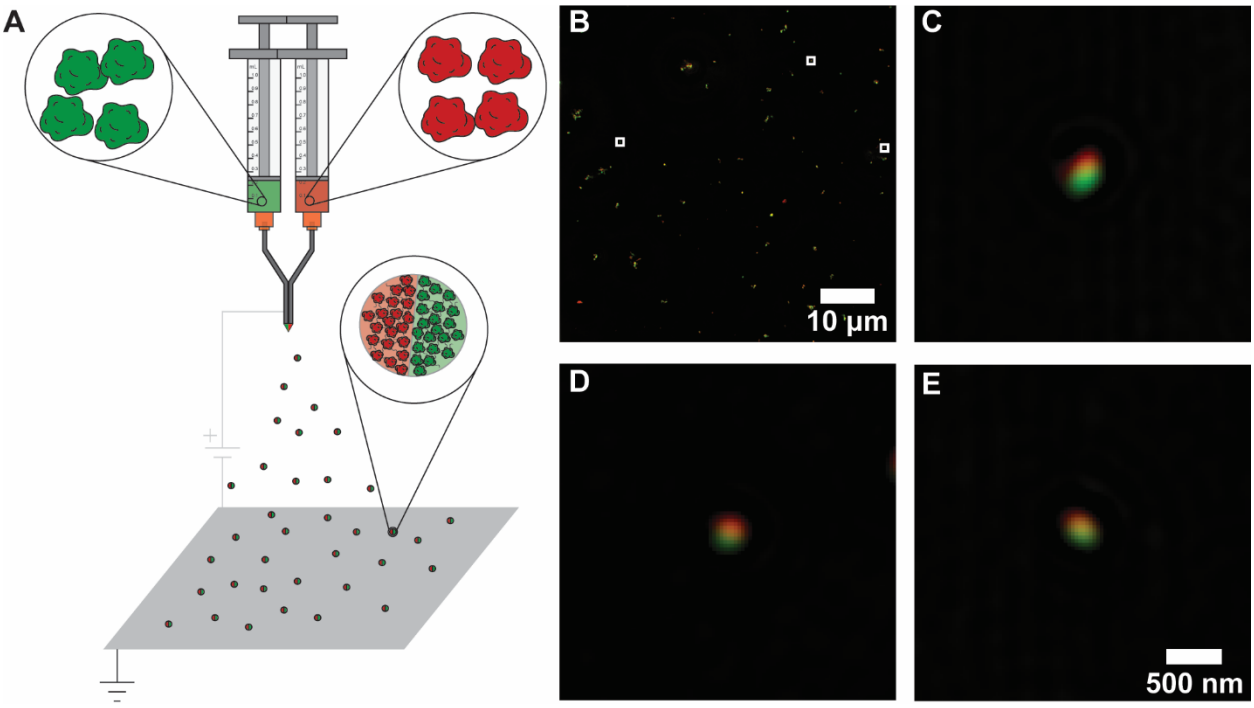

Figure 2.8 EHD co-jetting can be used to make bicompartmental SPNPs. (A) SPNPs containing Human Serum Albumin (HSA) in one compartment and Human Serum Transferrin (hTf) in the other were synthesized, with each compartment doped with BSA-Alexa-488 or hTf-Alexa-647, respectively. The particles were imaged using SIM. (B) The images were then deconvoluted. (C-E) Zoomed in images of individual particles are shown to showcase the bicompartmental nature of the particles.

2.4 Summary

In this work, we have developed a method for the synthesis of Synthetic Protein Nanoparticles fabricated using reactive electrojetting with tunable material compositions. Anisotropic SPNPs were also developed. As each compartment can be individually designed, this technique allows for the development of complex nanoparticles such that release kinetics of drug cargo from each compartment could be independently controlled, as shown in previous studies.[127,171] Novel

nanoparticle-based cancer vaccines, where each compartment is made of a different cancer antigen, could provide significant therapeutic advantages. Additionally, the use of functional proteins could also lead to the delivery of active gene therapy enzymes and nucleic acids. Recent work has shown how a treatment based on SPNPs cured mice in an intracranial murine model and prevented subsequent tumor recurrence from a secondary implant, suggesting immunity to cancer recurrence.[169] SPNPs have thus already started to demonstrate their potential in both the therapeutic and preventive clinical spaces. In the future, we aim to further develop these ASPNPs into a variety of clinical applications.

Chapter 3

Design of Synthetic Protein Nanoparticles for the Targeted Delivery of Enzymes

Part of the material for this chapter has been adapted with modifications from the following publication:

1. D. F. Quevedo, B. Zhang, Y. Hernandez, A. Berardi, R. Miki, J. Lahann, and C. F. Greineder "Synthetic Enzyme Nanoparticles Made by Electrohydrodynamic Co-jetting" *In Preparation*.

3.1 Background and Motivation

Proteins and enzymes are commonly used in the biomedical space. Enzymes, in particular, hold much promise, and have been in use therapeutically since the mid-1980s.[172] Enzymes have many advantages, including high-affinity and specificity to substrates, efficient reaction rates, and biodegradability. Enzymes tend to provide more specialized treatments and fewer side effects than traditional drugs, as well as an ability to treat deficiency diseases for medical applications.[173] While enzymes have the potential to revolutionize the therapeutic marketplace, using them in unmodified forms has significant drawbacks. In general, there are difficulties in maintaining enzymatic activity levels once they are in use, whether it is due to challenges from the immune system or harsh

environments upon uptake by cells, both of which could result in enzymatic deactivation or destruction.[174]

To address these challenges, enzymes can be stabilized and protected using a wide variety of techniques.[175,176] Medical enzymes are commonly modified by immobilizing them through adsorption or covalent bonding onto a solid support or packaging them into solid matrixes.[177,178] Immobilization and encapsulation techniques can improve the thermodynamic stability and thus improve performance. Encapsulation of enzymes in nanoparticles holds great promise. Packaging enzymes in nanoparticles could potentially increase their long-term stability and circulation time, while maintaining their activity, protecting them from degradation, and reducing immunological responses.[179]

While encapsulating enzymes show much promise clinically, most research has focused on using various systems that are impacted by problems with biocompatibility and degradability,[180] including liposomes,[181] polymeric nanoparticles,[182] sol-gel systems,[183] or inorganic based carriers such as mesoporous silica,[184] magnetic particles,[185] or carbon nanotubes.[186] As an alternative, enzymes encapsulated in constructs that are completely composed of proteins have been investigated, such as with Cross-linked Enzyme Aggregates (CLEAs),[187] or protein nanoparticles synthesized using coacervation.[91] However, these synthetic techniques have little capacity for customization when it comes to particle compartmentalization, which could open the door for particles that have multiple functions that are decoupled from each other or are able to deliver multiple incompatible therapeutics.

A recent advance in nanoparticle technologies has been the use of electrohydrodynamic (EHD) co-jetting to make synthetic protein nanoparticles (SPNPs). These particles are made of a

system where one component is a protein and the other a macromer, such as an oxidation-sensitive PEG chain. The macromers hold the proteins together in a nanoform and can impart the particles with additional functionalities, such as environment dependent degradation. SPNPs have shown significant promise as a translational therapeutic, as they have been shown to effectively treat glioblastoma in a murine model.[169] Additionally, particles made using EHD co-jetting are flexible, as they can be made from a variety of proteins and macromers, giving them potential for stimuli responsiveness and functionality. EHD co-jetting also allows for the formation of anisotropic (multicompartmental) SPNPs.[188] The flexibility in protein composition gives SPNPs potential for the delivery of a wide variety of therapeutics.

In this chapter, we present the development of enzyme loaded SPNPs generated using EHD co-jetting. We have used Catalase (CAT) and Glucose Oxidase (GOX) as proof-of-concept enzymes loaded into SPNPs to study the effects of loading on retained activity, show that enzyme-loaded SPNPs maintain their activity over time, and demonstrate the protection of the loaded enzymes from heat denaturation at physiologically relevant temperatures. Additionally, we show that we can easily conjugate targeting antibodies onto SPNPs. The antibody-targeted enzyme-loaded SPNPs show specific uptake, both in cells engineered to express the target receptor and in a disease model using primary cells, protecting those cells from ROS damage, and thus demonstrating the potential of SPNPs as delivery vehicles for therapeutic enzymes. Last, we show that we can make bicompartmental SPNPs that conduct a cascading enzymatic reaction, demonstrating the potential to structure enzymes in SPNPs at the nanoscale.

3.2 Methods

3.2.1 Particle Synthesis and Collection

Particles were synthesized using EHD co-jetting, as previously described. Briefly, a solution was prepared that contained a mixture of an enzyme of interest, such as Bovine Liver Catalase (Sigma-Aldrich#C40) or Glucose Oxidase (Sigma-Aldrich#G7141), and Human Serum Albumin (Cellastim S, InVitria) in a solvent mixture of 90% H_2O and 10% Ethanol (v/v%). The solution was then pressure driven through a needle at a rate of 0.1 mL hr^{-1}. At the same time, a voltage was applied, forming a Taylor cone at the tip of the needle. As the droplet was pulled away from the needle, the solvent mixture evaporated, leaving solid nanoparticles which landed on the collecting surface. After jetting, the particles were placed in a sealed container with 2.5 mL of 20% glutaraldehyde (v/v% in H_2O) and allowed to react. Particles were then collected in 100 mM glycine solution to quench any unreacted aldehydes. After collection, the particles were sonicated on ice and size selected using a modified version of a previously described technique.[189] Briefly, particles were centrifuged for 1 minute at 3200 RCF to remove large particles. The supernatant was then centrifuged first for 5 minutes at 3200 RCF, and the resulting supernatant for 5 minutes at 22300 RCF to further fine tune the size of the particles. Lastly, the resulting supernatant was then centrifuged for 40 minutes at 22300 RCF in order to isolate the desired particles. The desired SPNPs were then washed at least 4 times, followed by decanting and resuspension in DPBS + 0.01 % Tween 20.

3.2.2 Particle Characterization (Size, Shape, and Concentration)

SPNPs were characterized using various techniques to measure their size, shape, and concentration. Samples of particles that were jetted onto small silicon wafers were treated with vapor-phase glutaraldehyde, gold sputter-coated and imaged in their dry state with Scanning

Electron Microscopy (SEM) using a FEI Nova 200 SEM/FIB Microscope. Particle size and zeta potential was measured by dispersing hydrated particles in 0.22 μm filtered DPBS + 0.01 % Tween 20 and measuring them using Dynamic Light Scattering (DLS) and Electrophoretic Light Scattering (ELS) (respectively) with a Malvern ZSP ZEN-5600. All DLS and ELS measurements are the averages of a minimum of 3 measurement runs. Particle concentrations were measured using a Pierce BCA assay, using commercial BSA standards for calibration.

3.2.3 CD Spectroscopy of Jetted Proteins

To investigate how electrojetting affects enzymatic secondary structures, SPNPs were jetted as previously described, stored over night at 4 °C, and collected using 10 mM potassium phosphate, 100 mM potassium fluoride (pH: 7.4) to mimic the crosslinking process. The collected solution was then filtered using a 0.22 μm syringe filter, and the protein concentration measured by measuring the A_{280} of the protein using UV-Visible spectroscopy. 300 μL of sample was then placed in a Hellma quartz cuvette with a pathlength of 1 mm. The CD spectra from 185-260 nm of protein samples was measured using a Jasco J-815 CD Spectrometer. The measurement parameters used were a data pitch of 0.2 nm, digital integration time of 1 sec, bandwidth of 1.0 nm, scan speed of 50 nm min^{-1}, and a sample concentration of 0.15 mg mL^{-1}. Secondary structure analysis was conducted with the tools made available by DichroWeb.[157–161] Denatured enzyme was prepared by heating a sample of native enzyme, in the same conditions described above, to 80 °C.

3.2.4 Gel Electrophoresis of Jetted Proteins

To investigate the consistency between the protein ratio in the jetting solution vs the protein ratios in the resulting nanoparticles, SPNPs were jetted as previously described, stored over night at 4 °C, and collected as described above without glutaraldehyde treatment. The samples were then

analyzed by sodium dodecyl sulfate-polyacrylamide gel electrophoresis (SDS-PAGE) stained with Coomassie blue.

3.2.5 Activity Assays of Enzyme Loaded SPNPs

3.2.5.1 Enzyme Activity Assays

To investigate the activity of the CAT SPNPs, a previously described hydrogen peroxide degradation assay was used.[190] Briefly, CAT SPNPs were added to hydrogen peroxide diluted to 0.036% (w/w) in 50 mM potassium phosphate buffer at room temperature in a quartz cuvette. The activity (U/ml) of the SPNPs was calculated using:

$$\text{Activity } \left(\frac{\text{U}}{\text{mL}}\right) = s * \frac{2070}{\Delta t} \quad (1)$$

Where s is the slope of the linear portion of the recorded kinetic measurement, and Δt is the time in seconds required for A_{240} to decrease from 0.45 to 0.40. Duplicate measurements were done per sample. GOX loaded SPNPs' enzymatic activity was assayed using a commercially available assay following manufacturer instructions (Abcam, ab219924).

3.2.5.2 Long Term Activity of SPNPs

To investigate how enzymatic SPNP activity changed over time, the activity of freshly synthesized enzyme loaded SPNPs was measured over a two-week period. Samples were stored at either room temperature or 4 °C for the duration of the study. On the day of each measurement, the SPNPs were briefly sonicated, diluted, and their activity was measured as previously described.

3.2.5.3 Activity Stability of SPNPs at Elevated Temperatures

The enzymatic stability of SPNPs was investigated by measuring their activity after being exposed to elevated temperatures. Particles were briefly dispersed using tip sonication, diluted to

concentrations appropriate to each activity assay, and then heated at 40 °C for varying amounts of time. The tubes were subsequently allowed to come to room temperature and their activity measured as described above.

3.2.6 Surface Modification of Catalase SPNPs

To conjugate antibodies onto the surface of Catalase-loaded SPNPs, a two-step reaction was used. First, a 20x molar excess of Azidobutyric acid NHS ester (Lumiprobe, #63720) was added to SPNPs in a 1 mL volume of PBS+ 0.01%Tween, and allowed to tumble and react overnight at 4 °C. The particles were then washed 3 times to remove any unreacted Azidobutyric acid NHS ester by centrifuging at 23500 RCF for 1 hour, and subsequently resuspending the particle pellet in PBS. After washing, the protein concentration was measured using a BCA assay. YN1, R6.5, rat IgG, and human IgG were gifts from the Greineder lab. Antibodies were then added to the particle solution at a ratio of 2000 Ab per nanoparticle and tumbled overnight at 4 °C to react. The number of particles per mass of protein was calculated by measuring a known mass of particles by number concentration with Nanoparticle Tracking Analysis (NTA) using a Malvern Nanosight NS300, to give a ratio of $7.5x10^{11}$ particles/mg of protein. After the overnight reaction, the particles were washed 3 times with PBS as previously described.

3.2.7 Cell Culture

Ren–WT cells were cultured in Ren-WT media (RPMI 1640 supplemented with 10% (v/v) fetal bovine serum (FBS) and 1% (v/v) antibiotic antimycotic solution (100X)). Ren-mICAM cells were cultured with Ren-WT media with extra G418 (Geneticin) at a final concentration of 200 μg ml^{-1}.

3.2.8 Protection of Endothelial Cells from ROS by Targeted Catalase SPNPs

Ren-WT and Ren-mICAM cells were trypsinized to single cells and then plated to 96-well plates at a density of 35,000 cells/ well. Cells were cultured overnight to reach confluency. YN1 and IgG Catalase SPNPs were diluted in Ren-WT media to their final concentrations and incubated for 30 min at 37 °C. Then cells were subsequently washed 3 times with Ren-WT media to remove unbounded SPNPs. A H_2O_2 stock (8.8 M) was diluted in Ren-WT media to reach a final concentration of 4 mM. Cells were then incubated with 4 mM H_2O_2 solution at 37 °C cell culture incubator for 5 hr. Cell death was assessed based on the levels of lactate dehydrogenase (LDH) released to the culture media. LDH levels were measured using Pierce LDH Cytotoxicity Assay Kit (Thermo scientific, # 88953), following manufacturer instructions.

3.2.9 Confocal Microscopy and Cell Staining

REN cells were seeded in an 8-well chamber slide at a concentration of 100k cells per well and allowed to attach overnight. Catalase-loaded SPNPs were then dispersed in cell media to a final concentration of 10 μg/ml. Cells were treated for 30 minutes with 200 μL of particle solution, and then thoroughly washed with PBS. The cells were then fixed with 4% paraformaldehyde for 10 minutes and washed with PBS. Cells were permeabilized with Triton-X100, washed and blocked with PBS+ 1% BSA, and stained with Alexa-488 Phalloidin, along with a primary Rat YN1 antibody, and a Secondary Goat anti-Rat Alexa-555 Conjugate. The cells were finally washed, air dried, mounted with a glass cover slip using ProLong Diamond Antifade Mountant with DAPI, and allowed to cure for 24 hr prior to imaging. Micrographs were obtained using a Nikon A1 inverted confocal microscope with a 60X water immersion objective. Images were acquired with excitation at 401 nm, 488 nm, 555 nm, and 641 nm to image the nuclei, actin fibers, ICAM, and SPNPs, respectively. NIS-Elements and ImageJ software was used for image

acquisition and processing. Images were false colored and digitally treated identically between groups to help accentuate differences.

3.3 Results and Discussion

3.3.1 Electrohydrodynamic Jetting of Enzyme Loaded SPNPs

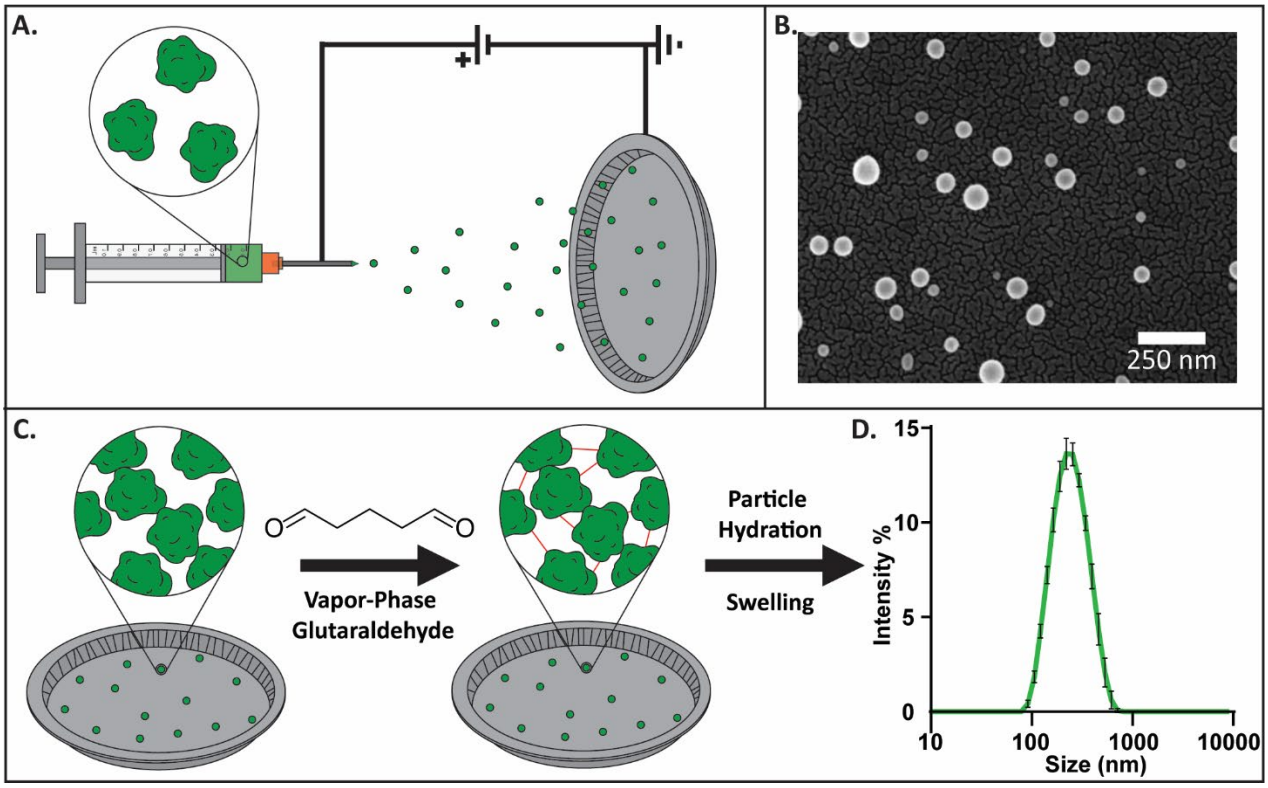

Figure 3.1 (A) Schematic of the preparation of Enzyme Loaded Synthetic Protein Nanoparticles (SPNPs) made using Electrohydrodynamic (EHD) co-jetting. (B) Particles made using EHD co-jetting immediately after formation, imaged using Scanning Electron Microscopy. Particles are formed and then (C) crosslinked using vapor phase glutaraldehyde as a macromer. (D) Nanoparticle size distributions are measured using dynamic light scattering.

Electrohydrodynamic (EHD) co-jetting was used to synthesize Synthetic Protein Nanoparticles (SPNPs) loaded with enzymes. Traditional EHD co-jetting has relied on solvent evaporation to solidify the resulting structures, but in EHD co-jetting of proteins, the resulting dry protein nanoparticles are unmodified and dissolve in aqueous conditions. SPNPs are thus made by modifying EHD co-jetting in a way inspired by reactive extrusion techniques common in chemical

engineering, by treating the particles with a crosslinking macromer during or immediately after the jetting process. Previous work with Human Serum Albumin SPNPs used short N-Hydroxylsuccinimide Polyethylene Glycol (NHS-PEG) chains as the macromer component in the particles, which react with the Lys residues in proteins to hold the proteins together in the SPNPs.[169] In preliminary studies that first explored the behavior of SPNPs loaded with enzymes, it was found that enzymatic SPNPs made with NHS-PEG lost most of their activity (<0.5% residual activity compared to equivalent amounts of free enzyme, data not shown). Circular Dichroism (CD) spectroscopy was used to investigate whether the secondary structure of the enzymes, which is vital to enzymatic function, was affected by the jetting process. It was found that the CD signal of native vs jetted enzyme had been changed, but not as significantly as full enzymatic denaturation (**Figure 3.2**). Due to this, our hypothesis became that the enzymes lost their activity due to the seven days at 37 °C required for the NHS-PEG reaction to result in stable SPNPs.

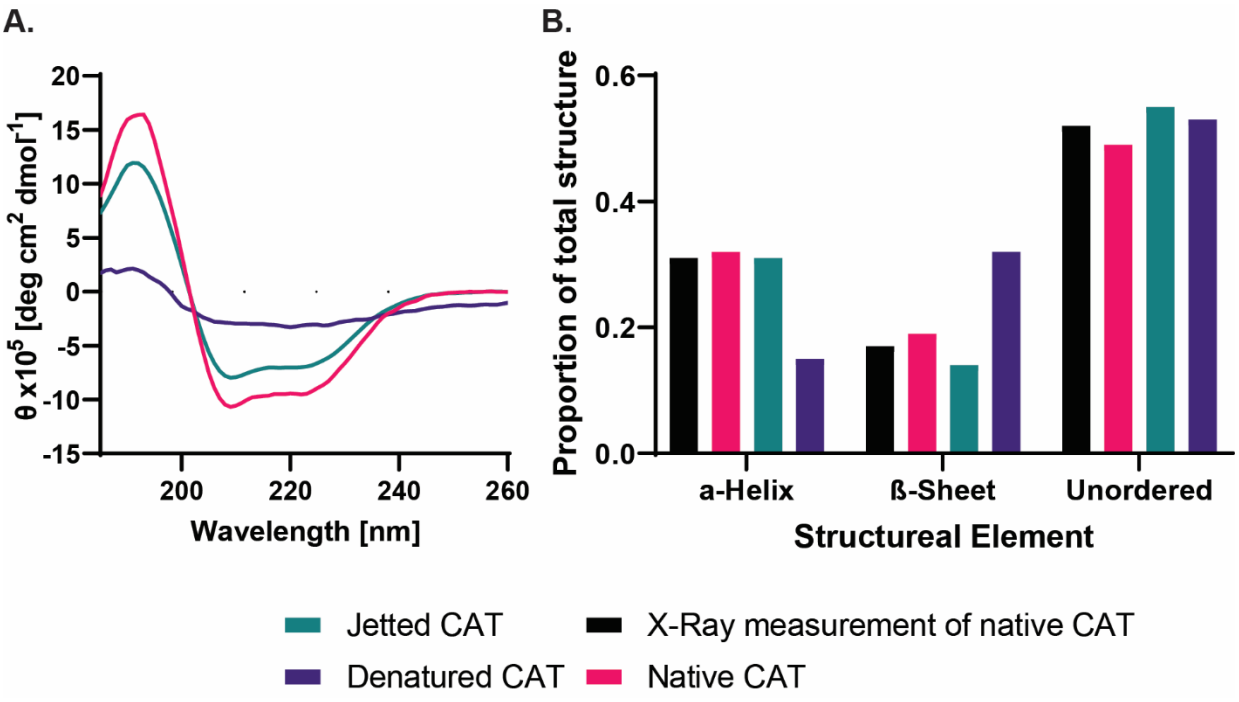

Figure 3.2 Analysis of jetted enzymes using Circular Dichroism (CD) Spectroscopy. (A) Catalase (CAT) was jetted and immediately hydrated without VPGA treatment, and measured using CD spectroscopy, alongside native and heat-denatured CAT. (B) CD spectra were then analyzed for secondary structure contents using K2d, a neural network method.

As an alternative, we sought to use glutaraldehyde (GA) as a macromer. Vapor-phase glutaraldehyde (VPGA) treatment, a common method used in crosslinking protein-based electrospun non-woven fiber scaffolds, was used to introduce GA to the particles. Particles were jetted using a solution of 10% (w/w) protein in 90:10 H_2O:EtOH (**Figure 3.1A**). The particles, when observed under scanning electron microscopy (SEM), were spherical and smooth, and had a relatively broad size distribution (**Figure 3.1B**), with an average diameter of 113±47 nm (**Figure 3.3**). The particles were then placed in a sealed container containing a 20% (v/v) aqueous solution of GA in a reservoir (**Figure 3.1C**). GA reacts with a various of amino acid residues in proteins, but mainly with tertiary amines, such as those in Lys residues.[164] The macromer acts to hold the proteins together as a crosslinker, making them stable in aqueous environments.

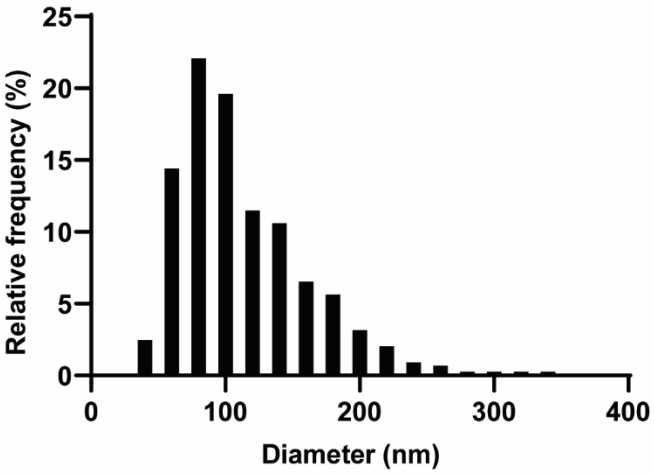

Figure 3.3 Particle size distribution of SPNPs prior to hydration. To determine size distribution, six different SEM micrographs (444 individual particles) were analyzed in MATLAB using the function imfindcircle(), and the resulting diameters converted to a frequency histogram

After VPGA treatment, the particles were immediately collected using a wet collection method, where they were scraped off the surface using a plastic razor and a PBS solution with 100 mM glycine, which reacts with any unreacted aldehydes. This quenching step is commonly used to remove any residual reactivity from GA, removing its cytotoxicity.[191,192] The particles were then size separated to narrow their size distribution using a previously developed serial centrifugation technique, where the particles went through a series of sonication, centrifugation, and decanting steps at increasing times and speeds, until the desired particle sizes were acquired.[193] After the particles were isolated, the particles were measured using dynamic light scattering (DLS), and the particles were found to have a narrow size distribution, with a z-average of 217 nm and PDI of 0.156 (**Figure 3.1D**), and have a volume swelling ratio of 7.09 (hydrated particle volume/ dry particle volume).

3.3.2 Tuning of Enzyme Activity by Loading

To study how enzyme activity would be maintained when particles were made using EHD co-jetting, two commonly used enzymes were selected. Catalase (CAT), an enzyme notable for its strong antioxidative ability, was selected as an example of an enzyme primed for therapeutics.[194] CAT exists in nearly all types of tissues and protects cells from reactive oxygen species (ROS) by rapidly catalyzing the degradation of hydrogen peroxide to water and oxygen (eqn. 2).[195]

$$2\,H_2O_2 \xrightarrow{\text{Catalase}} 2\,H_2O + O_2 \qquad [2]$$

While ROS participate in numerous physiologic processes, excessive production during acute infection, traumatic injury, hemolysis, ischemia, and reperfusion, among other pathophysiologic states can impair critical endothelial functions and result in secondary thrombosis, edema, and dysregulation of the innate immune system. ROS damage is manifested by a variety of signs, among them the exposure of various adhesion molecules such as VCAM-1 and ICAM.[196]

Glucose oxidase (GOX) was selected as an enzyme that is already in use in various industries. GOX is naturally produced by certain species of fungi and insects, and catalyzes the oxidation of β-D-glucose to D-glucono-δ-lactone and hydrogen peroxide (eqn. 3).[197]

$$O_2 + \text{ß-D-Glucose} \xrightarrow[\text{Oxidase}]{\text{Glucose}} \text{D-glucono-}\delta\text{-lactone} + H_2O_2 \qquad [3]$$

In nature, GOX acts as an anti-bacterial agent by producing hydrogen peroxide, but is now widely used in many sectors of society, such as the food industry, dairy production, preservatives, and in glucose meters.[197]

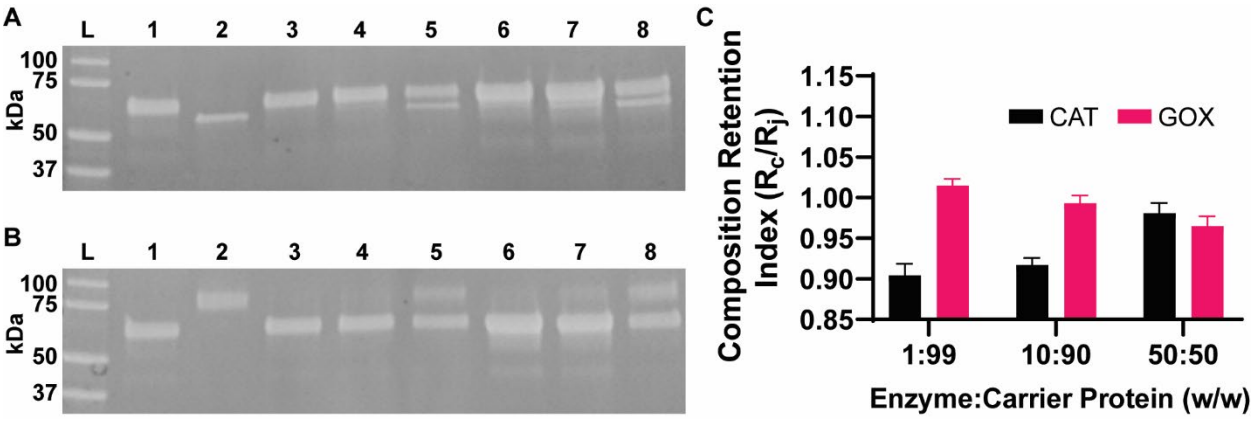

Figure 3.4 The mass of proteins that are loaded during synthesis are similar to the resulting mass in the particles. Mixtures of proteins at various mass ratios, either Human Serum Albumin (HSA) and Catalase (CAT) or HSA and Glucose Oxidase (GOX), were made, and then either used as is (control) , or jetted and collected (Jetted). (A-B) The samples were then analyzed using SDS-PAGE gel electrophoresis. The lanes are as follows: **L:** Ladder, **1:** HSA, **2:** Enz, **3:** Control, Enz:HSA-1:99 , **4:** Control, Enz:HSA -10:90, **5:** Control, Enz:HSA -50:50, **6:** Jetted, Enz:HSA -1:99 , **7:** Jetted, Enz:HSA -10:90, **8:** Jetted, Enz:HSA -50:50, where Enz is CAT for (A) and GOX for (B). (C)The SDS-PAGE was the analyzed using ImageJ, where the intensity ratio between the enzyme band and HSA band for each lane was calculated, and then a ratio calculated between the control ratio and the jetted ratio, termed the composition retention index. Values close to 1 are defined as the control and jetted samples being similar to each other. All tested ratios were within the range of 1.

The activity of each of the above enzymes was studied by modulating the ratio of each enzyme and a carrier protein, HSA, on a weight by weight basis. The protein ratio in the particles was confirmed by collecting the particles prior to crosslinking and checking their relative intensities by running the collected proteins on an SDS-PAGE gel stained with Coomassie Blue (**Figure 3.4**). SPNPs at a variety of enzyme ratios were synthesized and assayed. The particle masses were normalized to maintain the amount of enzyme loaded in the reaction solutions. It was found that in both GOX and CAT SPNPs, the retained activity of the enzymes in the particles decreased as more enzyme was loaded into the particles going from 84.8±6.4% to 31.3±0.3 % activity retention for CAT and 55.9±0.9% to 22.0±0.9% for GOX when they were loaded at a 5:95 Enzyme:HSA ratio compared to a 50:50 ratio (**Figure 3.5A**). This effect was to be expected, as it is generally accepted that when enzymes are immobilized, numerous different factors, such as

steric hinderance between enzymes and diffusion limitations, can result in decreased activity retentions.[176,198] A brief geometric analysis, described in **Appendix A**, shows how both enzymes could quite easily be diffusion limited in their SPNP form, though to date no studies have been performed testing this hypothesis.

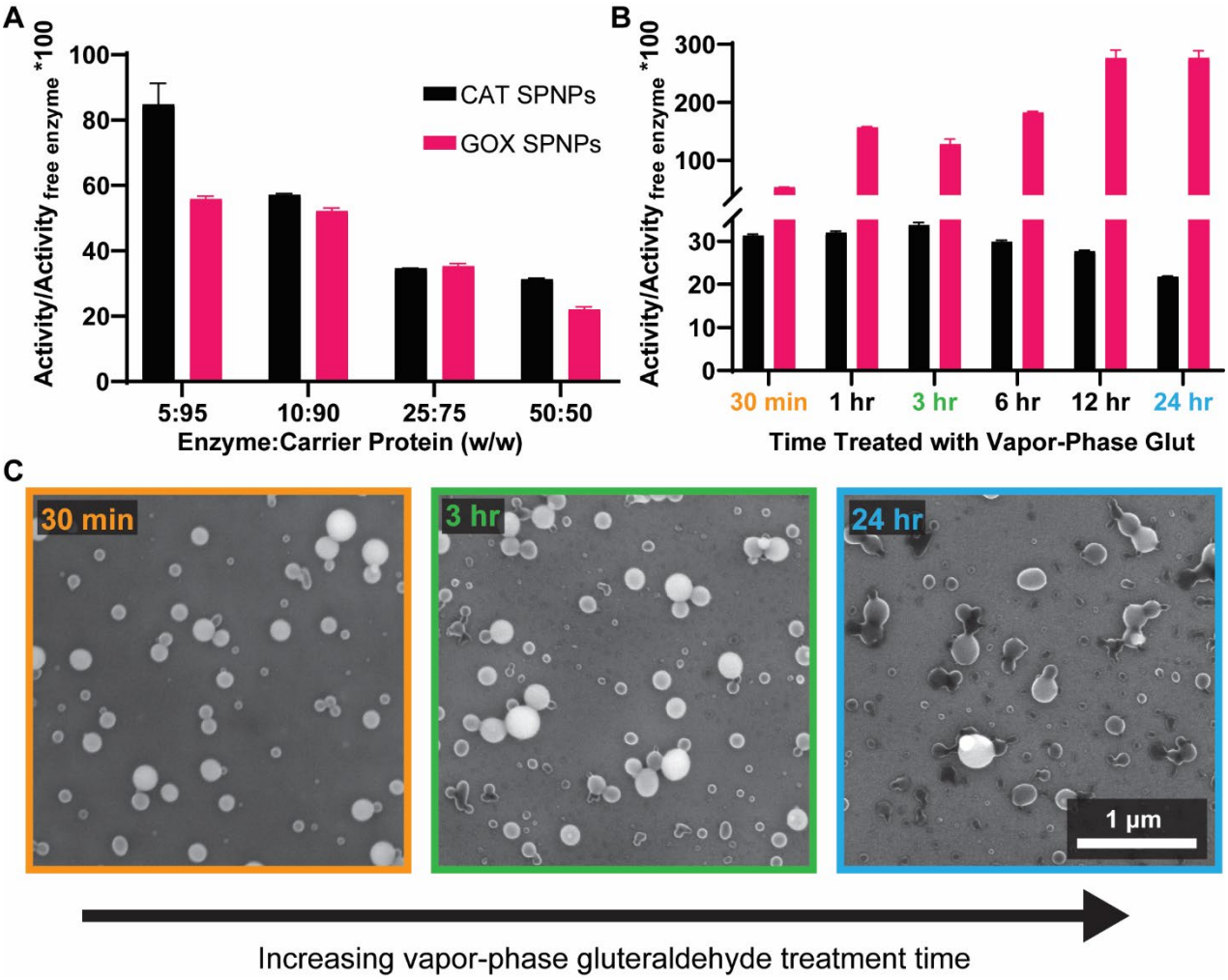

Figure 3.5 Effect of loading ratio and glutaraldehyde treatment time on enzyme activity and particle morphology. (a) The retained activity of enzyme loaded SPNPs is dependent on the loading ratio of enzyme to carrier protein. (b) Effects of vapor phase glutaraldehyde treatment time. When reacted for different amounts of time, both (b) the retained activities and (c) morphologies of the resulting particles are affected.

3.3.3 Tuning of Enzyme Activity by GA Treatment Time

To study how the VPGA treatment time would affect the retained activities of the enzymes, particles were treated with GA for various times, ranging from 30 minutes to 24 hours, and then collected and size separated. It was observed that particles fused together and lost much of their spherical morphology as they were treated for longer time periods (**Figure 3.5C**). However, in terms of activity retention, the two enzymes gave very different results. CAT SPNPs loaded at a 50:50 ratio had decreasing retained activity with longer treatment, going from 31.3±0.3% at a 30-minute treatment time to 22.0±0.9% for a 24-hour treatment time. For GOX SPNPs, not only was the opposite trend observed, but the unexpected result of enhanced activity was observed. As treatment time of GOX particles loaded at a 10:90 ratio increased from 30 minutes to 24 hours, the retained activity of the particles increased from 53.8±0.3% to 276.8±12.0% (**Figure 3.5B**).

The increase of activity as the GOX SPNPs were treated for longer periods of time with glutaraldehyde was surprising, but enzymes having increased activity after immobilization in different conditions has previously been reported in multiple studies,[199–202] and is theorized to occur for a variety of situation specific reasons, ranging from increased diffusion of substrate (substrate sponge effect), immobilization resulting in enzyme conformations with higher reaction rates, to the immobilization of the enzyme leading to advantageous thermodynamic reaction conditions.[203] The reason for the discrepancy between the two enzymes, or the increased activity observed as a function of VPGA treatment time may be due to the difference in size and complexity of the two enzymes, as CAT is an a 250kDa tetrameric complex, with each subunit containing an iron, while GOX is a smaller 160 kDa dimer and thus would be less impacted, and possibly even stabilized, by sterics.

Still, there could be several potential concerns with this study. If we were measuring enzyme activity in a non-linear region, that may explain the results. Also, the assay used to measure the GOX does not directly measure GOX activity, but rather a secondary cascade reaction made by Horseradish Peroxidase (HRP), which uses the H_2O_2 produced by GOX to oxidize a detector molecule, resulting a measurable change in A_{570nm}. This reaction has a linear region, where A_{570nm} increases in a linear fashion, and a subsequent non-linear region where the absorbance decreases. If a sample of measured GOX has activity over a certain threshold, it might seem like the enzyme is less active than it actually is, if the A_{570nm} is measured in endpoint mode (at the start of the reaction and then after a set time), as absorbance may quickly increase, and then decrease once the reaction enters the non-linear phase. We are sure that this did not happen, as the reaction was followed in kinetic mode, and all measurements used were from the linear region of the reactions.

To avoid false activity measurements due to variations in the assay, we only used kits from a single production batch. Additionally, the SPNPs that were treated for 30 minutes, which were used in subsequent experiments, gave very consistent measurements over a 6-month period, using various different kits, across different batches of particles, and in different experiments. Additionally, scattering of the nanoparticles themselves might interfere with the measurements, but when controls using SPNPs containing only HSA were measured, there was no signal at A_{570nm}. These results were confirmed for particle concentrations ranging over five orders of magnitude.

Last, incorrect particle concentrations could account for the unexpected results. The concentrations of the SPNPs were measured using a BCA assay, which is a protein assay that measures a color change that is dependent on the concentration of proteins in a particular solution. As the activity assays are highly dependent on accurate measurements of SPNP concentration, if the glutaraldehyde treatment time affects the readings of the BCA assay, it may lead to higher

readings. However, glutaraldehyde does not change the peptide backbone in proteins, and thus there is no reason to think that the protein modifications caused by the aldehyde reactions would change the BCA results. In addition, if there was an effect coming from incorrect mass measurements, we would have observed noticeable discrepancies between the yields of particles made with different treatment times. The particles measured were always from a single large batch of jetted particles that were then randomly split and treated for different time periods. With this in mind, no differences in yields were observed.

An additional experiment that may further elucidate the reasons behind the observed trends may be to measure GOX activity using a direct measurement of the enzyme products, as was done with CAT. These would involve either measuring oxygen consumption in the reaction by measuring pressure changes or measuring the produced D-glucono-δ-lactone by titration, as the molecule is acidic. By simplifying the measurements by removing the secondary enzyme reaction, it might explain the observed results.

3.3.4 Activity Retention of SPNPs In Different Temperature Conditions and Over Time

Key to medical applications is how therapeutics maintain their activities not just under physiological conditions, but also in pathological conditions and during long term storage. To investigate these factors, particle activity was found to be consistent over a 2 week period for SPNPs stored at room temperature or at 4 °C. Particles were also incubated for various amounts of time at 40 °C, which is representative of the temperature of a patient with a high fever. It was found that the particles maintained 82±9% and 78±2% of their initial activities after being in 40 °C for 20 minutes, for CAT and GOX SPNPs respectively. CAT SPNPs were able to maintain their activity much better than free CAT, which only maintained 47±0.2% of its initial activity. GOX, on the other hand, behaved differently, as the free enzyme lost none of its initial activity.

This was to be expected, as the working temperatures of GOX are both higher and broader than CAT, although why the activity of GOX in particle form dropped remains to be explained. (**Figure 3.6**).

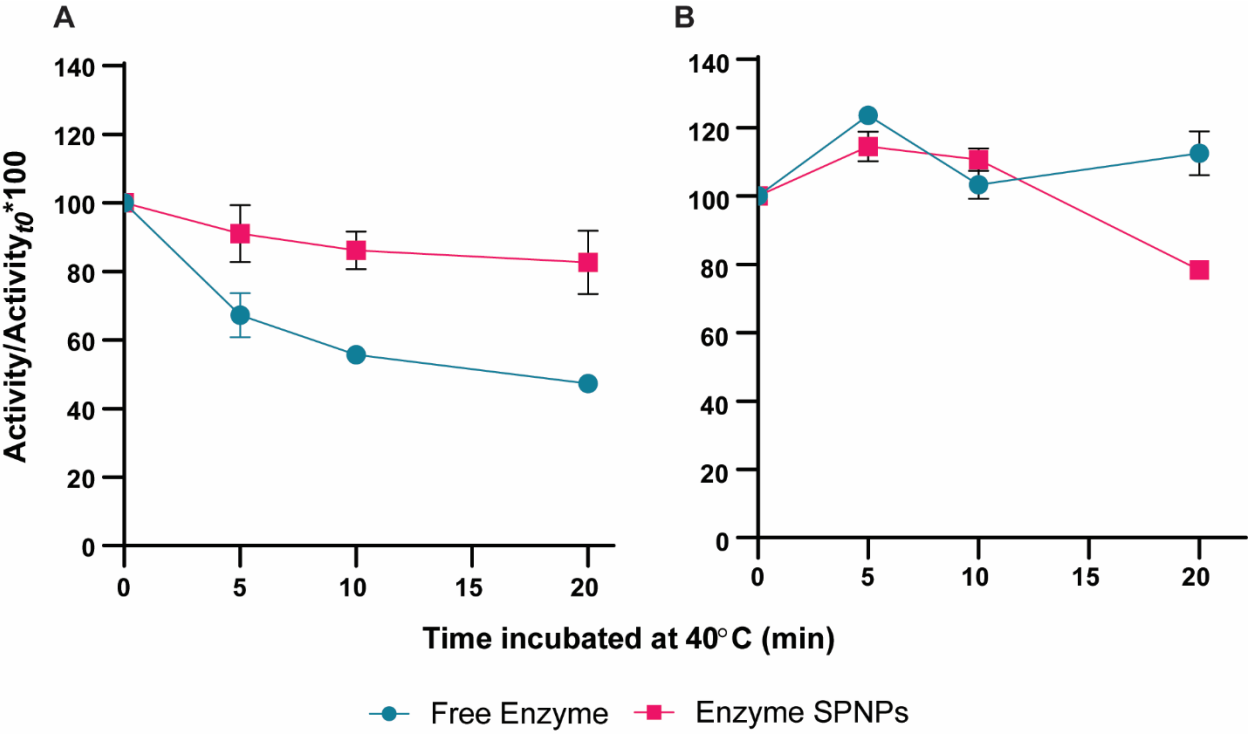

Figure 3.6 Enzyme loaded SPNP Activity Retention. (A) CAT and (B) GOX SPNPs and their free enzyme controls were exposed to 40 °C for varying amounts of time.

3.3.5 Using SPNPs to Protect Cells from Oxidative Damage

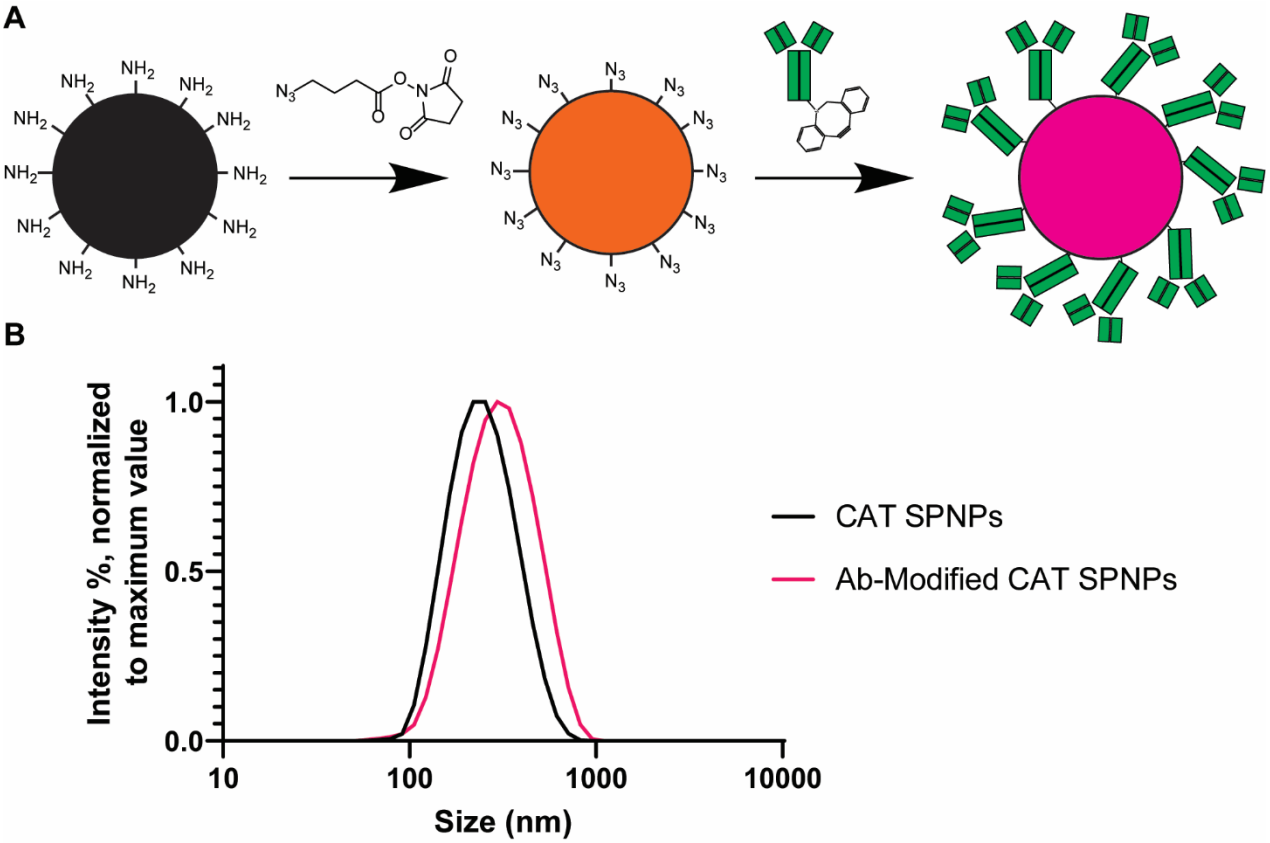

Figure 3.7 CAT SPNPs were Antibody (Ab) modified. (A) CAT SPNPs were surface modified by first reacting the proteins' surface amine groups with NHS-N_3, and subsequently reacting the resulting N_3 with DBCO modified Abs. (B) There was a measured size increase between the initial CAT SPNPs and the Ab-modified CAT SPNPs, using DLS.

As a potential use case for enzymatic SPNPs in medicine, we next sought to show how CAT SPNPs could be used to target endothelial cells and protect them from ROS damage. CAT SPNPs made using a 50:50 CAT:HSA ratio were synthesized as previously described using a 30-minute VPGA time, and subsequently surface modified using two sequential reactions. First azidobutyric acid NHS ester was incubated with the particles overnight at 4 °C to functionalize the SPNP surfaces with azides. The particles were then incubated overnight at 4 °C with antibodies functionalized with dibenzocyclooctyne (DBCO) to perform a copper-free click reaction with the azides on the particle surface. This reaction resulted in an increase of z-average of around 30 nm

from the unmodified CAT SPNPs to the antibody modified CAT SPNPs (**Figure 3.7**), and a very small decrease in zeta potential of 0.3 mV, measured using electrophoretic light scattering (going from -8.3 mV to -8.6 mV). These size and zeta potential differences were consistently seen when particles were modified with the various antibodies used.

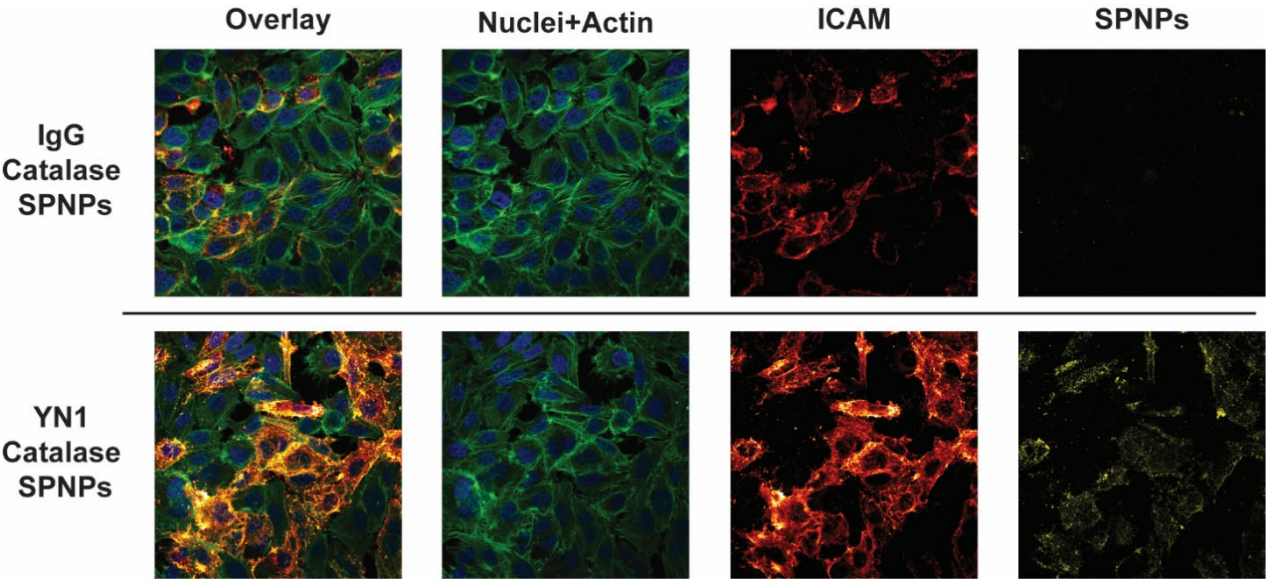

Figure 3.8 Binding of Antibody targeted enzyme loaded SPNP. Catalase loaded SPNPs were surface modified with anti-ICAM antibodies and given to a co-culture of ICAM expressing (ICAM+)/Wild-Type (WT) REN cells, and loaded with BSA-Alexa-647 to allow for fluorescent visualization. After a 30-minute incubation period, the cells were washed and stained with DAPI to cell nuclei (blue), Alexa 488 Phalloidin to actin (green), and an anti-ICAM antibody with an Alexa-555 secondary stain (red).

The selective targeting and protective potential of antibody targeted CAT SPNPs was first studied in a model *in vitro* system. REN cells, a human mesothelioma cell line, were genetically modified to express ICAM on their surface as previously reported.[204] To confirm high specificity of the antibodies, confocal microscopy was used on a co-culture of ICAM/WT REN cells treated with either non-specific IgG antibodies, or anti-ICAM YN1 rat antibodies, which were additionally loaded with fluorescent Bovine Serum Albumin. High particle uptake was only observed in cells staining positive for ICAM expression (**Figure 3.8**). Protective potential was then tested by

incubation with YN1 or IgG CAT SPNPs (**Figure 3.9**). After a 30-minute incubation period, the cells were washed and treated with 10 mM H_2O_2. The viability of the cells after the treatment was then measured, and it was found that the YN1 targeted nanoparticles were able to specifically protect up about 80% of ICAM-expressing cells, while non-specific controls provided no significant effect (**Figure 3.10**).

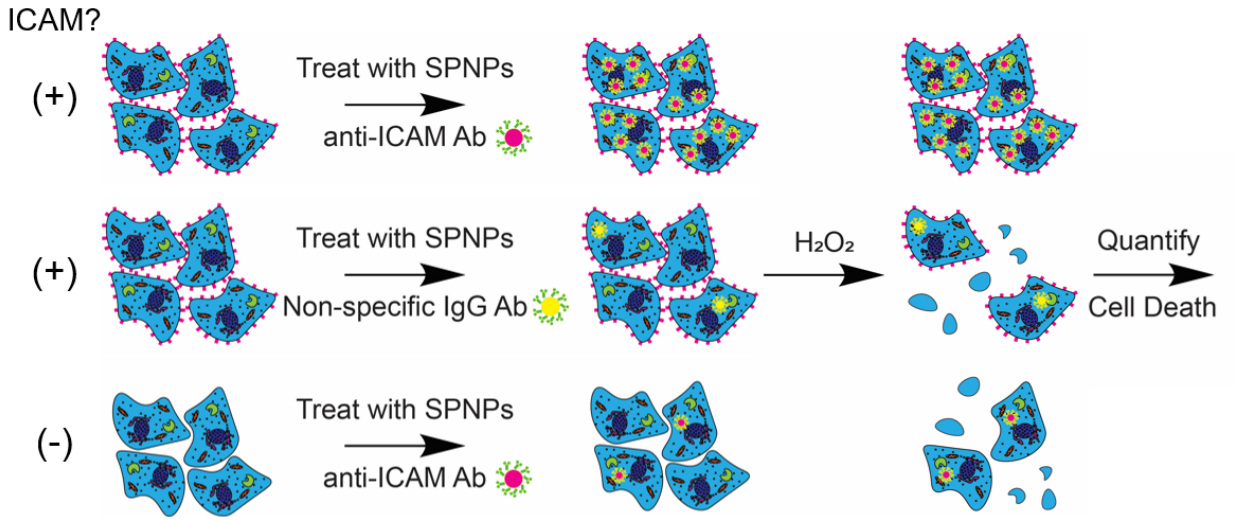

Figure 3.9 Cells were treated with various antibody modified CAT SPNPs to analyze them for their potential to protect cells from ROS.

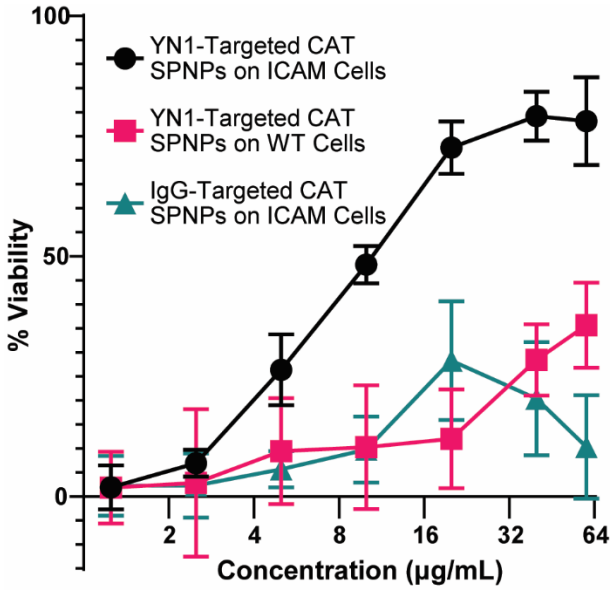

Figure 3.10 Targeted enzyme loaded SPNPs protect cells from ROS damage. ICAM expressing or WT REN cells were treated with Ab or IgG CAT SPNPs and exposed to 10 mM H_2O_2. Viability was then determined by measuring LDH released into the cell media as a marker of cell death, as compared to untreated cells.

Protection of cells in an *in vitro* inflammatory disease model was then investigated to better mimic clinical application. HUVEC cells were first treated with TNF-α to mimic an inflammatory pathology. TNF-α was used to induce expression of ICAM on the surface of the cells.[205] CAT SPNPs modified with R6.5, a human anti-ICAM, or IgG antibodies were then given to the cells. The cells were treated with H_2O_2 as previously described, and it was found that the particles were able to protect the 90% of cells, while non-specific and carrier controls had less effect, 70% and 35% protection, respectively (**Figure 3.11**). The ability of the SPNPs to specifically protect targeted cells and the retention of the enzymatic therapeutic activity shows the potential for these particles to be used as enzyme delivery vehicles.

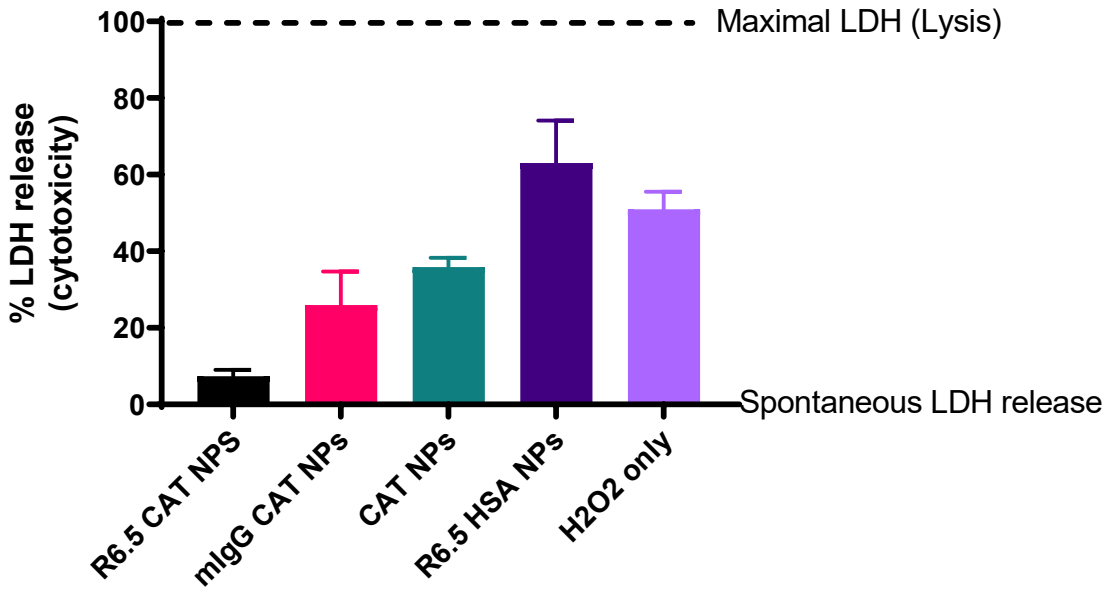

Figure 3.11 Protection of human primary cells in an inflammatory disease model. HUVECs were treated with TNF-α to mimic an inflammatory environment. Cells were then treated with Ab, IgG, or unmodified CAT SPNPs, along with an Ab carrier control for 30 minutes and then challenged with 10 mM H_2O_2. Cell viability was assayed by measuring LDH released.

3.3.6 Bicompartmental Enzyme Loaded SPNPs

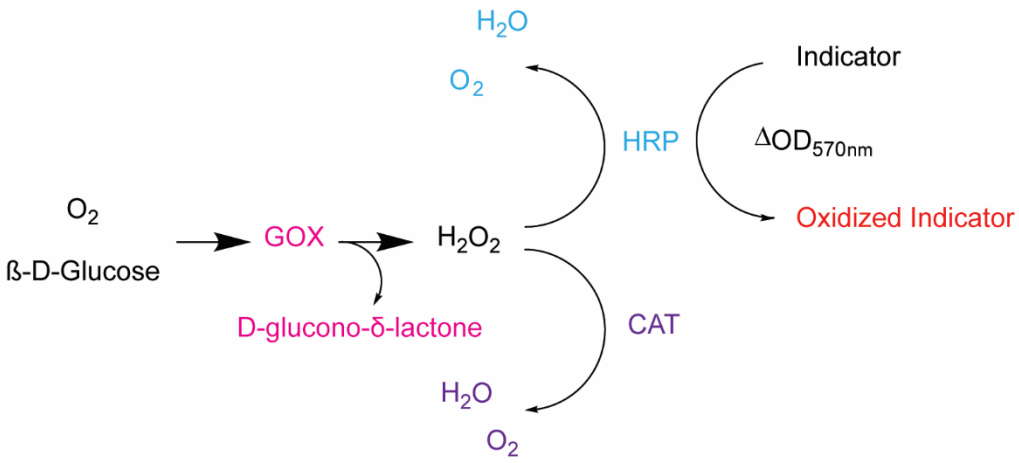

Figure 3.12 Enzymatic cascade model of GOX CAT and HRP. The two-step system has HRP consume the H_2O_2 produced by GOX, producing a color change in an indicator molecule. H_2O_2 can be scavenged by CAT when present, reducing the color change in the reaction.

There is strong interest in the biotechnology space for improving the efficiencies of enzymatic chemical reactions. One of the proposed methods to improve reactions is through the use of compartmentalized enzymes.[206] GOX and CAT are commonly used to study cascade enzymatic reactions, as the hydrogen peroxide produced by GOX is the substrate for CAT. Thus, the same assay used to measure GOX previously was adapted to measure the synergy between the enzymes when loaded in SPNPs (**Figure 3.12**).

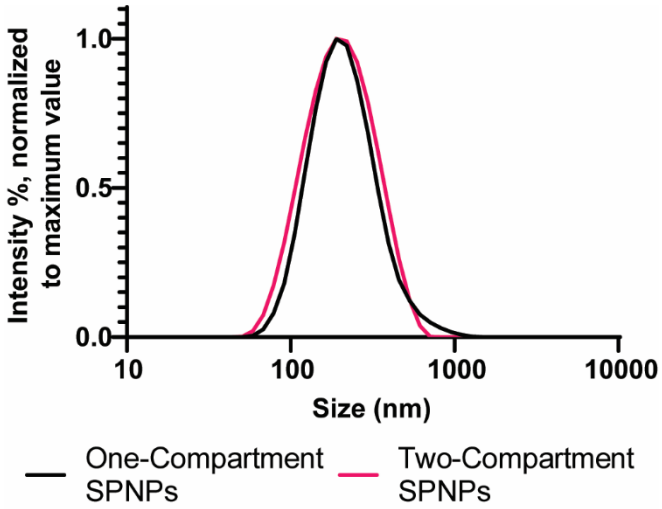

Figure 3.13 One and two compartment SPNPs have similar size distributions. Particles made using EHD co-jetting have similar size distributions, whether they are made with one or two compartments, as measured using DLS.

To showcase how synergistic enzymes could be loaded in anisotropic (bicompartmental) versions of the particles, SPNPs loaded with GOX in one compartment, and CAT in the other (GOX:CAT SPNPs) were synthesized using a parallel capillary system (**Figure 3.14A**).[115,122] Once size segregated, the anisotropic SPNPs had a similar size distribution as single compartment particles (**Figure 3.13**). The activity of GOX SPNPs and GOX:CAT SPNPs with the same amount of active GOX was measured, and there was a clear decrease in the change of absorbance when CAT was added (**Figure 3.14B**). This is the result that would be expected in a when a particle system containing GOX and CAT is present. The assay normally functions by having HRP use the

H_2O_2 produced by GOX to oxidize AbRed, a colorimetric detector molecule. When a portion of the H_2O_2 is consumed by CAT, a decreased amount of absorbance is observed, when compared to a particle system only containing GOX. These proof of concept results show the ability to load two enzymes in two compartment SPNPs, and further studies are planned to study possible synergistic effects of compartmentalizing enzymes in SPNPs.

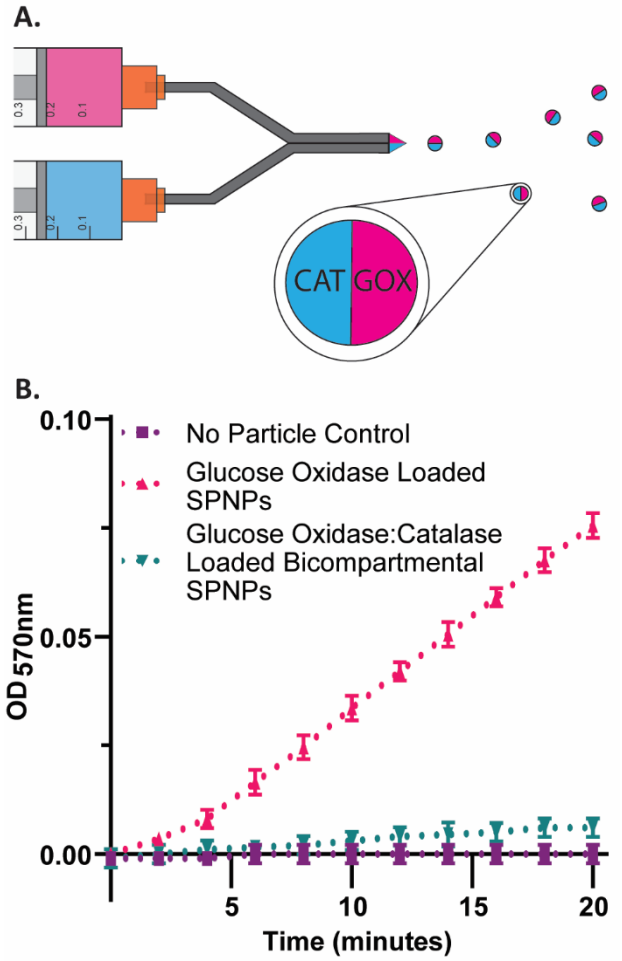

Figure 3.14 Two compartment enzymatic cascade SPNPs. (A) Two compartment SPNPs were synthesized using EHD co-jetting, resulting in particles with GOX in one compartment, and CAT in the other. (B) When placed in a reaction buffer containing HRP, Glucose, and a colorimetric indicator, the H_2O_2 produced by GOX was partially scavenged by CAT in the two compartment particles, leading to a reduced color change compared to single enzyme with equivalent amounts of GOX.

3.4 Summary

In this study, we report the development of a method to synthesize enzyme-loaded Synthetic Protein Nanoparticles (SPNPs). We show how two different proof-of-concept enzymes can be loaded into the particles at a variety of loading ratios, and how by changing the synthesis conditions, we can modulate the retained activities of the loaded enzymes. It was also shown how enzymatic particles could be targeted to specific cells using antibodies, and a small study was conducted to show the effectiveness of Catalase loaded SPNPs in protecting endothelial cells from reactive oxygen species damage. Notably, we were also able to show how two compartment particles, each loaded with a different enzyme, were able to conduct a cascade enzymatic reaction. While these experiments were all designed as proof-of-concept studies of enzyme loaded SPNPs, they all show the potential of these particles for a variety of potential applications in medicine.

Chapter 4

Characterization of Synthetic Protein Nanoparticles with Electrokinetic Microfluidics

Part of the material for this chapter has been adapted with modifications from the following publication:

1. D. F. Quevedo, C. J. Lentz, A. Coll de Peña, Y. Hernandez, N. Habibi, R. Miki, J. Lahann, and B. H. Lapizco-Encinas "Electrokinetic Characterization of Anisotropic Synthetic Protein Nanoparticles" *Beilstein Journal of Nanotechnology,* Under Review, 2020.

4.1 Background and Motivation

Over the past thirty years, nanoparticles have been developed for a broad variety of scientific applications, ranging from medical imaging to drug delivery and enzyme immobilization to industrial processes.[207,208] An emerging sector in nanotechnology has been the development of nanoparticles composed primarily of proteins.[209] Proteins have multiple desirable characteristics for use as the main material components of nanoparticles: they are biodegradable, naturally involved in biological molecule targeting, and are "smart" materials that can respond to various environmental cues such as pH, temperature, or target binding.[210] Protein nanoparticles (PNPs) have proven useful for the loading of active therapeutic enzymes and show promise as vaccines.[91,139] Using protein engineering techniques, there has also been significant advances in

self-assembled PNPs.[211,212] PNPs have successfully reached the clinic, with nab-paclitaxel (Abraxane®), a PNP made of Human Serum Albumin, being used for the treatment of metastatic breast cancer, non-small cell lung cancer, and pancreatic adenocarcinomas.[213] While current technologies allow for the synthesis of smart PNPs that release their active enzymatic payloads in oxidative environments,[91] a next step in further developing smart protein nanoparticle technologies is to develop a scalable method for producing sub-compartments within particles. By localizing proteins at the nanoscale, PNPs could have further applications in controlled release and delivery of therapeutics, theragnostics, and enzymatic cascades.[214]

Although previously developed methods to produce PNPs, such as coacervation,[139] self-assembly,[215] and pressure driven techniques,[216] allow for intraparticle spatial control of material composition through layer by layer techniques, no previous synthetic schemes are able to synthesize anisotropic protein nanoparticles with distinct hemispheres. To address this unmet need, we have adapted EHD co-jetting techniques, previously established by the Lahann lab, to create single-compartment and multicompartmental (i.e. anisotropic) synthetic protein nanoparticles (SPNPs and ASPNPs) that can be easily made from a variety of proteins.[119] A recent publication showcases how this versatile technique can be used to create particles that have significant potential as therapeutics, in particular their ability to treat glioblastoma.[169] To transition the promising results of these particles into the clinic, high-throughput purification and characterization techniques that are specific for anisotropic particles need to be developed.

In the last decade, the area of microfluidics, the field of science that studies the manipulation of minute volumes of fluids (microliters to picoliters),[217] has experienced a significant growth in bioanalytical applications.[217,218] Electrokinetics (EK) and electric-field driven processes are suitable for a wide range of applications due to their simplicity and robustness.

An applied electric potential can be used for both manipulating a bioparticle and its surrounding liquid, as electroosmotic (EO) flow can allow for "on the fly" dynamic flow re-direction within a device for further collection and analysis.[219] Both AC and DC electric potentials can be used to exploit differences in specific bioparticle properties, such as electrical charge, size, shape and polarizability.[220,221] An important fraction of miniaturized EK devices employ a combination of electrophoresis (EP), dielectrophoresis (DEP) and EO flow effects,[222] allowing for additional parameters to fine-tune a separation process. Particle characterization and manipulation with EK techniques offer the potential for developing novel separation schemes for the sorting and enrichment of bioparticles of interest. Furthermore, it has been shown that nonlinear EK effects, such as EP of the second kind,[223,224] are very effective mechanisms for controlling particle migration within microdevices. An advantageous strategy for enhancing nonlinear EK effects on particles is to use insulator-based EK devices, where insulating structures distort the electric field distribution generating regions within the device of higher electric field strength.[225] These are simple devices, usually made from a single substrate, making microscale EK methods promising for high-throughput purification applications. Furthermore, a recent development was the universal design parameter, the electrokinetic equilibrium condition (E_{EEC}) reported by Coll De Peña et al.,[225] that only depends on physical particle characteristics and can optimize the design of EK separations. E_{EEC}, as a unique particle-dependent parameter, can predict the required particle trapping voltages in any insulator-based EK device.

Microscale EK can be used to manipulate particles across size scales,[226] from proteins,[227–229] to viruses, [230] to cells,[231,232] to parasites.[233] Traditionally, these type of microscale studies were labeled as DEP methods, although more recently it has been reported that the major phenomena controlling particles in these systems was EP of the second kind.[225,234] DEP for the manipulation

of proteins was first reported in 1994 by Washizu et al.[235] via dielectrophoresis chromatography. Since then, other studies have demonstrated the potential of DEP for the manipulation of macromolecules.[236–238] However, microscale EK techniques for proteins are still developing. The Ros research group has reported both the trapping and streaming of protein particles employing devices with micro and nano insulating posts[228,239–241] as well as the sorting of protein nanocrystals with streaming insulator-based DEP.[242–244] The Swami and Chou groups have studied the enrichment of protein particles under conditions of high conductivity media employing devices with nano-gaps and reported both positive DEP and negative DEP.[227,245–247] Other studies have employed triangular insulating posts with nanogaps,[248] cylindrical insulating structures to enrich BSA particles,[249] or diamond-shaped post to separate PEGylated ribonuclease A from non-PEGylated molecules.[250]

The potential advantages of using microscale EK techniques with insulating structures include ease of manufacture and high-throughput parallel processing, making EK methods a key candidate for use in purifying SPNPs for clinical applications. Besides exploiting size differences, microscale EK techniques can also exploit differences in both electrical charge and dielectric properties, making them uniquely suited to process and purify SPNPs. EK techniques could also be used to differentiate between SPNPs and ASPNPs, since the anisotropic particles, whose polar ends have different properties, should have different behavior in the microdevices compared to their single compartment counterparts. In this work, we present the characterization of electrohydrodynamic (EHD) co-jetting synthesized SPNPs in a custom-built system, as well as the application of EK techniques to characterize SPNPs made of Bovine Serum Albumin (BSA) and Lysozyme. Two types of particles were synthesized: particles that were homogenous blends of proteins, and anisotropic particles. A total of eight distinct types of SPNPs were electrokinetically

characterized. The results illustrated that particle composition strongly influences the voltage at which SPNPs will trap in an insulator-based EK device. Moreover, homogeneous particles with a higher content of BSA showed lower trapping voltages. The results also indicated that particle anisotropy plays an important role in determining trapping voltage, as 50:50 homogeneous SPNPs required a much lower trapping voltage than 50:50 anisotropic SPNPs. All eight particle samples were characterized in terms of their electrophoretic mobilities, linear and nonlinear, and in terms of their E_{EEC}. These measurements expand the approach of using E_{EEC} to characterize nanoparticles and allow for the accurate prediction of SPNPs behavior in any EK device. The results obtained here shed light on the great potential of the use of insulator-based EK devices for the analysis and purification of protein nanoparticles.

4.2 Methods

4.2.1 Nanoparticle Synthesis, Purification and Characterization

Particles were synthesized using the EHD co-jetting method. The protein(s) of interest and 2kDa NHS-PEG-NHS copolymer were dissolved at 10% w/v and 1% w/v, respectively, in a 90:10 (ultra-pure H_2O:EtOH) solution. They were subsequently flown through a syringe at a rate of 0.1 mL/hr, and a voltage was applied between the needle and collecting surface to produce a Taylor cone. The voltage caused the droplet to be pulled towards the collecting substrate and subsequently break up into the nanometer sized spheres. In mid-flight, the solvents rapidly evaporate to form the solid nanoparticles. For bicompartmental particles, the needles were placed in a parallel configuration to create a laminar flow at their ends, as described previously, and all other conditions were identical. For the polycondensation reaction, where the NHS groups in the PEG copolymer react with lysine groups in the proteins, the nanoparticles were placed in a dry 37 °C

oven for 7 days. All SPNP synthesis reagents were purchased from Sigma Aldrich and Fisher Scientific.

After polycondensation, the particles were collected by scraping them off the collecting surface using a solution of Ultrapure H_2O + 0.01% Tween 20. The collected solution was then sonicated on ice, run through a Falcon 40 μm cell filter (Fisher Scientific), and then centrifuged at 3,200 RCF for 5 minutes to remove large particles. The resulting supernatant was then centrifuged at 21,130 RCF for 40 minutes to collect the desired particles.

Particles, in their dry state, were imaged using SEM to analyze their shape. To determine their hydrodynamic size distribution after being hydrated, the particles were suspended in Ultrapure H_2O + 0.01% Tween 20, sonicated on ice, and measured with dynamic light scattering (Malvern ZSP ZEN-5600), using standard settings. An average of at least three measurements are reported. Particle zeta potential was measured on the same instrument using a disposable folded capillary cell (DTS1070, Malvern) and using standard settings. Protein concentration was measured using a Pierce BCA assay using a BSA standard for the standard curve. Particle fluorescence was confirmed using a Leica DMi8 inverted microscope (Wetzlar, Germany) that was paired with a Leica DFC7000 T camera and the software LASX provided by the manufacturer.

4.2.2 Microdevice Fabrication

Microchannels with oval-shaped insulating posts (**Figure 4.1**) were made from polydimethylsiloxane (PDMS) employing standard soft lithography techniques. To create a device, PDMS (Dow Corning, Midland, MI) was cast onto a negative replica mold made with a silicon wafer (Silicon Inc., Boise, ID) and SU-8 3050 photoresist (MicroChem, Newton MA). After curing, the PDMS slab was sealed with a PDMS-coated glass wafer using a corona wand (Electro Technic Products, Chicago, IL), creating microchannels where all internal surfaces are

PDMS and have same wall zeta potential (ζ_W), ensuring consistent EOF. The microchannels were 10.16 mm long, 0.88 mm wide, 40 µm deep and contained one inlet and one outlet liquid reservoir.

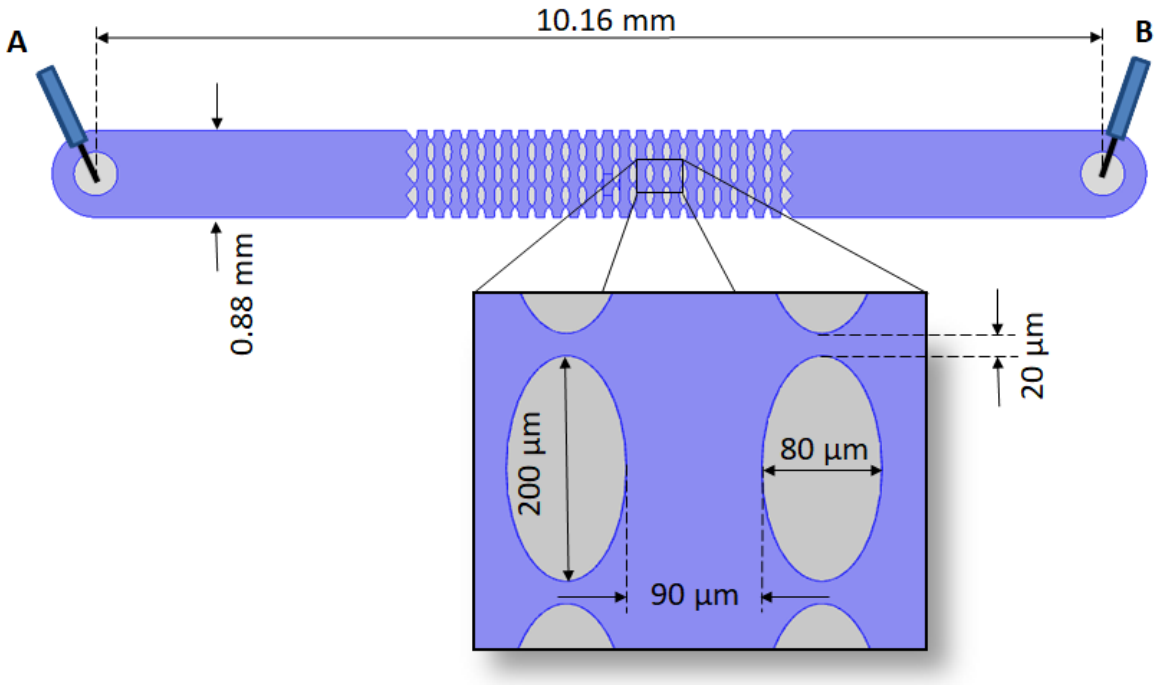

Figure 4.1 Schematic representation, with dimensions, of the iDEP device used in this study depicting the dimensions of the channels and the insulating posts.

4.2.3 Microfluidics Experimentation

Before placement in the microfluidic device, fully characterized SPNPs were pelleted by centrifugation at 21,130 RCF for 40 minutes and suspended at 2.5 mg/mL in Ultrapure H_2O + 0.01% Tween 20. Particles were then diluted to 250 µg/mL in the same suspending media used to fill the device (K_2HPO_4 buffer with a pH of 6.16 and a conductivity of 21.3 µS/cm, supplemented with 0.05% Tween 20) and subsequently sonicated to break up particle aggregates. A sample of suspended SPNPs (1-5 µL) was injected into a device before electrodes were inserted and the pressure was equalized. In order to determine the trapping voltage of one particular type of SPNP, a range of increasing voltages were tried on a single sample until particle trapping in the form of

bands was observed, such as the bands seen in **Figure 4.3c** and **Figure 4.3d**. Once this approximate trapping voltage was found, a new channel and sample was used to test voltages at and below the approximate trapping voltage. With the new sample, each time a new voltage was applied, the system was returned to neutral pressure, and voltages were decreased by 100 V increments until a smooth trapping band was no longer observed.

4.3 Results and Discussion

4.3.1 Synthetic Protein Nanoparticle Synthesis and Characterization

SPNPs were synthesized using a modification of the well-established technique of EHD co-jetting.[115,122,251] Generally, SPNP fabrication starts by dissolving a protein of interest and macromer of choice into a co-solvent system of water and an organic solvent, such as ethanol or ethylene glycol.[169] The mixture is then ejected through a small gauge needle toward a collecting surface. A high voltage (kV range) is placed between the needle and the collecting surface, which leads to the formation of a Taylor cone in the droplet of solution at the end of the needle. At the tip of the Taylor cone, the fluid jet breaks and nanoparticles are formed (**Figure 4.2A**). EHD co-jetting builds off electrospraying by incorporating a second parallel syringe to create multicompartmental, or anisotropic, structures. With the use of varying device designs and synthetic parameters, a variety of different particle and fiber architectures can be made.[123,252]

Bovine Serum Albumin (BSA) SPNPs were synthesized using EHD co-jetting, with BSA as the protein and a macromer composed of poly(ethylene glycol) (PEG, 2 kDa) terminally bifunctionalized with N-hydroxylsuccinimide esters (NHS) as the copolymer. The NHS esters react with the lysine groups in BSA to polymerize into insoluble SPNPs. The SPNPs were of uniform shape when imaged using scanning electron microscopy (SEM). We further analyzed the size distribution of the particles using ImageJ software and found that the particles had an average

diameter of 299±128 nm (**Figure 4.2B**). The particles were subsequently collected and suspended in buffer, leading to hydration. The average particle diameters had increased to 356±190 nm when measured using dynamic light scattering (DLS). The size distributions found by SEM and DLS were similar to those previously found with EHD jetting.[253] The size difference between the SEM and DLS measurements was a result of the particles solvation state, as they swell in water.

To test the potential of EK microfluidics as a high-throughput SPNP purification technique, a way to visualize our particles using fluorescent microscopy was needed. To achieve this, we incorporated commercially available Alexa Fluor dyes conjugated to BSA as fluorescent markers at 0.8% (w/w) of total protein into the initial electrospraying solution. After the purification steps described previously, we were able to clearly observe particles under typical microscopy conditions (**Figure 4.2C**).

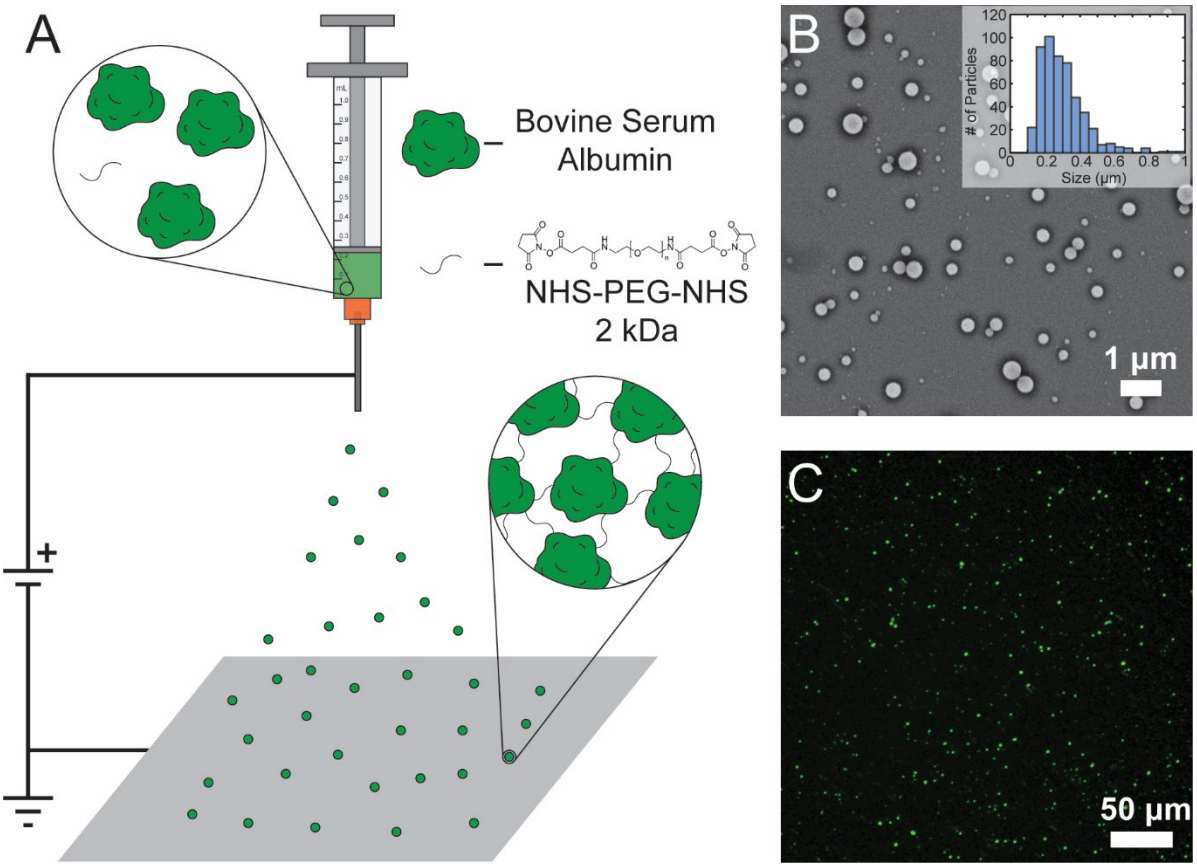

Figure 4.2 Fabrication process of Synthetic Protein Nanoparticles (SPNPs). (A) Representation of the electrohydrodynamic co-jetting process. (B) SEM image demonstrating the morphology of the SPNPs as synthesized, (C) Image of SPNPs loaded with BSA-Alexa 488 to make them visible for characterization through microscale electrokinetic experimentation. Fluorescence was confirmed using a fluorescent microscope.

4.3.2 Effect of Size Differences and Fluorescent Dyes

For potential applications in theragnostics where fluorescent markers in the particles could be needed, we were interested in first investigating whether the incorporation of different fluorescent dyes in our particles would affect the particle behavior in EK microfluidics. Thus, we synthesized BSA SPNPs loaded with Alexa Fluor-488 (SPNP-BSA-488) or Alexa Fluor-555 (SPNP-BSA-555) and explored their behavior in an EK device. The resulting particles were fully characterized, and it was found that the SPNP-BSA-488 and SPNP-BSA-555 had hydrodynamic diameters of 373±180 nm and 356±190 nm, respectively (**Figure 4.3A**). The zeta potentials of the

SPNPs (ζ_p) were also measured in a K_2HPO_4 buffer, which was the same buffer used in EK experiments, using electrophoretic light scattering and found to be -20.0±0.6 mV for the SPNP-BSA-488 and -17.4±0.6 mV SPNP-BSA-555.

The EK devices to study these particles were made using microdevice manufacturing techniques as previously described. Standard soft lithography techniques were used to cast polydimethylsiloxane (PDMS) onto molds, and the resulting microdevices were sealed with PDMS-covered glass wafers to ensure all the internal walls had the same zeta potential (ζ_w). These microchannels were designed to include an inlet and an outlet liquid reservoir where electrodes are placed, and an array of PDMS insulating posts located at the center of the channel **(Figure 4.3B**). Particles are introduced at the inlet reservoir prior to applying an electric potential. In the devices, as the electric potential is applied particles will begin migrating in the device towards either the inlet or outlet reservoirs. The particles stop migrating, or "trap", at a certain voltage due to the constrictions between the insulating posts. The voltage at which a particle traps is directly related to the properties of the particle (e.g., electrical charge, size, shape, and polarizability); therefore, every particle type will trap at a different voltage. These differences in trapping voltage can be used to separate and characterize particles. The trapping voltages can also be used to estimate the E_{EEC}, a parameter that can be used to find the trapping behaviors across any microdevice design, for each particle type. These calculations will be covered later in this study.

SPNP-BSA-488 and SPNP-BSA-555 were both measured in the EK microdevices and both particle types were found to trap at the same potential, 500 V (**Figure 4.3C** and **Figure 4.3D**). This result, suggesting that the presence of the dye does not affect the EK response, has been reported in the literature in similar EK microdevices.[254] This lack of a difference in trapping voltage even

in the presence of different fluorescent dyes shows that the dye molecules themselves have no evident effect on the particles' EK behavior.

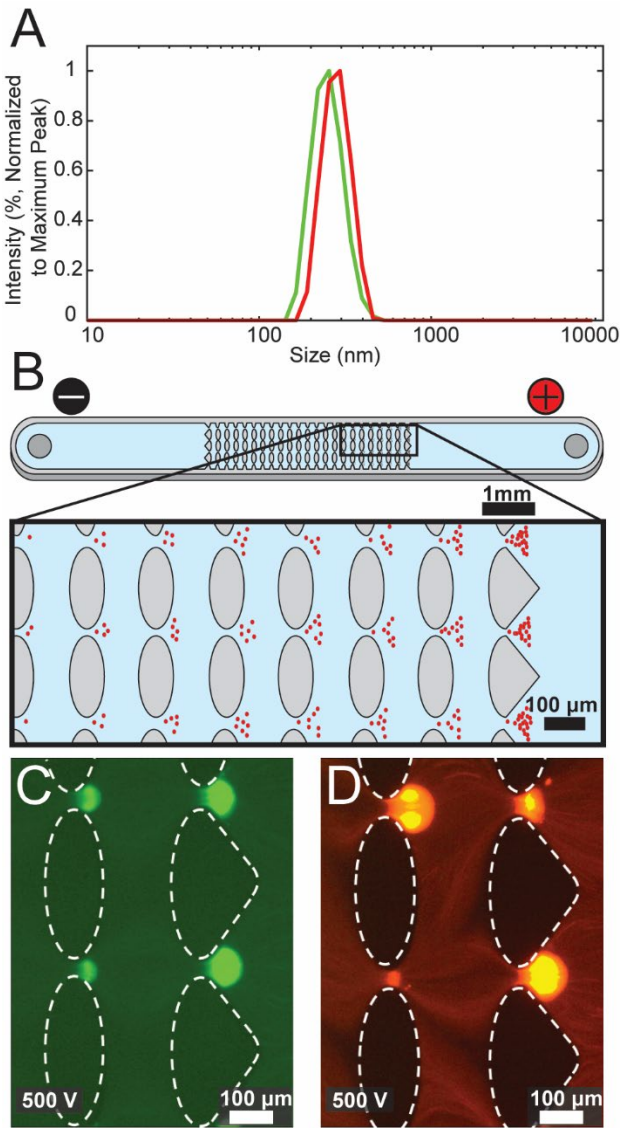

Figure 4.3 Results illustrating the effect of the fluorescent dye on dielectrophoretic trapping. (A) DLS size distributions of BSA SPNPs labeled with Alexa Fluor-488 (green) and Alexa Fluor-555 (red). (B) A schematic representation of the EK microfluidic devices used, and how particles trap within the devices (insert). (C) Trapping of SPNP-BSA-488 and (D) Trapping of SPNP-BSA-555. Both types of SPNPs were trapped at an applied voltage of 500 V, exhibiting very similar trapping behavior. Flow direction is from positive to negative (right to left) in images b, c, and d.

4.3.3 Electrokinetic Response of SPNPs Composed of Different Proteins

EK microfluidics could potentially be used to separate SPNPs of two different proteins based on size and ζ_p, and thus we next investigated the trapping voltages of SPNPs composed of two commonly used model proteins, BSA and Lysozyme. The two proteins have significantly different isoelectric points: 11.35 for lysozyme and 5.4 for BSA. This difference in isoelectric point implies that the two particles behave differently in an EK device. SPNPs were synthesized whose main protein was lysozyme (SPNP-Lys-488) or BSA (SPNP-BSA-488). The particles were fully characterized (**Table 4.1**). SPNP-Lys-488s were of a similar size distribution and ζ_p as the BSA SPNPs, when measured in EK buffer (**Figure 4.4**). While surprising, considering the different isoelectric points, the lack of a difference in ζ_p was likely due to the buffer used, as when the particles were measured in DPBS, they had significantly different ζ_p of -3.5±0.5 mV and 11.2±0.9 mV for the SPNP-BSA-488s and SPNP-Lys-488s, respectively.

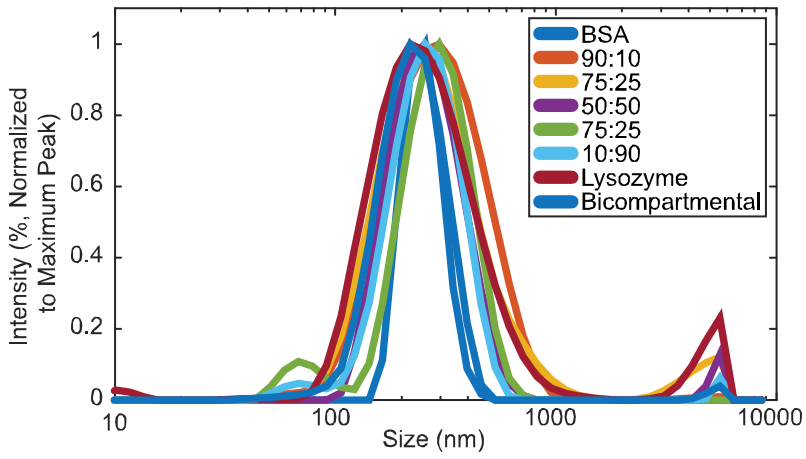

Figure 4.4 Plot of SPNP size distributions measured with dynamic light scattering.

The SPNP-Lys-488s were then analyzed using an EK device as previously described, and the particles trapped at 2300 V. This voltage significantly differed from the 500 V obtained for SPNP-BSA-488s, suggesting that the two particle types could be easily differentiated using EK microfluidics.

4.3.4 Electrokinetic Response of SPNPs as Function of Particle Composition

Possible SPNP therapeutics could be made from a mixture of different proteins in a single particle, such as a mixture of a carrier protein and an active protein like an enzyme.[91] To investigate the sensitivity of EK microfluidics to detect differences in blends of two proteins in single particles, SPNPs were made that were composed of a variety of ratios of BSA and Lysozyme. The particle compositions sizes and ζ_p are described in **Table 4.1**. The particles were then analyzed using an EK microdevice. Generally, when the amount of Lysozyme in the particles was increased, the voltage required to trap the particles increased as well (**Figure 4.6**). This shows promise for EK microfluidics to detect SPNPs that are composed of blends of different proteins. Images depicting the trapping of the eight particles samples are included in **Figure 4.5**.

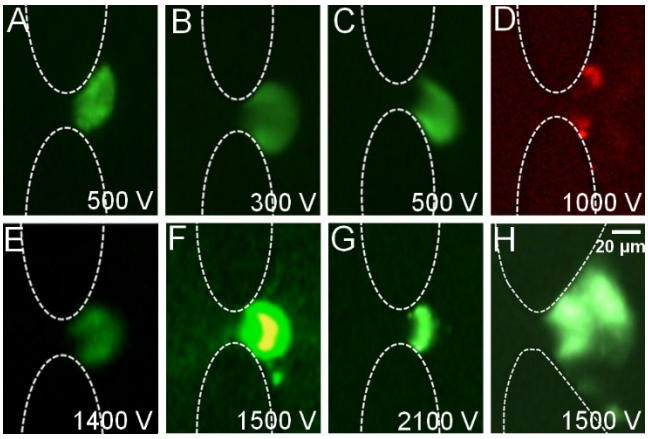

Figure 4.5 Images depicting the EK trapping of the eight types of SPNPs used in this study

Table 4.1 Composition of the eight distinct types of PNPs studied here, listing the percentage composition of BSA and Lysozyme as well as their respective hydrodynamic diameters and zeta potentials.

Particle Sample	Particle Composition	Hydrodynamic Diameter (nm)	ζ_p (mV)
BSA	100% BSA	356±190	-20.0±0.6
Lysozyme	100% Lysozyme	277±130	-20.5±2.2
90:10 blend	90% BSA 10% Lysozyme	367±201	-20.6±1.0
75:25 blend	75% BSA 25% Lysozyme	302±168	-14.6±0.5
50:50 blend	50% BSA 50% Lysozyme	360±169	-14.5±0.9
25:75 blend	25% BSA 75% Lysozyme	304±100	-22.1±1.9
10:90 blend	10% BSA 90% Lysozyme	266±94	-20.3±1.8
50:50, bicompartmental	Compartment 1: 100% BSA Compartment 2: 100% Lysozyme	322±172	-14.1±2.7

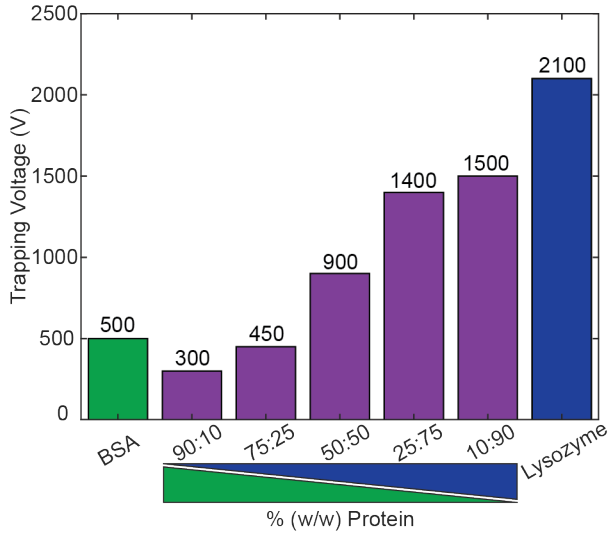

Figure 4.6 Experimental results of the trapping voltage of the seven types of SPNPs composed of BSA, Lysozyme, or blends of both proteins. The bottom image illustrates how the trapping voltages trended as function of the SPNPs composition, where the voltage required to trap the particles increased as the amount of Lysozyme increased. Images of trapped SPNPs are included in Figure S3.

4.3.5 Electrokinetic Response of ASPNPs

A final point of interest was whether EK microfluidics can differentiate particles based not only on general composition, but also on local anisotropy. Thus ASPNPs, with one hemisphere composed entirely of BSA, and the other of lysozyme, were synthesized. Note that compositionally this would be equivalent to the 50-50 particles tested earlier (**Figure 4.7A**). However, when the trapping voltage of the ASPNPs was measured, it was found to be 1500 V, making a 600 V difference in trapping voltage between ASPNPs and particles made of a 50:50 w/w ratio of BSA and lysozyme (**Figure 4.7B**). This voltage differential is significantly larger than the possible step sizes of EK microfluidics, which are in the range of 23 V to 50 V.[225] Although the two particle types were identical in material composition, EK microfluidics were able to differentiate the subpopulations purely by the distribution of matter within each particle.

That this was observed is to be expected, but the specifics behind the physics are yet to be explained. An unexplained facet of this is the fact that the bicompartmental particles had a higher trapping voltage than its isotropic counterpart. It would make intuitive sense for the anisotropic particles to have a lower trapping voltage, as they would have a natural polarity due to their material distribution, and thus be easier to polarize, ergo require a lower voltage to trap, but the opposite result was observed. It is unknown why this happened, but it might be that the behavior of the anisotropic particles is a result of them acting like two particles that are physically attached to each other. This hypothesis would require a more in-depth quantitative examination to prove its validity that is outside the scope of this work, due to the complex kinetics that occur in electrokinetic devises,[255] many of which can be calculated, but some more novel effects such as non-linear electrokinetic phenomena,[256–258] which cannot currently be calculated. Given this, the unique trapping voltage of ASPNPs vs protein blend SPNPs is still notable, as it shows the potential of ASPNPs to be sorted using EK microfluidics.

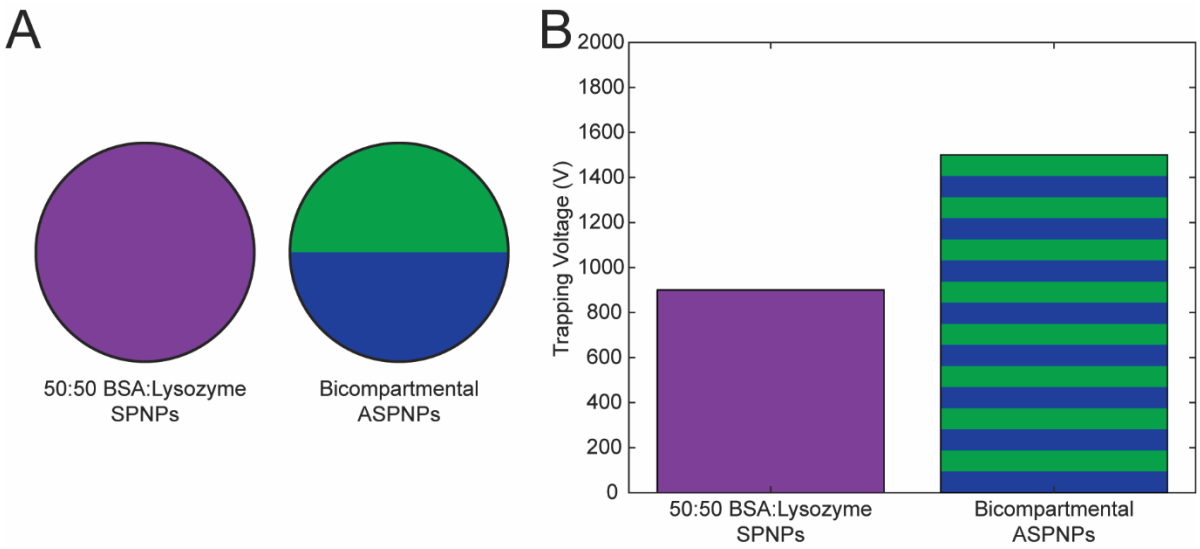

Figure 4.7 PNP material distribution and trapping voltage characteristics. (A) Schematic representation of SPNPs composed of a homogeneous mixture of BSA and Lysozyme, and ASPNPs made in a bicompartmental configuration. (B) Illustration of the trapping voltages of the two types of SPNPs, which were significantly different between the two types of particles.

4.3.6 Estimation of Non-Linear Electrokinetic Parameters

Having obtained the applied voltage necessary to trap each type of SPNP, it was then possible to derive the electric field magnitude at which each SPNP type would have zero velocity (E_{EEC}). The previously developed technique[225] to calculate particle E_{EEC} relies on the fact that trapped particles (**Figure 4.8A**) trap along isoelectric lines (**Figure 4.8B**). The lowest magnitude isoelectric line, the line passing through the midpoint of the constriction, forms a "barrier" which only particles with an E_{EEC} higher than the electric field magnitude along this line can pass through. With this information obtained from experiments, the E_{EEC} of each SPNP listed in **Table 4.2** was calculated by simulating the electric field within a constriction using COMSOL Multiphysics at the trapping voltage of each particle.

The nonlinear electrophoretic mobility ($\mu_{EP}^{(3)}$) was obtained,[259] since both μ_{EO} and $\mu_{EP}^{(1)}$ were experimentally obtained a priori, employing particle image velocimetry and current monitoring measurements.[260] Knowing both the linear and nonlinear EP mobilities is an essential component for the design of EK particle separations.

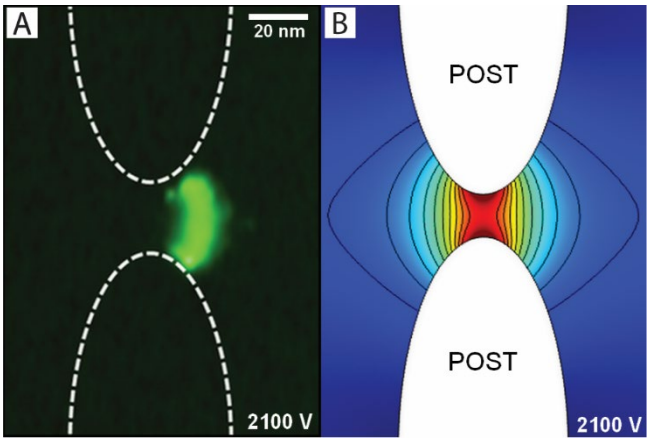

Figure 4.8 (A) Image of trapped Lysozyme SPNPs at 2100 V. (B) Plot of electric field magnitude inside post constriction with black isoelectric field lines at an applied voltage of 2100 V.

Table 4.2 Electrokinetic properties of the eight distinct types of SPNPs studied here.

Particle Sample	$\boldsymbol{EP}^{(1)}$ Mobility $\boldsymbol{\mu}_{\boldsymbol{EP}}^{(1)}$ ($m^2V^{-1}s^{-1}$)	$\boldsymbol{EP}^{(3)}$ Mobility $\boldsymbol{\mu}_{\boldsymbol{EP}}^{(3)}$ ($m^4V^{-3}s^{-1}$)	$\boldsymbol{E}_{\boldsymbol{EEC}}$ (V/m)
BSA	-1.44E-08	-1.15E-18	2.31E+05
Lysozyme	-1.45E-08	-1.37E-19	6.68E+05
90:10	-1.49E-08	-3.17E-18	1.38E+05
75:25	-1.04E-08	-1.51E-18	2.08E+05
50:50	-1.05E-08	-3.78E-19	4.15E+05
25:75	-1.58E-08	-1.43E-19	6.46E+05
10:90	-1.43E-08	-1.28E-19	6.92E+05
Bicompartmental	-1.01E-08	-1.37E-19	6.92E+05

4.4 Summary

In summary, we have shown a potential high throughput method to characterize and manipulate synthetic protein nanoparticles. We synthesized eight distinct types of SPNPs with a variety of different characteristics, ranging from different fluorescent dyes, protein compositions, and particle anisotropies (homogenous vs. anisotropic). Particles were tested in EK microfluidic devices with oval-shaped insulating posts, illustrating the potential of EK techniques for the rapid enrichment and characterization of SPNPs. Notably, the results illustrated that by employing insulator-based EK microfluidics, we differentiated between SPNPs by two distinct characteristics: protein composition and anisotropy. The electric potential required to electrokinetically "trap" and enrich homogenous SPNPs depends on the particle composition, i.e., the relative fractions of BSA and Lysozyme. The higher the Lysozyme fraction within the SPNPs, the higher the electric potential required. In terms of particle anisotropy, homogenous SPNPs required a much lower electric potential to be electrokinetically trapped than ASPNPs separated into two hemispheres. Furthermore, a complete EK characterization for all eight SPNPs samples was reported, which includes particle zeta potential, two types of electrophoretic mobility and the electrokinetic equilibrium condition (E_{EEC}).[225] This latter parameter is an essential component that integrates the main EK phenomena acting on the particles, and has the potential to be used for the design and optimization of these systems. The E_{EEC} is analogous to an EK signature, that is, this value remains constant for a particular particle type in any insulator-based EK system. Differences in particle dielectric properties can be exploited for the design of EK-based separation processes. These results show the promise for EK microfluidics to be used as a technique for the characterization and separation of synthetic protein nanoparticles. .

Chapter 5

Toward Medical Applications of EHD Co-jetted Nanoparticles

5.1 Background and Motivation

Neuroblastoma is a solid extracranial cancer of the nervous system. It mainly affects children under fifteen years old and accounts for 15% of childhood cancer deaths.[261] A treatment for certain high-risk patients uses iodine-131 meta-iodobenzylguanidine (I-131 MIBG, **Figure 5.1A**). MIBG is a norepinephrine analogue that localizes to adrenergic cells.[262] Neuroblastoma cells overexpress adrenergic transporters, such as the norepinephrine transporter (NET), and thus take up MIBG at higher rates than other tissues; because of this, when modified with I-131, MIBG is used as radiotherapy.[263] I-131 MIBG treatment, as a targeted therapy, avoids many of the side effects seen in other cancer treatments and is highly efficacious, but its radioactivity causes a need for specialized facilities and harsh conditions for patients.[264] MIBG is a norepinephrine analogue that localizes to adrenergic cells.[262] Neuroblastoma cells overexpress adrenergic transporters, such as the norepinephrine transporter (NET), and thus take up MIBG at higher rates than other tissues. Because of this, when modified with I-131, MIBG is used as radiotherapy.[263] I-131 MIBG treatment, as a targeted therapy, avoids many of the side effects seen in other cancer treatments and is highly efficacious, but its radioactivity causes a need for specialized facilities and harsh conditions for patients.[264]

Particles fabricated through EHD co-jetting can be made of a variety of polymers. Work done in this chapter was done at the beginning of my studies before the thorough development of

Synthetic Protein Nanoparticles (SPNPs), and thus was done using nanoparticles made from poly(lactic-co-glycolic acid) (PLGA, **Figure 5.1C**). PLGA is a biodegradable co-polymer that that has been in use in the drug delivery field for decades, is a component in a large number of FDA approved therapeutic devices, and so was, at the time of this study, a more clinically validated material compared to protein nanoparticles.[265] Additionally, the synthesis of a number of chemically modifiable PLGA variants is well established, which gives more flexibility for surface modifications of NPs vs SPNPs.[122] The azide-alkyne Huisgen cycloaddition, commonly known as a copper catalyzed click reaction, is an example of a reaction that can be used with poly(lactic acid-co-2-methoxy-3-oxo-3-(2-oxopropoxy)propyl pent-4-ynoate) (PLGA-Alkyne) (**Figure 5.1D**). The side group in PLGA-Alkyne can be reacted in gentle conditions with molecules containing azide (N_3) groups. By carefully designing reaction schemes, sequences of molecules can be added to the surfaces of NPs.

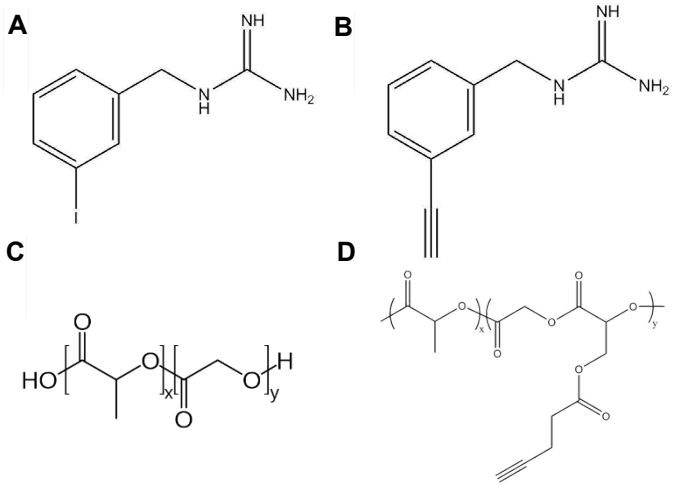

Figure 5.1 A variety of polymers and molecules were used to make NPs for neuroblastoma targeting. (A) meta-iodobenzylguanidine (MIBG), (B) meta-acetylenbenzylguanidine (MABG), (C) poly(lactic-co-glycolic acid) (PLGA), (D) poly(lactic acid-co-2-methoxy-3-oxo-3-(2-oxopropoxy)propyl pent-4-ynoate) (PLGA-Alkyne)

As an alternative to I-131 MIBG treatment, a NP system that uses MIBG to home to neuroblastoma cells and then releases chemotherapy agents in their immediate vicinity may result in a better treatment for the disease. This treatment would contain no radioactive properties and therefore reduce harsh conditions, which would increase patient compliance and reduce costs. In this section, methods to modify PLGA NPs with PEG, followed by MABG, were explored. It was found that the attempted reaction schemes, an azide-alkyne Huisgen cycloaddition with MABG, was incompatible with PLGA nanoparticles. Additionally, an *in vitro* model for the testing of targeting of neuroblastoma cells was developed and validated. Potential alternative reaction schemes are discussed.

5.2 Methods

5.2.1 Materials

Poly(lactic-co-glycolic acid) 5002A (Purasorb®) was purchased from Corbion. Twenty kDa 8-arm star PEG-Azide was purchased from Creative PEGWorks. Dulbecco's Modified Eagle Medium (DMEM), Ham's F12 nutrient mixture, fetal bovine serum (FBS), non-essential amino acids (NEAA), penicillin-streptomycin(pen-strep) and Trypsin were purchased from Gibco. Desipramine Hydrochloride was purchased from Toronto Research Chemicals. All other reagents were purchased from Thermo Fisher or Sigma Aldrich and were of reagent grade or higher. MABG was synthesized using the reaction scheme shown in **Figure 5.2** courtesy of Dr. Artak Shahnas. Briefly, the nitrile group in **Figure 5.2A** was reduced using Lithium aluminiumhydride as a reducing agent. After a workup with K_2CO_3, the trimethylsilyl (TMS) group was deprotected, whereby the 3-Ethynyl-benzylamine (**Figure 5.2B**) could be obtained in a yield of 70%. The obtained amine in **Figure 5.2B** was then reacted at 60 °C in Tetrahydrofuran with 3,5-Dimethylpyrazole-1-carboxamidine (**Figure 5.2C**) and Triethylamine. Upon complete reaction of

the starting material, the final product MABG (**Figure 5.2D**), was obtained in a yield of 85% using the ion exchanger Amberlite IRA 400. All compounds were characterized by 1H-NMR, 13C-NMR, IR, and mass spectroscopy.

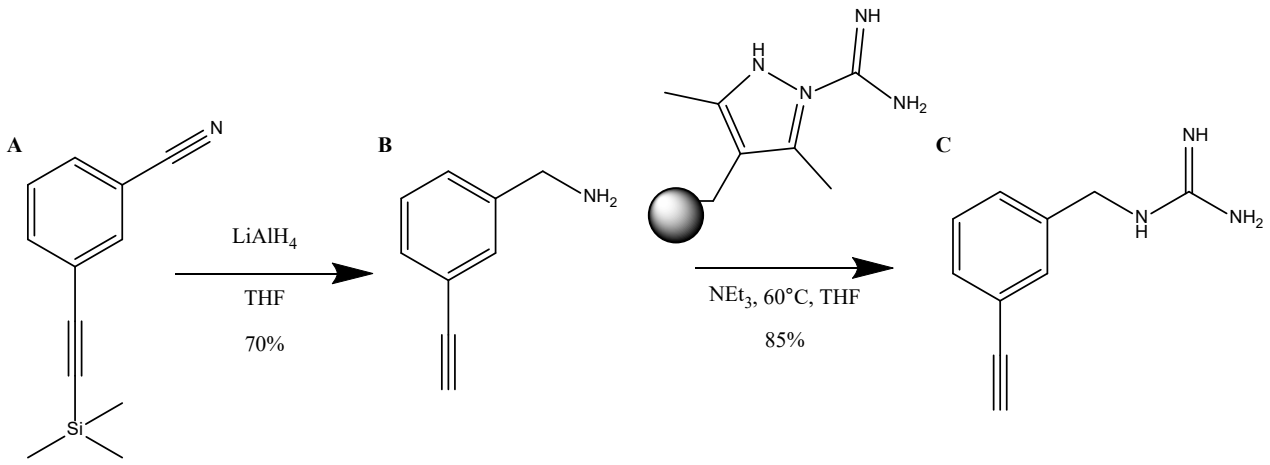

Figure 5.2 Reaction for the synthesis of MABG. MABG was synthesized by starting with reactant (A), which was reduced to product (B). Subsequent amidation resulted in (C), MABG

5.2.2 Synthesis and Characterization of PLGA and PLGA-Alkyne NPs Using EHD Jetting

PLGA and PLGA-Alkyne NPs were synthesized using EHD co-jetting using a previously established method.[189] Briefly, PLGA-5002A was dissolved at a 10% w/v concentration in a 97:3 mixture of Chloroform and dimethylformamide (DMF), and further spiked with 5% (w/v) of cetyl trimethylammonium bromide (CTAB). For PLGA-Alkyne particles, a 75:25 PLGA-5002A: PLGA-Alkyne polymer mixture was used. PLGA-Alkyne was synthesized by Dr. Domenic Kratzer at KIT. The solution was electro-jetted, and the particles collected using a wet collection scrapping method, like that described in previous chapters. Particles were size segregated as previously described,[189] and subsequently measured for hydrodynamic diameters using dynamic light scattering (DLS) or for both size and number concentration with nanoparticle tracking analysis (NTA) using a Malvern Nanosight

5.2.3 Synthesis and Characterization of PLGA and PLGA-Alkyne NPs Using a Single Emulsion Technique

PLGA and PLGA-Alkyne NPs were synthesized using single emulsion to be able to thoroughly investigate the reactions in detail, using a previously established method.[266] PLGA-5002A was dissolved at a concentration of 1% (w/v) in Chloroform, which was subsequently diluted 3x in an aqueous solution of 5% (w/v) Polyvinyl Alcohol. The resulting solution was then submerged in ice water, and a total energy of 55 W was delivered to the solution using a tip sonicator in pulse mode, 1 second on, 5 seconds off. The chloroform was then removed from the solution using a rotary evaporator at 38 °C for 1 hour. For PLGA-Alkyne particles, a 75:25 PLGA-5002A:PLGA-Alkyne polymer mixture was used. Fluorescent NPs were synthesized by doping the jetting solution with 1% PLGA-Rhodamine, (w/w%) of total polymer, courtesy of Jason Gregory.

The resulting particles were washed 3 times by centrifuging them for 50 minutes at 4,900 RCF, and subsequently resuspending the resulting pellet in ultra-pure H_2O. The hydrodynamic diameters of the resulting particles were measured using DLS, and the number, concentration, and particle size with NTA.

5.2.4 NP Surface Modifications

PLGA-Alkyne particles were surface modified using two sequential copper catalyzed click reactions (**Figure 5.3**). PLGA-Alkyne particles were suspended in a 0.9 mL volume of ultra-pure H_2O + 0.1% Tween and the solution sonicated to disperse the particles. 0.1 mL of a 10x mixture of Copper(II) Sulfate Pentrahydrate and (+)-Sodium L-ascorbate (prepared by dissolving 13.3 mg Copper(II) Sulfate Pentrahydrate and 53.3 mg (+)-Sodium L-ascorbate in 1 ml of ultra-pure H_2O + 0.1% Tween) was added. For the first reaction, 90 mg of 8-arm star PEG-Azide was added to

the particle solution and tumbled for 24 hours at room temperature. The solution was then chelated with EDTA to remove any insoluble copper ions, and subsequently washed 5x using ultra-pure H_2O + 0.1% Tween. For the second reaction, the same dilutions and Copper(II) Sulfate Pentrahydrate/(+)-Sodium L-ascorbate solution was prepared, and 24.98 mg of MABG dissolved in 50 µL of dimethyl sulfoxide was added to the reaction mixture. The particles were then chelated and washed as previously described. For fluorescent stand in reactions, the same reaction conditions were followed, with the replacement of MABG in the second reaction with 1 mg of Cy5-Azide. Particles were imaged using a Nikon Eclipse 80i Fluorescent Microscope on a 10X objective.

5.2.5 Particle Characterization Using Scanning Electron Microscopy

Particle samples were prepared for Scanning Electron Microscope (SEM) by washing them 10x with Ultra-Pure H_2O, followed by sonication to disperse the particles. Multiple serial dilutions of particles were prepared, and 10µL of each particle solution was then drop casted onto a silicon wafer. The samples were then gold sputter coated and imaged using a Nova 200 Nanolab SEM.

5.2.6 Cell Culture

SK-N-BE(2) cells were cultured on plastic cell culture dishes using a 1:1 (v/v) mixture of DMEM and Ham's F12 supplemented with 1% NEAA and 10% FBS. Cells were passaged every 3-5 days, or when 80% confluent. Cells were only cultured in media supplemented with pen-strep during experiments.

5.2.7 NET Upregulation and Blocking of Neuroblastoma Cell Lines Using Vorinostat and Desipramine

The cytotoxic and protein expression responses of Vorinostat and Desipramine in SK-N-BE(2) cells were tested. Cytotoxicity was tested using a commercially available XTT assay. NET

expression was quantitatively measured using a Wes Simple Western, following manufacturer instructions. A rabbit anti-NET antibody was used as the primary antibody (Abcam, ab41559).

5.3 Results and Discussion

We first set out to design a NP system that could target neuroblastoma through the use of NET. As NET is a channel transporter, and not a surface ligand, it is expected to have low overall avidity to an MIBG derivative that is unable to go through the channel. To counteract the expected weak interactions, a PLGA system that could take advantage of multivalency was designed. Multivalency is an interaction common in biology where a system of ligands and receptors, such as MIBG and NET, that have multiple reversible and simultaneous weak interactions. Much like Velcro, the combined, numerous interactions can lead to strong binding, and thus multivalency is a way to create strong targeting to NP systems with otherwise weak interactions.[267] Multivalency has been shown, through both *in vitro* and *in silico* experiments, to be a way to amplify targeting interaction in NPs that otherwise, on their own, are weak.[268,269] This binding affinity improvement can both increase the residence time of NPs in tumors, which is key to providing therapeutic effects, and counteract the decrease of affinity observed when ligands are bound to PEG linkers.[270]

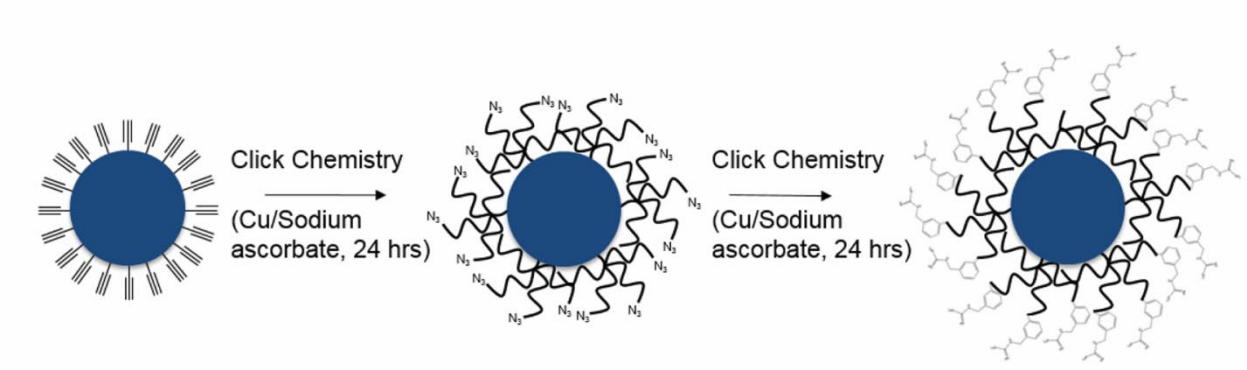

Figure 5.3 Proposed reaction sequence to produce MABG targeted PLGA NPs

PLGA-Alkyne NPs were first synthesized using EHD co-jetting, but after multiple attempts, it was found that while the particles behaved as expected after the first click reaction, which PEGylates the surface of the particles, there was a very poor yield of particles after the second click reaction to attach MABG onto the surface (**Figure 5.3**). Additionally, multiple attempts at conducting *in vitro* uptake and targeting assays were inconclusive, and we were unable to determine whether the particles were unable to target due to the MABG hypothesis not being valid, or manufacturing problems with the fully functionalized NPs.

To investigate the reason behind this loss of particles, a higher yield synthetic route for the PLGA NPs, single phase emulsion, was utilized to be able to thoroughly investigate the reactions in detail. A systematic search was then conducted to diagnose the low yield. First, fluorescent NPs were PEGylated, and subsequently reacted with a Cy5-Alkyne, which was used as a fluorescent stand in for MABG. After thorough washing to remove unreacted reagents, the reaction was confirmed with fluorescent microscopy (**Figure 5.4**).

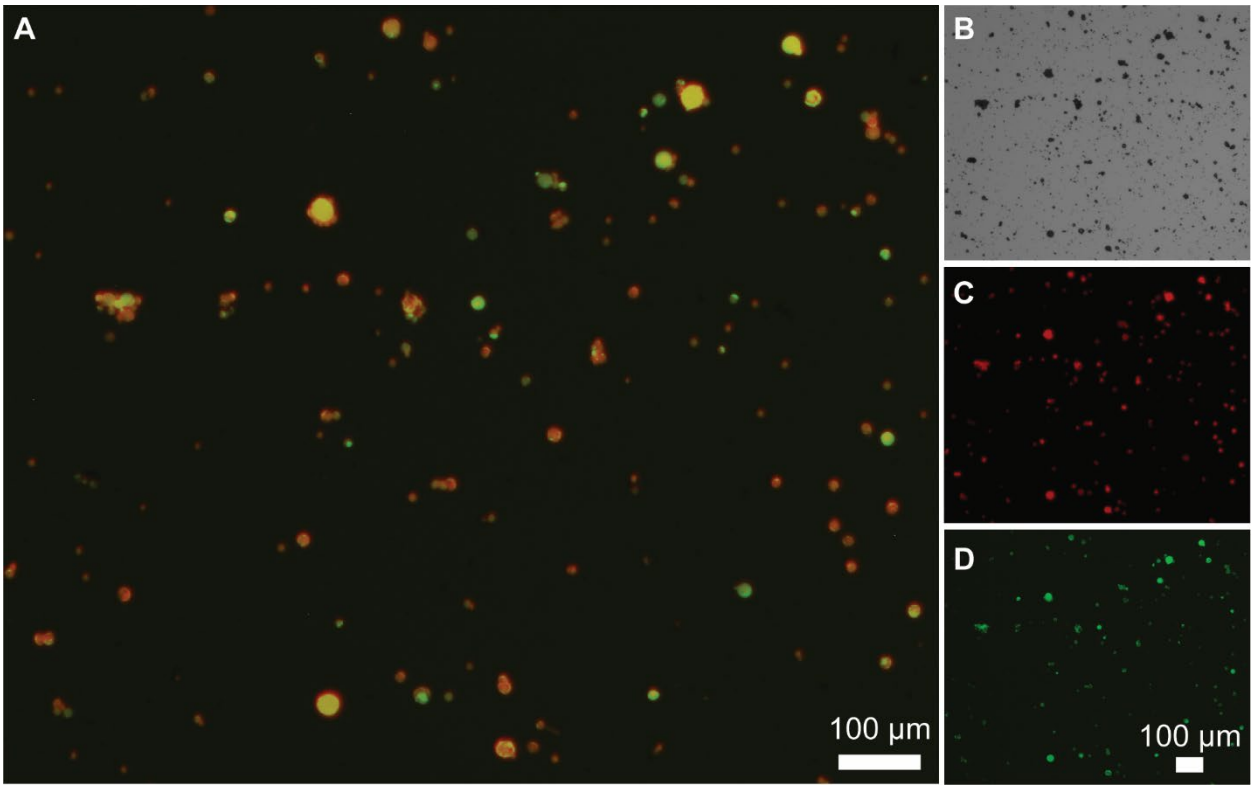

Figure 5.4 The ability of PLGA NPs to be surface modified was confirmed using a fluorescent MABG analogue. PLGA nanoparticles were reacted with two sequential copper catalyzed click reactions, one to PEGylate the particles, and the second to react Cy5-Alkyne, a stand in for MABG, with the terminal azides on the particles. (A) Co-localization of Green (Fluorescent PLGA) and Red (Cy5-Alkyne) channels imply success of click reactions. (B-D) are bright field, Cy5, and fluorescent PLGA channels, respectively. Controls (no Cy5-Alkyne, and no PEG-Azide but yes Cy5-Alkyne) showed only green fluorescence, not shown). Scale bar 100 µm.

The emulsion synthesized PLGA particles were then reacted using the full reaction sequence and measured after each reaction using DLS. A small but notable size increase was observed after the MABG reaction, potentially implying that the reaction had occurred. (**Figure 5.5**). The NPs were also characterized using NTA. The size measurements using NTA agreed with the results from DLS. Number concentration was also acquired, and it was found that similar to the EHD co-jetted particles, there was a very poor yield from the MABG reaction, with only a 3.06% yield.

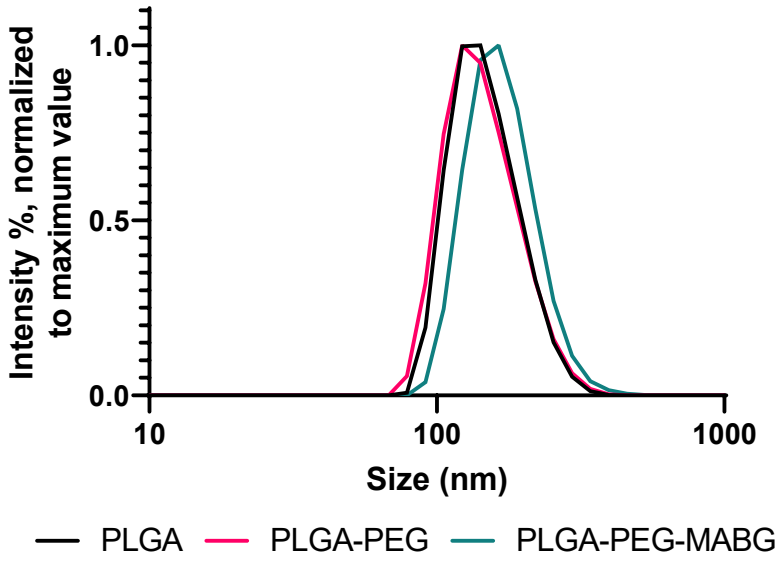

Figure 5.5 Nanoparticle hydrodynamic diameter of functionalized PLGA NPs. Particles were measured using DLS before and after each functionalization reaction. A notable size increase was observed after the second reaction, where MABG is added to the particles.

Unlike the EHD co-jetted particles, the yield of the emulsion particles was high enough to observe particles using SEM. PLGA, PLGA-PEG, PLGA-PEG-MABG, and PLGA-Control were imaged using SEM. PLGA-Control particles were particles that were treated under the same reaction buffers, and treated like PLGA-PEG-MABG, but without any reagents. PLGA (**Figure 5.6A**), PLGA-PEG (**Figure 5.6B**), and PLGA-Control NPs (**Figure 5.6C**), showed no morphological differences, in contrast to the PLGA-PEG-MABG NPs, which appeared to be degraded (**Figure 5.6D**). We concluded PLGA particle degradation likely resulted from acid-induced hydrolysis. We predict this may have occurred in response to deprotonation of MABG, or an unidentified byproduct of the click chemistry reaction.

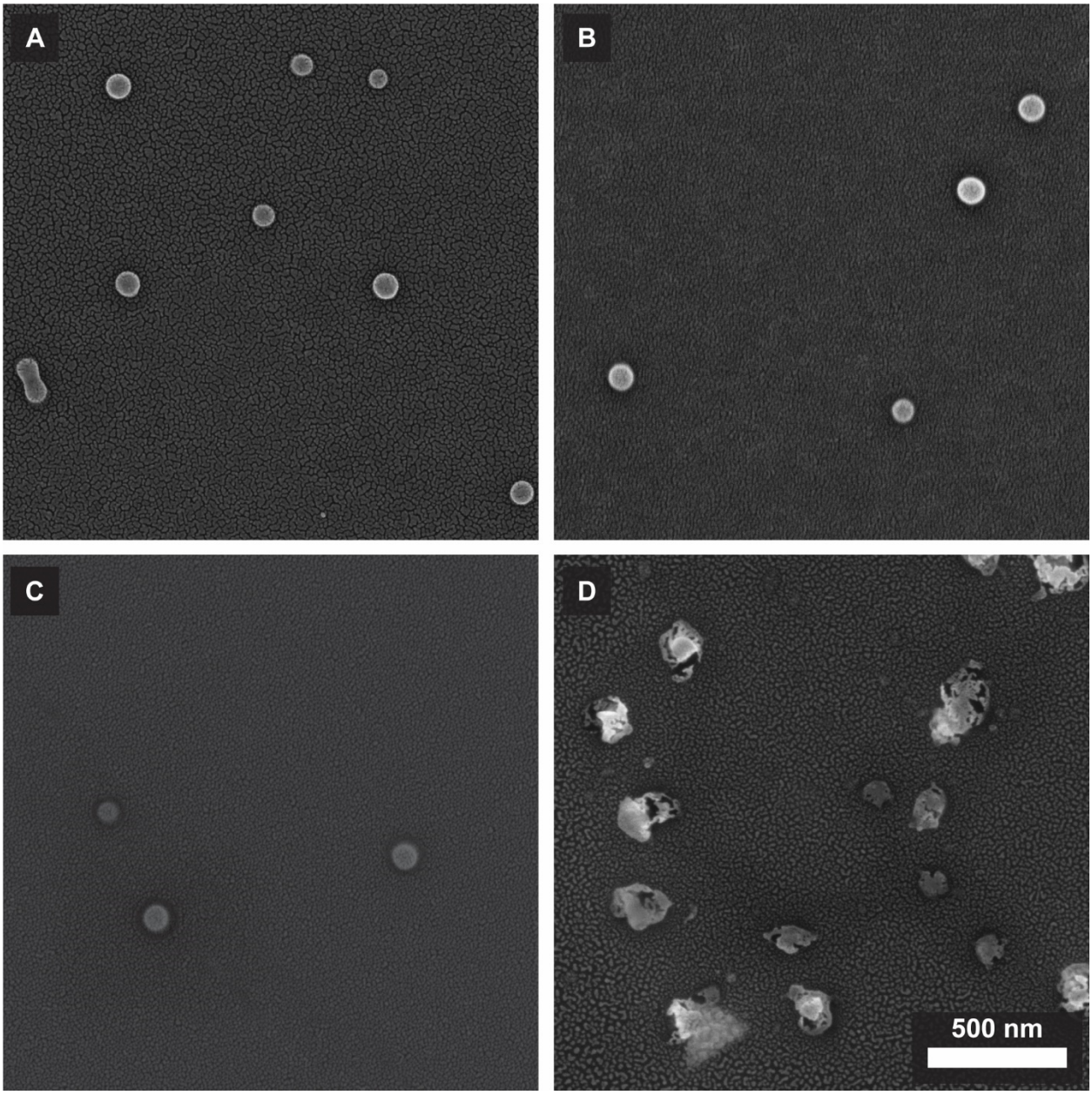

Figure 5.6 SEM of modified PLGA particles. (A) PLGA, (B)PLGA-PEG, (C)PLGA-Control, and (D)PLGA-PEG-MABG particles were imaged using SEM. It was found that MABG caused degradation of the PLGA NPs during the conjugation reaction, possibly due to acidic degradation induced by the presence of MABG.

During the three years that this project lasted, a biological system for the testing of specific targeting by MIBG analogues was developed. Using SK-N-BE(2) cells, the dose response of Vorinostat, a NET upregulator, and Desipramine, an NET antagonist, was quantified. It was found

that SK-N-BE(2) cells showed a dose dependent upregulation of NET when treated with Vorinostat, with cells treated with 2.5 µM of Vorinostat expressing 43% more active NET, as measured with a quantitative western blot (n=1), without significant cell death (n=3). Desipramine was found, as expected, to not affect NET expression, and concentrations that were previously used to block NET by Dr. Asish Misra in our lab and in the literature, were not found to affect cell viability (**Figure 5.7**).

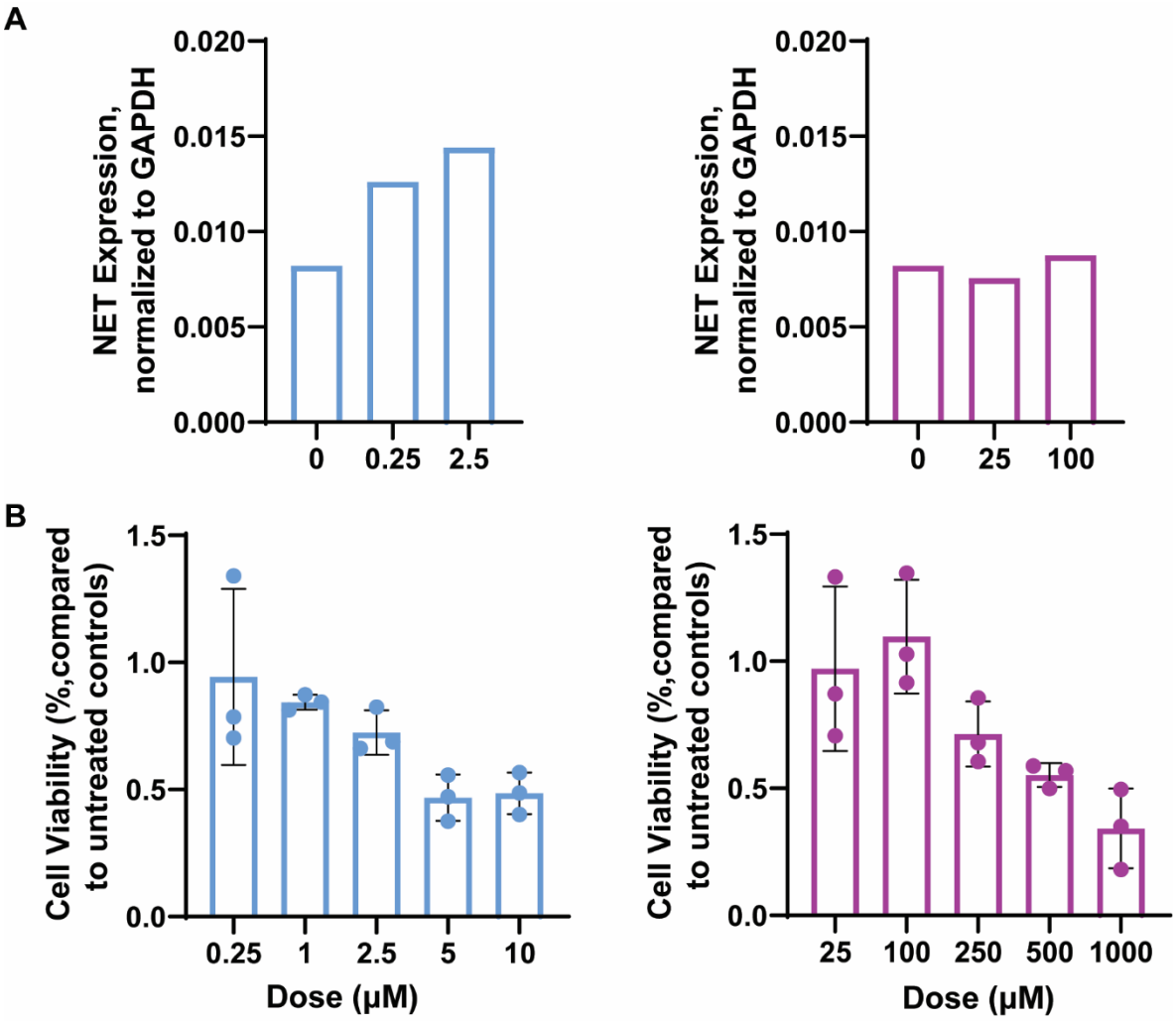

Figure 5.7 NET upregulator Vorinostat increases NET expression in SK-N-BE(2) cells, and NET antagonist Desipramine has no cytotoxic effects at relevant doses. (A) NET expression was measured using a quantitative Western Blot (n=1), and (B) toxicity using an XTT assay (n=3).

5.4 Conclusions

Here, a method for how to use MABG to target PLGA nanoparticles is thoroughly investigated. It was found that while it is possible to conduct copper-catalyzed click reactions with nanoscale PLGA NPs, MABG induces a degradation reaction on the PLGA NPs and is fundamentally incompatible with the particles as a targeting modality, under the investigated conditions. Additionally, a method to upregulate NET expression without significant cytotoxicity was characterized. New methods developed in the intervening years since this work was conducted, such as the surface modification of synthetic protein nanoparticles with azides, make it so that it may be possible to study how MABG can be used as a targeting moiety for the treatment of neuroblastoma. While the findings of this study were disappointing, they were informative, and lay the groundwork to study the use of MABG to target blastomas.

Chapter 6

Conclusions and Future Directions

In this thesis, various methods for the fabrication of Synthetic Protein Nanoparticles (SPNPs) using Electrohydrodynamic (EHD) co-jetting were developed, an investigation of how different synthetic parameters affect biological responses was conducted, and anisotropic SPNPs were fully characterized. Additionally, a method for loading active enzymes into SPNPs was developed and characterized, and their therapeutic and technological potentials explored. Furthermore, a method for characterizing single compartment and two-compartment SPNPs using electrokinetic microfluidics was demonstrated. Last, exploratory work was shown on how a small molecule might be conjugated onto the surface of a nanoparticle for cancer therapeutics. SPNPs are a novel technology, and thus there is plethora of available research routes available for further exploration and development.

6.1 Toward *in silico* Guided Nanoparticle *in vitro* Experiments

In Chapter 2, SPNPs made from a variety of proteins and with different macromers were tested for how certain parameters – the proteins and macromers used – would affect how the particles would behave in a biological setting, specifically their uptake and degradation behavior. In the field of nanoparticle-based drug delivery, these studies are usually conducted using many assumptions that treat nanoparticles as if they were small molecules. For example, in the studies we conducted, we selected a concentration of particles to incubate cells with and used this same concentration for all the studied SPNPs. This assumes that all nanoparticles will physically behave

the same, regardless of nanoparticle composition. While this is a perfectly acceptable practice when a small molecule (e.g. Vorinostat) is being examined, it may not make sense for nanoparticles. A small molecule will quickly diffuse to a steady concentration in surrounding media. As it is consumed by the cell, the concentration in the media above the cell will quickly equilibrate and be mostly homogeneous at the relevant time scales, following a steady-state kinetics approximation. On the other hand, nanoparticles are more complex (e.g. have size distributions, interact with each other as well with the surrounding environment, etc.), and are influenced by not just diffusion, but also a host of other interactions and physical forces, such as aggregation and sedimentation. This leads to particles demonstrating variable measured uptakes that may not be based on affinities of the particles to the cells, but on variations in particle settling and aggregation.[271–273]

The targeting v. aggregation conundrum has been of particular concern in the field of nanotoxicology, where there are broad efforts to create *in silico* tools to help screen the millions of new nanoforms that are being created in industry for environmental and health hazards, both short term effects such as toxicity, or effects that could result from long term exposure such as genetic mutations. The consensus in the field is that it would be unethical and financially untenable to test all the materials being created in the most relevant models (i.e. *in vivo* murine models). To address this, the initial approach was to conduct *in vitro* testing to screen materials to identify potential toxic/hazardous materials for further *in vivo* testing.[272,274–276] This approach has problems, particularly the potential of erroneous or misleading results coming not from the toxic potential of the particles, but due to the diffusion/sedimentation concerns described previously. As a result, models have been developed that seek to predict how particles behave *in vitro*. The foremost current example is the Distorted Grid (DG) model, where particle qualities, like density,

effective density, size distribution, alongside characteristics of the surrounding media, like viscosity and temperature, are used to model how quickly particles will deposit at the bottom of a modeled well of cells.[277] These models have gained wide acceptance in the field of nanotoxicology but have gained little traction in nanomedicine. With the field beginning to adopt more high throughput techniques for drug delivery and toxicity,[278,279] similar to the ones that are used in nanotoxicology, and the synthetic flexibility of our SPNPs showing their potential as candidates in high throughput screening for optimal nanoformulations, implementing models such as the DG model into work flows can serve as a tool for quality control and "sanity" checks, preventing the *in vivo* testing of improperly targeted materials. By thoroughly characterizing the particles, and subsequently modeling to reflect experimental conditions,[280] much insight could be gained about particle behavior, whether differences observed are due to true targeting effects or are just an artifact from the particle formulation (i.e. identify false positives/negatives).

As an example, a meta-analysis was conducted of uptake results from unrelated, unpublished uptake studies conducted by Nahal Habibi in order to have a real-world data set to compare the DG model against (personal communication, experimental details omitted by request).[281] Note that none of these particles should specifically target the cells used, theoretically. The same particles were then characterized for a variety of parameters, following established nanotoxicological protocols,[282] and then the deposited fraction was calculated in the same experimental conditions with the DG model, using a custom built MATLAB based macro, which is available upon request (**Figure 6.1**).

Comparing the results between the experiment and the model provide several new insights. For instance, this modeling system can explain discrepancy between experiment and theory. Take the uptake results for 200 nm HSA and hTf particles for example. The particles had different

uptake levels measured, implying some degree of targeting or increased affinity between the particles and the cells. On their own, these results are anomalous, as no targeting would be expected in the cells used for these proteins types, but the DG model, based solely on the measured material properties of the SPNPs, was able to predict the measured uptake differences. Upon further inspection, it was found that the model recognized small differences in the size distributions of the particles and was able to quantify the impact of these differences on relative sedimentation, and thus measured uptake, rates.

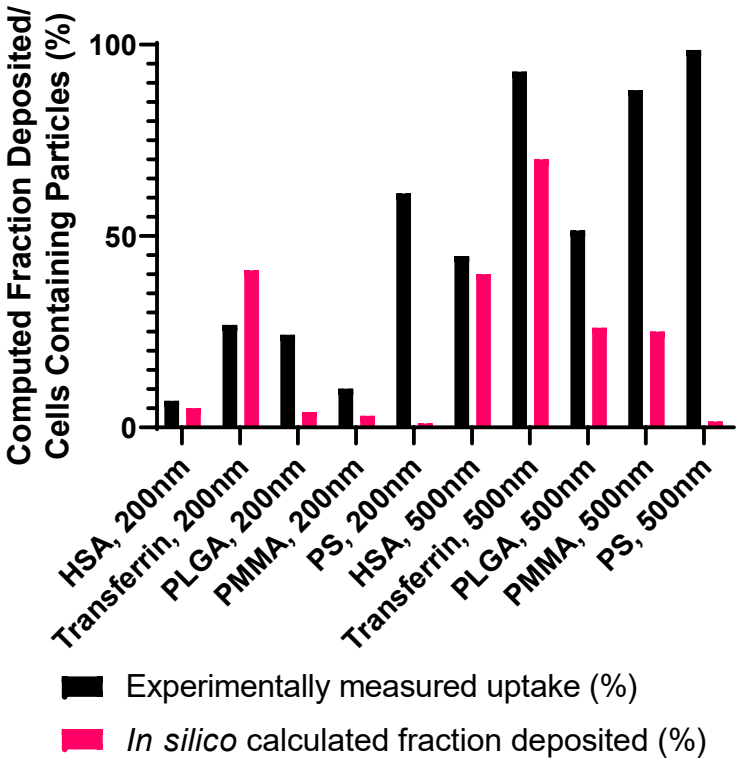

Figure 6.1 *In silico* models can be used as sanity checks and troubleshooting tools for *in vitro* NP uptake experiments. Various NP and SPNP formulations were given to cells, and the results compared to deposited fractions as calculated by the DG model.

While these models have potential in being used in screening workflows to rule out false negatives or positives, they also have weaknesses that could be improved upon. Take for example the contrast between the real uptake and the predicted deposition of amine-modified Polystyrene

(PS) particles, where the model predicted very low uptake rates, while the actual experiment resulted in high uptake rates for both sizes of PS NPs. This was due to the amines in the particles being positively charged, a parameter that the model does not consider,[277] leading to charge induced uptake by the cells, whose surface charge is negative. The results presented here provide an initial workflow that could be expanded, improved, and integrated into high throughput screening of various nanocarriers. These type of *in silico* based checks could improve the accuracy of results, reduce experimental error, and overall improve the translatability of *in vitro* results into *in vivo* models by ensuring that particles are truly giving potentially positive results because of their engineered qualities, and not physics based anomalies due to experimental conditions.

6.2 Towards Shape Control of SPNPs

In Chapter 2, SPNPs were found to be quite flexible in their components, and the compositions were shown to have significant effects on the biological behaviors of the particles. Another factor in particle behavior has been found to be the particle shape.[283,284] Preliminary work was conducted to see how particle shape could be modified prior to the macromer polycondensation reaction in SPNPs.

HSA SPNPs were synthesized, using the NHS-PEG macromers described in Chapter 2, and then a sample was either immediately placed in a 37 °C incubator for 1 week (**Figure 6.2A**), or placed in a 37 °C high humidity incubator for 6 hours prior to the 1 week incubation (**Figure 6.2B**). As can be seen, the particles that were treated as normal maintained their usual geometry, but the particles that were incubated at high humidity first were morphed into "pancake" architectures. These pancake shapes are normally seen with EHD jetting when the jetting parameters are specifically selected to have low volatility, and thus the particles are not fully solid prior to landing on the collection surface and "melt", forming the "pancakes". By treating the

particles after jetting, the humidity in the environment partially hydrates the particles, and creates the same effect. The key difference between the two methods is that changing the jetting conditions so that the particles result in "pancakes" normally changes not just the particle geometry, but also other characteristics, namely the size of the particles. By using humidity to modify the particles, the SPNPs have different shapes but retain similar sizes.

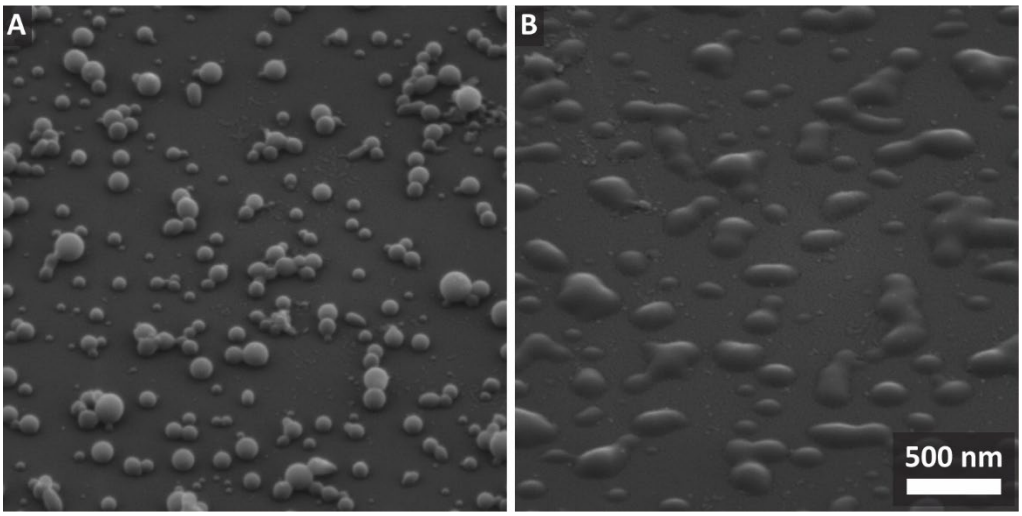

Figure 6.2 SPNPs can be shape shifted after jetting. HSA SPNPs were either (A) treated as described in Chapter 2 as a control, or (B) incubated in a high humidity incubator for 6 hours, changing their shape to a "pancake-like" geometry.

Another key factor in NP delivery is what happens to the particles once they are inside cells. NPs are taken up by cells through a variety of different mechanisms, but they almost always end up being localized in endosomes which have high levels of enzymes and an acidic environment which can reduce therapeutic effect, be it through the breakdown of small molecule therapeutics, or denaturation of enzyme therapies such as those used in Chapter 3. A popular strategy of particles' escaping endosomes is through pH triggered swelling.[285–287] Thus, preliminary experiments were conducted that attempted to control pH dependent swelling in SPNPs. It was found that the swelling could be controlled by modulating the material composition of the particles. For example, when bicompartmental particles were made with HSA loaded with branched 25 kDa

Polyethyleneimine (PEI) in one compartment, and hTf in the other, it was found that particles showed little pH dependent swelling (**Figure 6.3A**). This contrasts to SPNPs made from hTf, that when incubated for 24 hours at a pH 4.5, increased in size from 120 nm to 300 nm (**Figure 6.3B**).

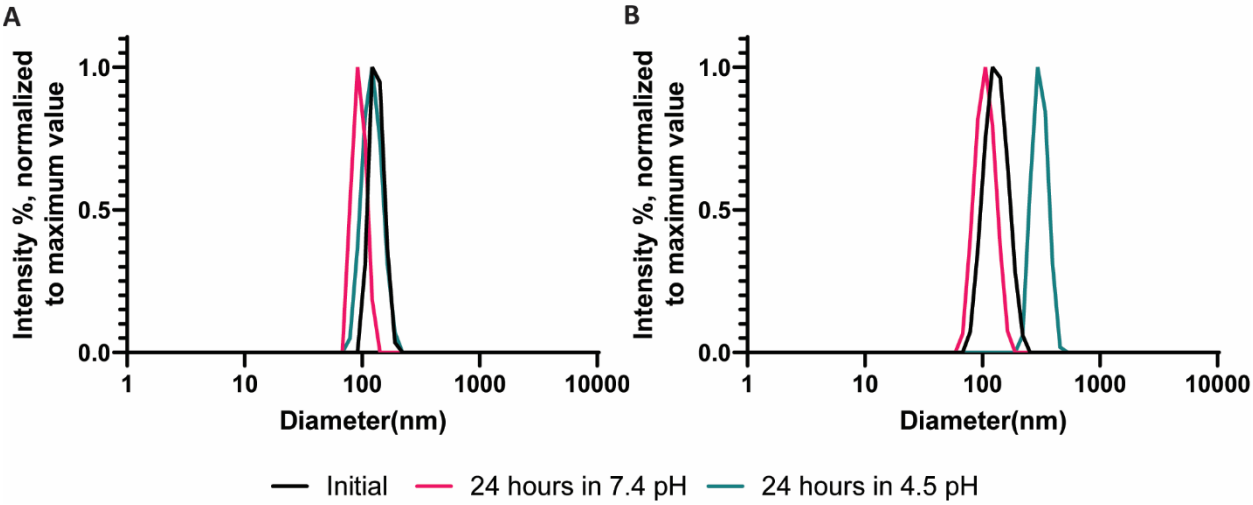

Figure 6.3 SPNPs display material dependent stimuli responsive swelling. SPNPs made in either a (A) bicompartmental configuration with HSA PEI in one compartment and hTf in the other, or (B) wholly made from hTf, showed different swelling behaviors when place in a pH 4.5 media for 24 hours.

With further development, the two results presented here leave two routes of possible research: shape control of particles and controllable stimuli responsive swelling. The first technique could be modified (shorter high humidity incubation times, different humidity treatments, combination with stretching methods, etc.) to create high aspect ratio SPNPs, leading to potentially improved *in vivo* behavior.[288,289] In the second technique, the mechanisms behind differential swelling behaviors could be further investigated and used to finely tune swelling behavior in the SPNPs, allowing for controlled endosomal escape.

6.3 Toward Externally Controllable SPNPs

As was shown in Chapter 3, SPNPs can be loaded with and maintain the activity of enzymes after loading. SPNPs that contain enzymes can be envisioned as the precursors to true

medical “nanomachines”, machines that can be controlled and perform functions at the nano- scale. The main missing component to using SPNPs as machines is some kind of external or programable control, since currently the SPNPs are only able to be controlled through relatively simple means such as substrate or reaction selection, or antibody targeting.

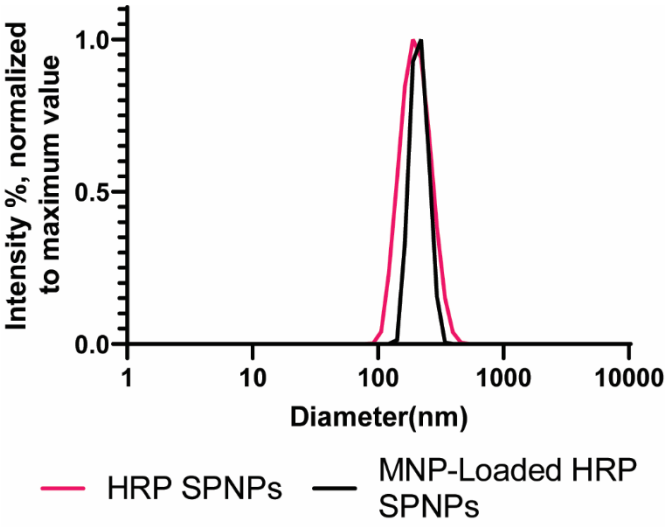

Figure 6.4 Loading SPNPs with magnetic nanoparticles (MNPs) does not significantly change their sizes. HRP SPNPs were made with and without MNPs, and their sizes measured using DLS.

As an early foray into developing enzymatic SPNPs into nanomachines, external control of the particles was implemented by loading enzymatic SPNPs with Horseradish Peroxidase (HRP), a popular biotechnology enzyme, and iron oxide Magnetic Nanoparticles (MNP, 0.05% w/w of protein), using the Glutaraldehyde (GA) macromers. MNPs were made following a method described by Roh and Lahann.[290] The inclusion of MNPs the had no significant effect on the size of the resulting particles.

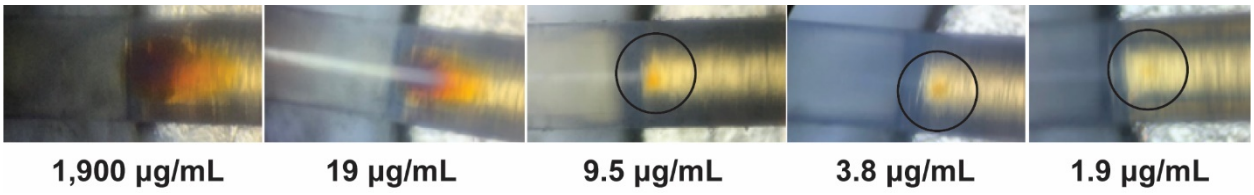

Figure 6.5 Enzyme and MNP loaded SPNPs can be trapped magnetically in a microfluidic system. Various concentrations of SPNPs were loaded into a simple microfluidic device and were trapped using an external rare earth magnet.

These particles were then placed in a flow through microfluidic system and it was found that a strong rare earth magnet was able to capture particles on the inside of the tubing. Trapped particles were observed at concentrations down to 1.9 µg/mL through light microscopy (**Figure 6.5**). Particles were trapped, washed, and then reacted with a 1-step TMB solution, which would change color upon reaction with active HRP. It was found that the particles, after being trapped, were still active. The reaction efficiencies for particles trapped in the flow through reactor (i.e. substrate was flowed over the trapped pellet and samples from the product measured) and in a batch reaction system (i.e. in a microplate assay) were then calculated using the following formula:

$$Reaction\ Efficiency = \frac{P}{S*E*t} \quad [1]$$

Where P is the amount of product in absorbance units in the flow-through as measured by a plate reader, S the mass of substrate placed in the reaction, E the mass of enzyme used, and t the time duration of the reaction. It was found that the particles in the flow reactor were 2 orders of magnitude more efficient than the same amount of free enzyme in batch reactor conditions, 6.88×10^5 Abs·mg^{-2}·s^{-1} for the "flow" reactor vs 1.07×10^3 Abs·mg^{-2}·s^{-1} for the "batch" reactor. These results are promise and suggest a future route for research for the development of nanomachines.

6.4 Toward the Delivery of Biological Therapeutics

Gene-therapy holds promise for eradicating some 4,000 described monogenetic diseases, such as Angelman Syndrome,[291] Cystic Fibrosis,[292] Coffin-Lowry Syndrome,[293] and Huntington's disease,[294] as well as countless acquired diseases. However, traditional gene-therapies rely on viral-based delivery platforms which suffer from a host of limitations, such as limited tissue specific tropism, variable immunogenicity, toxicity, and limited transgene size.[295] There have been a variety of attempts to develop non-viral gene delivery platforms using a variety of carrier systems, such as liposomes,[296] nanogels,[297] dendrimers,[298] and many others.[299]

Synthetic Protein Nanoparticles (SPNPs) developed by the Lahann lab show significant promise as potential gene delivery vectors. Work by Gregory et al. showed that HSA SPNPs are able to effectively deliver siRNA *in vivo* to a glioblastoma bearing mice, a treatment that when combined with ionized radiation results in long term survival, a rare achievement in the treatment of gliomas.[169] As shown in Chapters 2 and 3, the proven potential to load SPNPs with active targeting proteins, such as Transferrin, or the possibility to load active gene-modifying enzymes, such as Cas9 enzymes,[300] adds to the innovative potential of using SPNPs as a gene delivery carrier vehicle.

To investigate whether SPNPs could be used for the non-viral gene delivery of plasmid DNA, we first set out to investigate whether plasmid DNA (pDNA) could be electrojetted. HSA and eGFP pDNA was electrojetted, with eGFP at a concentration of 50 ng/mL in the jetting solution and crosslinked using NHS-PEG macromers. The particles were imaged using SEM (**Figure 6.6**), and it was found that the pDNA did not affect particle morphology, as compared to unloaded SPNPs (see Chapter 2 as a comparison).

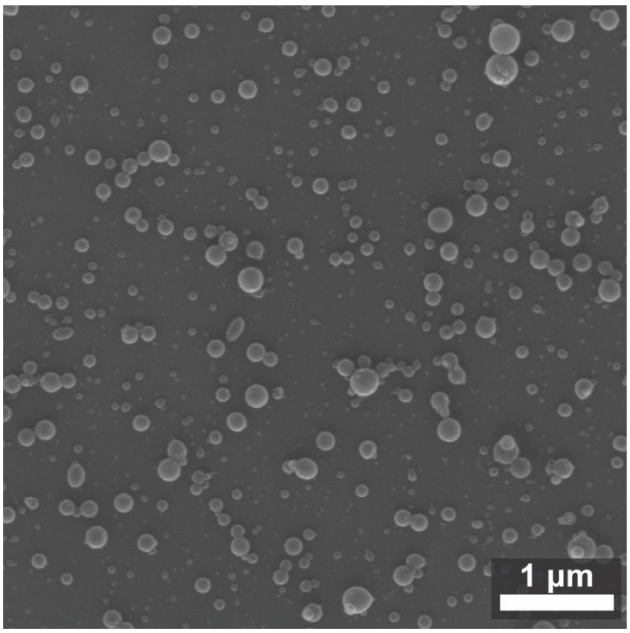

Figure 6.6 HSA SPNPs loaded with eGFP pDNA. SPNPs can be synthesized with unchanged morphology to contain pDNA.

The particles, unmodified eGFP pDNA, or electrojetting collectate containing HSA and eGFP pDNA was then used to transfect MDA-MB-231 cells in a preliminary study. Lipofectamine 3000 was used to transfect the non-particle controls. It was found that the SPNPs were unable to induce any expression of eGFP in the cells, but it was found that the electrojetted pDNA was still able to transfect the cells with eGFP. It was hypothesized that this lack of effectiveness may have been due to difficulties with endosomal escape of the particles, as extensive evidence showed that HSA SPNPs are readily taken up by cells (see Chapters 2 and 3).

To investigate whether endosomal escape was affecting pDNA transfection, a small library of bicompartmental SPNPs was synthesized. The particles were designed to have a gene delivery compartment, which was loaded with eGFP DNA, and a second endosomal escape compartment, loaded with either branched 25 kDa PEI or Pluronic F127 (shortened to F127). It was hypothesized that PEI, a cationic polymer shown to cause endosomal escape through the proton sponge effect, or F127, a PEG based surfactant which could disrupt phospholipid bilayers and thus also potential

cause endosomal escape.[126] Particles were made of one of two proteins, HSA, or Human Transferrin, hTf, as both proteins have shown promise in various drug delivery applications (see Chapter 2).

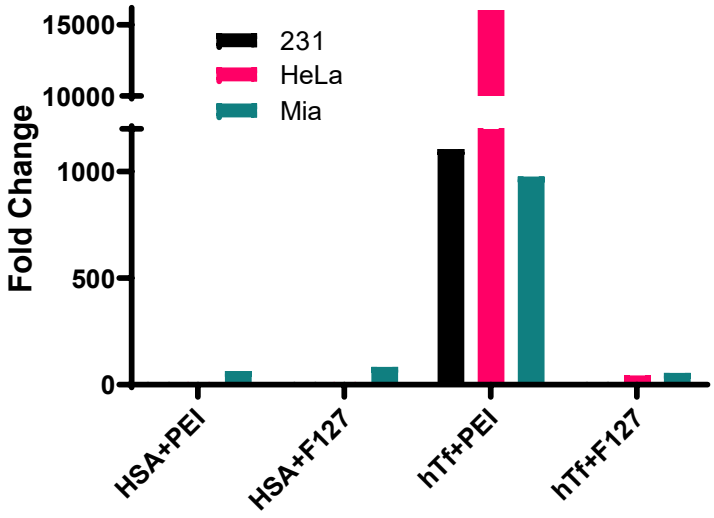

Figure 6.7 Bicompartmental SPNPs can transfect a variety of cancer cells with eGFP pDNA. A small library of bicompartmental SPNPs was built, with one compartment loaded with pDNA, and the other designed for endosomal escape, loaded with either Polyethyleneimine or Pluronic F127. The x-axis denoted the protein that the SPNPs are composed of, and the endosomal escape polymer used.

A variety of cancer cell lines, HeLa, MIA-PaCa-2 and MDA-MB-231, were then treated with the library of particles at a concentration of 10 μg/mL of SPNPs overnight, and the expression of eGFP in the cells analyzed using qPCR (**Figure 6.7**). It was found that SPNPs made from hTf and that contained PEI in the endosomal escape compartment were able to significantly transfect all cell lines with eGFP expression. It is important to note that it was difficult to quantify gene delivery with the particles using eGFP as the delivered gene. eGFP is valuable as its expression can be directly observed in cells through fluorescent microscopy, but its fluorescence is not linearly related to the expression levels of the protein.

To quantify expression, we were forced to use qPCR, which is labor intensive for high-throughput applications.

In this section, the potential to use SPNPs as a gene delivery device was demonstrated. First, the effect of EHD co-jetting on plasmid DNA was quantified, and it was shown that electrojetted pDNA is still able to transfect cells with eGFP DNA. Notably, we were able to transfect a variety of cancer cell lines with eGFP pDNA by using a bicompartmental SPNPs made from Human Transferrin, using PEI as an endosomal escape polymer. Future work should focus on the development of a high throughput method to assay gene expression induced by SPNPs, perhaps by using a reporter gene like luciferase that is able to give results quickly and quantitatively on large-scale microplate assays. This work shows the potential to further develop SPNPs into an effective gene delivery device.

6.5 Future Outlook

The work presented in this dissertation provides a foundation for the synthesis, use and processing of Synthetic Protein Nanoparticles as a tool for drug delivery. A versatile method for their synthesis using a variety of materials was developed. The methods described are flexible and allow for multiple routes of research that can be further pursued. For example, particles with diverse geometries and anisotropies could be developed to deliver drugs in preprogrammed, material dependent, and stimuli responsive fashions. One could also envision the development of "nanobiomachines", SPNPs completely made from bio-derived materials such as proteins and carbohydrates, that are able to use enzymes in a preprogrammed manner to self-actuate, self-locomote, and perform actions, such as catalyze a chemical reaction, or transcribe cells with a genes, once at the desired location.

Much development is left to create technologies such as these, namely more sophisticated macromers whose chemistries are more controllable, work at smaller time scales, and use more bio-derived materials – perhaps engineered proteins with artificial amino acid residues. Additionally, release profiles of different drugs must be characterized, both in single and multi-compartment configurations of SPNPs, to completely characterize their therapeutic potentials. These, and many other unforeseeable hurdles must be crossed, but SPNPs made by EHD co-jetting hold significant potential to be impactful nanodevices.

Appendices

Appendix A

A Brief Geometric Analysis of Substrate Diffusion in Enzyme Loaded Synthetic Protein Nanoparticles

Applying 1D diffusion, we find that the following equation can be used to estimate whether a chemical reaction in a sphere will be diffusion limited:

$$Ø = \frac{qr^2}{DC}$$

Where q is the reaction rate of the chemical reaction, r is the radius of the sphere, D is the rate of diffusion of the substrate, and C is the bulk concentration of the substrate. Ø is a dimensionless number. In this analysis, it is assumed that the substrate concentration is high enough for q to be independent of C, and C(r)>>0. In a sphere, if Ø << 6, the diffusion rates are high enough to feed the reaction, and thus the reaction is not diffusion limited. This can translate over to a nanoparticle loaded with enzymes. In a particle that is diffusion limited, reaction rates will seem lower than an equivalent particle system that is not diffusion limited (higher C, smaller r).

Using this, we can estimate whether the two particle systems investigated are diffusion limited. Assuming that proteins have a mass to volume ratio of.[301]

$$V = (1.212 * 10^{-3}) * M\ (Da)$$

Alongside knowing the reaction rates of our proteins (2.8x106 molecules/protein for Catalase, 641 molecules/protein for Glucose Oxidase), the concentration of substrate in our

reaction, and the diffusion rates of the substrates in the nanoparticle (assuming Glucose will diffuse similarly to water in our particles,[302] and the rate for Hydrogen Peroxide was obtained from literature),[303] we can calculate Ø for the particles, and for particles that are made of enzymes at different loading rates :

Protein	*(w/w%)*	*Ø*
Catalase	5:95	585.7
	10:90	1193.6
	25:75	3164.0
	50:50	7034.8
GOX	5:95	0.0099
	10:90	0.0203
	25:75	0.0540
	50:50	0.1202

This result is intuitive. Catalase, which is the enzyme with the fastest known turnover rate, is incredibly diffusion limited, as all substrate that approaches the surface is quickly reacted. To achieve a particle that is not diffusion limited with the sizes possible using EHD co-jetting, particles would have to be loaded in the range of 0.0001% loading (around 2 enzyme molecules per nanoparticle). Glucose Oxidase, on the other hand, has a much slower reaction rate and this results in that all the particles are not diffusion limited. Even particles that are completely made of enzyme have Ø=0.31.

To compare these results to experimental data, it is most useful to look at the retained activities of the particles as a function of loaded enzyme(**Figure 3.5A**). As can be seen, both particle types seem to be diffusion limited, as the retained activities decrease as the amount of

enzyme in the particles increase. This disagrees with the analysis that predicts that the GOX particles should not be diffusion limited and thus the activity should stay constant, regardless of the loading.

This analysis does not cover the full picture. The substrates likely do not have the diffusion rates that are found in literature, as they have never been studied in this specific system. For example, it is well known that carbohydrates interact with proteins, HSA in particular, and this likely reduces the diffusion constant of glucose within the SPNPs.[304–307] Additionally, this analysis does not take into account enzyme inactivation, which is most likely occurring in the particles at some level. A full analysis of these particles would require measurements of the diffusion constants of each substrate within the protein matrices, which is outside the scope if this study.

Appendix B

Useful Protocols for Nanoparticle Surface Modification and Confocal Microscopy

Surface Modification with Copper Catalyzed Click Chemistry

This is a general protocol for the surface modification of Nanoparticles that are functionalizes with azide or alkyne groups. It can be modified for specific applications. Brands described were the ones used, but may be substituted

Materials Needed

- DI H_2O + 0.1%Tween
- Copper(II) Sulfate Pentrahydrate ($CuSO_{4.5}H_2O$)
- (+)-Sodium L-ascorbate ($C_6H_7NaO_6$)
- 0.01M Ethylenediaminetetraacetic acid (EDTA)
- 15 mL Centrifuge Tubes (Falcon Brand)
- 2.0 mL Microcentrifuge Tubes (Fisher Brand)

Procedure

1. Quantify your particle yield, be it by particle number, mass, or assays such a BCA
2. Pellet your particles, remove the supernatant, and resuspend the pellet in 900 µL of DI H_2O + 0.1% Tween. Sonicate for 5 sec at 1 sec on/5 sec off to disperse particles.
3. Make a 10x solution of Copper(II) Sulfate Pentrahydrate and (+)-Sodium L-ascorbate (13.3 mg $CuSO_{4.5}H_2O$ + 53.3 mg $C_6H_7NaO_6$ in 1 mL of DI H_2O + 0.1% Tween). Mix

until orange. Do not make a stock, place on rotator immediately after solubilizing and keep on rotator until used.

4. Add 100 µL of 10x $CuSO_4.5H_2O/C_6H_7NaO_6$ solution to the particle solution.
5. Add your desired mass of reactant. Aim for 5-10x molar excess to the estimated number of corresponding click reaction groups on your particles, be it azide or alkyne
6. Place on a rotator at room temperature, covered in foil, for 24 hours.
7. If the solution is clear: Wash with 5x with DI water and 0.1% tween.
8. If the solution is brown, or the pellet is brown if when you centrifuge down the particles for washing:
    a. Centrifuge and remove supernatant. Add 2 ml of EDTA solution and resuspend pellet. Leave for 2 hours or until solution is clear (but not more than 3 hr). If after 3 hr the solution is still brown, centrifuge, remove supernatant, and incubate with EDTA again. If you used too much copper, it might take a couple of times of this. Make sure to wash 5x with DI/tween after this to remove all the EDTA, as it is pretty toxic.

Cell Staining to Image Cells for Nanoparticle Uptake

This protocol is to stain cells after conducting an uptake experiment. This procedure begins after the incubation time of cells with particles is over. The volumes suggested assume that the cells were cultured in an 8 well chamber slide with removable wells (Nunc Lab-Tek II Chamber Slide System), but the volumes may be adjusted to be higher or lower, as long as the volumes used completely cover the bottom of each well. The specific dyes described here will stain a nuclei blue (DAPI laser line), and the actin fibers green (FITC laser line). This protocol has been used to stain HeLa, REN, and SK-N-BE(2) with good results, and should work with most adherent cell lines, but the specific dye concentrations may need to be adjusted to obtain optimal images.

Materials Needed

Percentage values are all mass based, except for formalin and Alexa-488 Phalloidin, which is volume based.

- Sterile PBS for cell fixation steps
- Clean PBS, no need for sterility but should be a container specifically used for staining
- Fixing Solution
    - PBS + 4% formalin, or commercial methanol free fixing agent. 200 µL per sample.
- Permeabilization Solution
    - PBS + 0.1% Triton-X + 1% BSA. 250 µL per sample.
- Blocking Solution
    - PBS + 1% BSA, 1 mL per sample.

- Staining Solution
    - PBS + 2.5% Alexa-488 Phalloidin + 1% BSA. 250 µL per sample.
- Prolong Diamond + DAPI
    - Allow to come to room temp before use, Around 10 µL per sample.
- Coverslips for your desired application
    - Be careful, coverslips of the wrong thickness can distort images in confocal microscopy.
    - I like corning brand (Corning #2980225) for chamber slides.

Procedure

Cell Fixation

- Remove experimental media, and carefully wash each well with sterile PBS (with same volume used in experiment, gently sway slide back and forth 3-4 times for all washes)
- Remove PBS
- Add 200 µL 4% formalin/PBS mix, incubate for 10 min
- Remove formalin
- Wash at least 2 times w/PBS

Stop point: Samples can be stored at this point for a week at 4 °C, covered well in foil, preferably with lid parafilmed. I try to stain within 2-3 days.

Alexa-488 Phalloidin Stain

- Incubate with 200 µL of 0.1%Triton-X+1% BSA in PBS for 3-5 minutes.

    - Very time sensitive. Try to treat all your wells for the same amount of time to ensure even staining.
- Wash at least 3 times w/ PBS + 1% BSA, leave last wash in the well. The last wash should stay in the well for 20-30 minutes.
    - This is your non-specific staining blocking step. The longer you incubate, the dimmer your Actin stain will be, but the lower your background. HeLa cells worked well with a 20-minute incubation.
- Remove the PBS wash and place 200 μL of the below solution in each well.
    - PBS + 2.5% Alexa-488 Phalloidin + 1% BSA
- Incubate in a dark box for 20 minutes.
- Wash at least 2 times w/PBS

Fixing with Prolong Diamond + DAPI

- Remove last wash, remove slide wells, and allow to air dry in the dark (around 20-30 minutes).
- Place a drop of Prolong Diamond + DAPI (around 10 μL) on each well, and place coverslip on top.
    - Be gentle and careful, try to avoid bubbles.
    - Allowing the Prolong Diamond to fully come to room temp, and letting it sit for 20 or so minutes so all the bubbles rise will help with this.
- Allow Prolong Diamond to cure in a dark place for at least 24 hr.

Tips for a successful stain:

- My recommendation is that you stain no more than 2 slides at a time until you are well practiced at the procedure.
- Make your solutions before you start working.
- You can make stocks of 100X Triton-X and 10X BSA, but keep track of when you make the solutions, store at 4 °C, and do not use past 2-3 months, or if you see visible precipitates.
- Work in the dark to stop photobleaching. My practice is to use a non-direct source of light to see by.
- Key is consistency, patience, gentleness, and consistency. Yes, that was on purpose, getting consistent stains is probably the hardest part of all of this.
- Take your time, except for the points that have specific incubation times. If you rush it, you will reduce with the quality of your stain.
- Make sure to minimize touching the bottom of the well with your pipette. My practice is to pick a corner, and always have that be the part you touch when removing volumes.
- Always switch tips when removing solutions, but you can reuse tips when adding solutions if you are sure that no part of the well has been touch by the tip.
- When adding liquids to wells, “waterfall” them down the walls of the well. Do not directly release the volume over the bottom of the well, this can damage/cause cells to detach.
- Placing coverslip atop the cells with the Prolong Diamond without introducing bubbles is tricky. I recommend practicing either with a slide that has nothing in it, or with your controls, before working with experimental samples.

References

1. Bayda, S., Adeel, M., Tuccinardi, T., Cordani, M. & Rizzolio, F. The history of nanoscience and nanotechnology: From chemical-physical applications to nanomedicine. *Molecules* **25**, (2020).

2. Feynman, R. There's plenty of room at the bottom. in *Feynman and Computation* **XXIII**, 63–76 (2018).

3. Editorial: 'Plenty of room' revisited. *Nature Nanotechnology* **4**, 781 (2009).

4. Gramling, H. M., Kiziroglou, M. E. & Yeatman, E. M. Nanotechnology for Consumer Electronics. in *Nanoelectronics: Materials, Devices, Applications* **1**, 501–526 (2017).

5. Friederich, P. *et al.* Toward Design of Novel Materials for Organic Electronics. *Adv. Mater.* **31**, 1808256 (2019).

6. Shafique, M. & Luo, X. Nanotechnology in transportation vehicles: An overview of its applications, environmental, health and safety concerns. *Materials* **12**, 2493 (2019).

7. Adams, A. *et al.* Vantablack properties in commercial thermal infrared imaging systems. in *Infrared Imaging Systems: Design, Analysis, Modeling, and Testing XXX* (eds. Krapels, K. A. & Holst, G. C.) **11001**, 28 (SPIE, 2019).

8. Theocharous, S. P., Theocharous, E. & Lehman, J. H. The evaluation of the performance of two pyroelectric detectors with vertically aligned multi-walled carbon nanotube coatings. *Infrared Phys. Technol.* **55**, 299–305 (2012).

9. de Keijzer, M. Meet the Future: The Creation of New Pigments. in *Conservation of Modern Oil Paintings* 61–75 (Springer International Publishing, 2019). doi:10.1007/978-3-030-19254-9_4

10. Elvin, G. Nanotechnology in Architecture. in *Nanotechnology for Energy Sustainability* 967–996 (Wiley-VCH Verlag GmbH & Co. KGaA, 2017). doi:10.1002/9783527696109.ch39

11. Baglioni, P. & Chelazzi, D. Nanoscience for the Conservation of Works of Art. in *Nanoscience for the Conservation of Works of Art* (eds. Baglioni, P. & Chelazzi, D.) (Royal Society of Chemistry, 2013). doi:10.1039/9781849737630

12. Schlather, A. E., Gieri, P., Robinson, M., Centeno, S. A. & Manjavacas, A. Nineteenth-century nanotechnology: The plasmonic properties of daguerreotypes. *Proc. Natl. Acad. Sci. U. S. A.* **116**, 13791–13798 (2019).

13. Shabunya-Klyachkovskaya, E. V., Kulakovich, O. S. & Gaponenko, S. V. Surface enhanced Raman scattering of inorganic microcrystalline art pigments for systematic cultural heritage studies. *Spectrochim. Acta - Part A Mol. Biomol. Spectrosc.* **222**, 117235 (2019).

14. Peer, D. *et al.* Nanocarriers as an emerging platform for cancer therapy. *Nat. Nanotechnol.* **2**, 751–760 (2007).

15. Shi, J., Votruba, A. R., Farokhzad, O. C. & Langer, R. Nanotechnology in drug delivery and tissue engineering: From discovery to applications. *Nano Lett.* **10**, 3223–3230 (2010).

16. Nakamura, H., Jun, F. & Maeda, H. Development of next-generation macromolecular drugs based on the EPR effect: challenges and pitfalls. *Expert Opin. Drug Deliv.* **12**, 53–64 (2015).

17. Kukowska-Latallo, J. F. *et al.* Nanoparticle targeting of anticancer drug improves therapeutic response in animal model of human epithelial cancer. *Cancer Res.* **65**, 5317–5324 (2005).

18. Brannon-Peppas, L. & Blanchette, J. O. Nanoparticle and targeted systems for cancer therapy. *Adv. Drug Deliv. Rev.* **64**, 206–212 (2012).

19. Indira, T. K. & Lakshmi, P. K. Magnetic Nanoparticles-A Review. *Intyernational J. Pharm. Sci. Nanotechnol.* **3**, 1035–1042 (2010).

20. Fu, C. & Ravindra, N. M. Magnetic iron oxide nanoparticles: Synthesis and applications. *Bioinspired, Biomim. Nanobiomaterials* **1**, 229–244 (2012).

21. Brenner, J. S. *et al.* Red blood cell-hitchhiking boosts delivery of nanocarriers to chosen organs by orders of magnitude. *Nat. Commun.* (2018). doi:10.1038/s41467-018-05079-7

22. Wayteck, L. *et al.* Biomaterials Hitchhiking nanoparticles : Reversible coupling of lipid-based nanoparticles to cytotoxic T lymphocytes. *Biomaterials* **77**, 243–254 (2016).

23. Anselmo, A. C. & Mitragotri, S. Cell-mediated delivery of nanoparticles: Taking advantage of circulatory cells to target nanoparticles. *Journal of Controlled Release* (2014). doi:10.1016/j.jconrel.2014.03.050

24. Anselmo, A. C. *et al.* Exploiting shape, cellular-hitchhiking and antibodies to target nanoparticles to lung endothelium: Synergy between physical, chemical and biological approaches. *Biomaterials* (2015). doi:10.1016/j.biomaterials.2015.07.043

25. Mura, S., Nicolas, J. & Couvreur, P. Stimuli-responsive nanocarriers for drug delivery. *Nature Materials* **12**, 991–1003 (2013).

26. Cheng, R., Meng, F., Deng, C., Klok, H. A. & Zhong, Z. Dual and multi-stimuli responsive polymeric nanoparticles for programmed site-specific drug delivery. *Biomaterials* **34**, 3647–3657 (2013).

27. Pelaz, B. *et al.* Diverse Applications of Nanomedicine. *ACS Nano* **11**, 2313–2381 (2017).

28. Shi, J., Kantoff, P. W., Wooster, R. & Farokhzad, O. C. Cancer nanomedicine: Progress, challenges and opportunities. *Nature Reviews Cancer* **17**, 20–37 (2017).

29. Barenholz, Y. (Chezy). Doxil® — The first FDA-approved nano-drug: Lessons learned. *J. Control. Release* **160**, 117–134 (2012).

30. Yang, Y., Wang, L., Wan, B., Gu, Y. & Li, X. Optically Active Nanomaterials for Bioimaging and Targeted Therapy. *Frontiers in Bioengineering and Biotechnology* **7**, 320 (2019).

31. Battistelli, G., Cantelli, A., Guidetti, G., Manzi, J. & Montalti, M. Ultra-bright and stimuli-responsive fluorescent nanoparticles for bioimaging. *Wiley Interdiscip. Rev. Nanomedicine Nanobiotechnology* **8**, 139–150 (2016).

32. Du, J., Xu, N., Fan, J., Sun, W. & Peng, X. Carbon Dots for In Vivo Bioimaging and Theranostics. *Small* **15**, 1805087 (2019).

33. Wolfbeis, O. S. An overview of nanoparticles commonly used in fluorescent bioimaging. *Chemical Society Reviews* **44**, 4743–4768 (2015).

34. Kircher, M. F. *et al.* A brain tumor molecular imaging strategy using a new triple-modality MRI-photoacoustic-Raman nanoparticle. *Nat. Med.* **18**, 829–834 (2012).

35. Chen, F., Ehlerding, E. B. & Cai, W. Theranostic nanoparticles. *J. Nucl. Med.* **55**, 1919–1922 (2014).

36. Gao, D. & Yuan, Z. Photoacoustic-based multimodal nanoprobes: From constructing to biological applications. *Int. J. Biol. Sci.* **13**, 401–412 (2017).

37. Chen, X., Song, J., Chen, X. & Yang, H. X-ray-activated nanosystems for theranostic applications. *Chemical Society Reviews* **48**, 3073–3101 (2019).

38. Guo, X., Shi, C., Wang, J., Di, S. & Zhou, S. PH-triggered intracellular release from actively targeting polymer micelles. *Biomaterials* **34**, 4544–4554 (2013).

39. Gao, W., Chan, J. M. & Farokhzad, O. C. PH-responsive nanoparticles for drug delivery. *Molecular Pharmaceutics* **7**, 1913–1920 (2010).

40. Alejo, T., Uson, L. & Arruebo, M. Reversible stimuli-responsive nanomaterials with on-off switching ability for biomedical applications. *Journal of Controlled Release* **314**, 162–176 (2019).

41. Lu, C. & Urban, M. W. Stimuli-responsive polymer nano-science: Shape anisotropy, responsiveness, applications. *Progress in Polymer Science* **78**, 24–46 (2018).

42. Hu, Q., Katti, P. S. & Gu, Z. Enzyme-responsive nanomaterials for controlled drug delivery. *Nanoscale* **6**, 12273–12286 (2014).

43. Pan, U. N. *et al.* Protein-Based Multifunctional Nanocarriers for Imaging, Photothermal Therapy, and Anticancer Drug Delivery. *ACS Appl. Mater. Interfaces* **9**, 19495–19501 (2017).

44. Chen, Q. *et al.* Drug-induced self-assembly of modified albumins as nano-theranostics for tumor-targeted combination therapy. *ACS Nano* **9**, 5223–5233 (2015).

45. Chou, L. Y. T., Zagorovsky, K. & Chan, W. C. W. DNA assembly of nanoparticle superstructures for controlled biological delivery and elimination. *Nat. Nanotechnol.* **9**, 148–155 (2014).

46. Xing, P. & Zhao, Y. Multifunctional Nanoparticles Self-Assembled from Small Organic Building Blocks for Biomedicine. *Adv. Mater.* **28**, 7304–7339 (2016).

47. Chaudhary, A. & Yadav, R. D. A review on virus protein self-assembly. *Journal of Nanoparticle Research* **21**, 1–13 (2019).

48. Anselmo, A. C. & Mitragotri, S. Nanoparticles in the clinic: An update. *Bioeng. Transl. Med.* **4**, (2019).

49. CDER. New Drugs at FDA: CDER's New Molecular Entities and New Therapeutic Biological Products. *FDA* (2016). Available at: https://www.fda.gov/drugs/development-approval-process-drugs/new-drugs-fda-cders-new-molecular-entities-and-new-therapeutic-biological-products. (Accessed: 5th June 2020)

50. de Lázaro, I. & Mooney, D. J. A nanoparticle's pathway into tumours. *Nature Materials* **19**, 486–487 (2020).

51. Darrow, J. J., Avorn, J. & Kesselheim, A. S. FDA Approval and Regulation of Pharmaceuticals, 1983-2018. *JAMA - J. Am. Med. Assoc.* **323**, 164–176 (2020).

52. Wilhelm, S. *et al.* Analysis of nanoparticle delivery to tumours. *Nature Reviews Materials* **1**, 1–12 (2016).

53. Huynh, E. & Zheng, G. Cancer nanomedicine: Addressing the dark side of the enhanced permeability and retention effect. *Nanomedicine* **10**, 1993–1995 (2015).

54. Nel, A., Ruoslahti, E. & Meng, H. New Insights into 'permeability' as in the Enhanced Permeability and Retention Effect of Cancer Nanotherapeutics. *ACS Nano* **11**, 9567–9569 (2017).

55. Nakamura, Y., Mochida, A., Choyke, P. L. & Kobayashi, H. Nanodrug Delivery: Is the Enhanced Permeability and Retention Effect Sufficient for Curing Cancer? *Bioconjugate Chemistry* **27**, 2225–2238 (2016).

56. Kim, S. M., Faix, P. H. & Schnitzer, J. E. Overcoming key biological barriers to cancer drug delivery and efficacy. *J. Control. Release* **267**, 15–30 (2017).

57. Danhier, F. To exploit the tumor microenvironment: Since the EPR effect fails in the clinic, what is the future of nanomedicine? *Journal of Controlled Release* **244**, 108–121 (2016).

58. Nichols, J. W. & Bae, Y. H. EPR: Evidence and fallacy. *Journal of Controlled Release* **190**, 451–464 (2014).

59. Sindhwani, S. *et al.* The entry of nanoparticles into solid tumours. *Nat. Mater.* **19**, 566–575 (2020).

60. Gerlowski, L. E. & Jain, R. K. Microvascular permeability of normal and neoplastic tissues. *Microvasc. Res.* **31**, 288–305 (1986).

61. Matsumura, Y. & Maeda, H. A New Concept for Macromolecular Therapeutics in Cancer Chemotherapy: Mechanism of Tumoritropic Accumulation of Proteins and the Antitumor Agent Smancs. *Cancer Res.* **46**, 6387–6392 (1986).

62. Shang, L., Nienhaus, K. & Nienhaus, G. U. Engineered nanoparticles interacting with cells: Size matters. *Journal of Nanobiotechnology* **12**, 1–11 (2014).

63. Zhang, S., Li, J., Lykotrafitis, G., Bao, G. & Suresh, S. Size-dependent endocytosis of nanoparticles. *Adv. Mater.* **21**, 419–424 (2009).

64. Sparreboom, A. *et al.* Comparative Preclinical and Clinical Pharmacokinetics of a Cremophor-Free, Nanoparticle Albumin-Bound Paclitaxel (ABI-007) and Paclitaxel Formulated in Cremophor (Taxol). *Clin. Cancer Res.* **11**, 4136–4143 (2005).

65. Desai, N. Technology: A Drug Delivery Platform Utilising Endothelial gp60 Receptor-based Transport and Tumour-derived SPARC for Targeting". *Drug Deliv. Rep.* **505**, 1–9 (2010).

66. Minshall, R. D. *et al.* Endothelial cell-surface gp60 activates vesicle formation and trafficking via G(i)-coupled Src kinase signaling pathway. *J. Cell Biol.* **150**, 1057–1069 (2000).

67. Tiruppathi, C., Song, W., Bergenfeldt, M., Sass, P. & Malik, A. B. Gp60 activation mediates albumin transcytosis in endothelial cells by tyrosine kinase-dependent pathway. *J. Biol. Chem.* **272**, 25968–25975 (1997).

68. Sehnal, D., Rose, A., Koča, J., Burley, S. & Velankar, S. Mol*: towards a common library and tools for web molecular graphics. in *Proceedings of the workshop on molecular graphics and visual analysis of molecular data* 29–33 (2018). doi:10.2312/molva.20181103

69. Arunachalam, B., Phan, U. T., Geuze, H. J. & Cresswell, P. Enzymatic reduction of disulfide bonds in lysosomes: Characterization of a gamma-interferon-inducible lysosomal thiol reductase (GILT). *Proc. Natl. Acad. Sci. U. S. A.* **97**, 745–750 (2000).

70. Saito, G., Swanson, J. A. & Lee, K. D. Drug delivery strategy utilizing conjugation via reversible disulfide linkages: Role and site of cellular reducing activities. *Adv. Drug Deliv. Rev.* **55**, 199–215 (2003).

71. Arroyo, M., De La Mata, I., Acebal, C. & Castillón, M. P. Biotechnological applications of penicillin acylases: State-of-the-art. *Applied Microbiology and Biotechnology* **60**, 507–514 (2003).

72. Wiegand, G. & Remington, S. J. Citrate synthase: structure, control, and mechanism. *Annual review of biophysics and biophysical chemistry* **15**, 97–117 (1986).

73. Adelstein, R. S. & Eisenberg, E. Regulation and Kinetics of the Actin-Myosin-ATP Interaction. *Annu. Rev. Biochem.* **49**, 921–956 (1980).

74. Rayment, I. *et al.* Structure of the actin-myosin complex and its implications for muscle contraction. *Science (80-.).* **261**, 58–65 (1993).

75. Daniels, T. R. *et al.* The transferrin receptor and the targeted delivery of therapeutic agents against cancer. *Biochim. Biophys. Acta - Gen. Subj.* **1820**, 291–317 (2012).

76. Leader, B., Baca, Q. J. & Golan, D. E. Protein therapeutics: a summary and pharmacological classification. *Nat. Rev. Drug Discov.* **7**, 21–39 (2008).

77. Reichert, J. M. Monoclonal antibodies in the clinic. *Nature Biotechnology* **19**, 819–822 (2001).

78. Strohl, W. R. Current progress in innovative engineered antibodies. *Protein and Cell* **9**, 86–120 (2018).

79. Muzykantov, V. R. Targeting of superoxide dismutase and catalase to vascular endothelium. *J. Control. Release* **71**, 1–21 (2001).

80. Beckman, J. S. & Koppenol, W. H. Nitric oxide, superoxide, and peroxynitrite: the good, the bad, and ugly. *Am. J. Physiol.* **271**, C1424-37 (1996).

81. Nicholls, P. Classical catalase: Ancient and modern. *Arch. Biochem. Biophys.* **525**, 95–101 (2012).

82. Singla, A. K., Garg, A. & Aggarwal, D. Paclitaxel and its formulations. *Int. J. Pharm.* **235**, 179–192 (2002).

83. Habibi, N., Quevedo, D. F., Gregory, J. V. & Lahann, J. Emerging methods in therapeutics using multifunctional nanoparticles. *Wiley Interdisciplinary Reviews: Nanomedicine and Nanobiotechnology* e1625 (2020). doi:10.1002/wnan.1625

84. Thao, L. Q. *et al.* Doxorubicin and paclitaxel co-bound lactosylated albumin nanoparticles having targetability to hepatocellular carcinoma. *Colloids Surfaces B Biointerfaces* **152**, 183–191 (2017).

85. Maruyama, T. *et al.* Improved anticancer effects of albumin-bound paclitaxel nanoparticle via augmentation of EPR effect and albumin-protein interactions using S -nitrosated human serum albumin dimer. *Biomaterials* **140**, 162–169 (2017).

86. Ruttala, H. B. & Ko, Y. T. Liposome encapsulated albumin-paclitaxel nanoparticle for enhanced antitumor efficacy. *Pharm. Res.* **32**, 1002–1016 (2015).

87. Ruttala, H. B. *et al.* Layer-by-layer assembly of hierarchical nanoarchitectures to enhance the systemic performance of nanoparticle albumin-bound paclitaxel. *Int. J. Pharm.* **519**, 11–21 (2017).

88. Chen, J. *et al.* Radionuclide I-131 Labeled Albumin-Paclitaxel Nanoparticles for Synergistic Combined Chemo-radioisotope Therapy of Cancer. *Theranostics* **7**, 614–623 (2017).

89. Ruttala, H. B. & Ko, Y. T. Liposomal co-delivery of curcumin and albumin/paclitaxel nanoparticle for enhanced synergistic antitumor efficacy. *Colloids Surfaces B Biointerfaces* **128**, 419–426 (2015).

90. Neil P. Desai. Nanoparticle Compositions of Albumin and Paclitaxel. (2014).

91. Estrada, L. H., Chu, S. & Champion, J. A. Protein nanoparticles for intracellular delivery of therapeutic enzymes. *J. Pharm. Sci.* **103**, 1863–1871 (2014).

92. Hawkins, M. J., Soon-Shiong, P. & Desai, N. Protein nanoparticles as drug carriers in clinical medicine. *Adv. Drug Deliv. Rev.* **60**, 876–885 (2008).

93. Tan, Y. L. & Ho, H. K. Navigating albumin-based nanoparticles through various drug delivery routes. *Drug Discov. Today* **23**, 1108–1114 (2018).

94. Yeates, T. O., Liu, Y. & Laniado, J. The design of symmetric protein nanomaterials comes of age in theory and practice. *Curr. Opin. Struct. Biol.* **39**, 134–143 (2016).

95. Arai, R. Hierarchical design of artificial proteins and complexes toward synthetic structural biology. *Biophys. Rev.* **10**, 391–410 (2018).

96. Molino, N. M. & Wang, S. W. Caged protein nanoparticles for drug delivery. *Curr. Opin. Biotechnol.* **28**, 75–82 (2014).

97. Kaczmarczyk, S. J., Sitaraman, K., Young, H. A., Hughes, S. H. & Chatterjee, D. K. Protein delivery using engineered virus-like particles. *Proc. Natl. Acad. Sci.* **108**, 16998–17003 (2011).

98. Zhen, Z. *et al.* RGD-modified apoferritin nanoparticles for efficient drug delivery to tumors. *ACS Nano* **7**, 4830–4837 (2013).

99. Kawakami, N. *et al.* Design of Hollow Protein Nanoparticles with Modifiable Interior and Exterior Surfaces. *Angew. Chemie - Int. Ed.* **57**, 12400–12404 (2018).

100. Ecker, D. M., Jones, S. D. & Levine, H. L. The therapeutic monoclonal antibody market. *mAbs* **7**, 9–14 (2015).

101. Weber, C., Coester, C., Kreuter, J. & Langer, K. Desolvation process and surface characterisation of protein nanoparticles. *Int. J. Pharm.* **194**, 91–102 (2000).

102. Von Storp, B., Engel, A., Boeker, A., Ploeger, M. & Langer, K. Albumin nanoparticles with predictable size by desolvation procedure. *J. Microencapsul.* **29**, 138–146 (2012).

103. Langer, K. *et al.* Human serum albumin (HSA) nanoparticles: Reproducibility of preparation process and kinetics of enzymatic degradation. *Int. J. Pharm.* **347**, 109–117 (2008).

104. Dreis, S. *et al.* Preparation, characterisation and maintenance of drug efficacy of doxorubicin-loaded human serum albumin (HSA) nanoparticles. *Int. J. Pharm.* **341**, 207–214 (2007).

105. Herrera Estrada, L. P. & Champion, J. A. Protein nanoparticles for therapeutic protein delivery. *Biomater. Sci.* **3**, 787–799 (2015).

106. Fathi, M., Donsi, F. & McClements, D. J. Protein-Based Delivery Systems for the Nanoencapsulation of Food Ingredients. *Comprehensive Reviews in Food Science and Food Safety* **17**, 920–936 (2018).

107. Shao, S., Shen, X. & Guo, M. Zinc-loaded whey protein nanoparticles prepared by enzymatic cross-linking and desolvation. *Int. J. Food Sci. Technol.* **53**, 2205–2211 (2018).

108. Chang, T. Z., Stadmiller, S. S., Staskevicius, E. & Champion, J. A. Effects of ovalbumin protein nanoparticle vaccine size and coating on dendritic cell processing. *Biomater. Sci.* **5**, 223–233 (2017).

109. Tsoras, A. N. & Champion, J. A. Cross-Linked Peptide Nanoclusters for Delivery of Oncofetal Antigen as a Cancer Vaccine. *Bioconjug. Chem.* **29**, 776–785 (2018).

110. Deng, L. *et al.* Double-layered protein nanoparticles induce broad protection against divergent influenza A viruses. *Nat. Commun.* **9**, 359 (2018).

111. Fiers, W. *et al.* M2e-based universal influenza A vaccine. *Vaccine* **27**, 6280–6283 (2009).

112. Turley, C. B. *et al.* Safety and immunogenicity of a recombinant M2e–flagellin influenza vaccine (STF2.4xM2e) in healthy adults. *Vaccine* **29**, 5145–5152 (2011).

113. Chang, T. Z., Deng, L., Wang, B.-Z. & Champion, J. A. H7 Hemagglutinin nanoparticles retain immunogenicity after >3 months of 25 degrees C storage. *PLoS One* **13**, e0202300 (2018).

114. Arnold, F. H. Directed Evolution: Bringing New Chemistry to Life. *Angew. Chemie Int. Ed.* **57**, 4143–4148 (2018).

115. Roh, K., Martin, D. C. & Lahann, J. Biphasic Janus particles with nanoscale anisotropy. *Nat. Mater.* **4**, 759–63 (2005).

116. Saha, S. *et al.* Chemically controlled bending of compositionally anisotropic microcylinders. *Angew. Chemie - Int. Ed.* **51**, 660–665 (2012).

117. Rahmani, S. & Lahann, J. Recent progress with multicompartmental nanoparticles. *MRS Bull.* **39**, 251–257 (2014).

118. Lee, K. J., Yoon, J. & Lahann, J. Recent advances with anisotropic particles. *Current Opinion in Colloid and Interface Science* **16**, 195–202 (2011).

119. Lahann, J. Recent progress in nano-biotechnology: Compartmentalized micro- and nanoparticles via electrohydrodynamic co-jetting. *Small* **7**, 1149–1156 (2011).

120. Jordahl, J. H. *et al.* 3D Jet Writing: Functional Microtissues Based on Tessellated Scaffold Architectures. *Adv. Mater.* **30**, (2018).

121. Jordahl, J. H., Ramcharan, S., Gregory, J. V. & Lahann, J. Needleless Electrohydrodynamic Cojetting of Bicompartmental Particles and Fibers from an Extended Fluid Interface. *Macromol. Rapid Commun.* **38**, 1600437 (2017).

122. Rahmani, S. *et al.* Chemically orthogonal three-patch microparticles. *Angew. Chemie - Int. Ed.* **53**, 2332–2338 (2014).

123. Yoon, J., Eyster, T. W., Misra, A. C. & Lahann, J. Cardiomyocyte-Driven Actuation in Biohybrid Microcylinders. *Adv. Mater.* **27**, 4509–4515 (2015).

124. Bhaskar, S., Roh, K. H., Jiang, X., Baker, G. L. & Lahann, J. Spatioselective modification of bicompartmental polymer particles and fibers via huisgen 1,3 -dipolar cycloaddition. *Macromol. Rapid Commun.* **29**, 1655–1660 (2008).

125. Misra, A. C., Luker, K. E., Durmaz, H., Luker, G. D. & Lahann, J. CXCR4-Targeted Nanocarriers for Triple Negative Breast Cancers. *Biomacromolecules* **16**, 2412–2417 (2015).

126. Misra, A. C., Bhaskar, S., Clay, N. & Lahann, J. Multicompartmental particles for combined imaging and siRNA delivery. *Adv. Mater.* **24**, 3850–3856 (2012).

127. Rahmani, S., Park, T. H., Dishman, A. F. & Lahann, J. Multimodal delivery of irinotecan from microparticles with two distinct compartments. *J. Control. Release* **172**, 239–245 (2013).

128. Shi, J., Kantoff, P. W., Wooster, R. & Farokhzad, O. C. Cancer nanomedicine: Progress, challenges and opportunities. *Nat. Rev. Cancer* **17**, 20–37 (2017).

129. Senapati, S., Mahanta, A. K., Kumar, S. & Maiti, P. Controlled drug delivery vehicles for cancer treatment and their performance. *Signal Transduct. Target. Ther.* **3**, 1–19 (2018).

130. Xin, Y., Yin, M., Zhao, L., Meng, F. & Luo, L. Recent progress on nanoparticle-based drug delivery systems for cancer therapy. *Cancer Biol. Med.* **14**, 228–241 (2017).

131. Ragelle, H., Danhier, F., Préat, V., Langer, R. & Anderson, D. G. Nanoparticle-based drug delivery systems: a commercial and regulatory outlook as the field matures. *Expert Opin. Drug Deliv.* **14**, 851–864 (2017).

132. Habibi, N., Quevedo, D. F., Gregory, J. V. & Lahann, J. Emerging methods in therapeutics using multifunctional nanoparticles. *Wiley Interdisciplinary Reviews: Nanomedicine and Nanobiotechnology* e1625 (2020). doi:10.1002/wnan.1625

133. Blanco, E., Shen, H. & Ferrari, M. perspective Principles of nanoparticle design for overcoming biological barriers to drug delivery. **33**, 941–951 (2015).

134. Geiger, B. C., Wang, S., Jr, R. F. P., Grodzinsky, A. J. & Hammond, P. T. Cartilage-penetrating nanocarriers improve delivery and efficacy of growth factor treatment of osteoarthritis. **1**, (2018).

135. Rahmani, S. *et al.* Chemically orthogonal three-patch microparticles. *Angew. Chemie - Int. Ed.* **53**, 2332–2338 (2014).

136. Varadharajan, D., Turgut, H., Lahann, J., Yabu, H. & Delaittre, G. Surface-Reactive Patchy Nanoparticles and Nanodiscs Prepared by Tandem Nanoprecipitation and Internal Phase Separation. **1800846**, 1–11 (2018).

137. Jain, A., Singh, S. K., Arya, S. K., Kundu, S. C. & Kapoor, S. Protein Nanoparticles: Promising Platforms for Drug Delivery Applications. *ACS Biomaterials Science and Engineering* **4**, 3939–3961 (2018).

138. Gawde, K. A. *et al.* Paclitaxel and di-fluorinated curcumin loaded in albumin nanoparticles for targeted synergistic combination therapy of ovarian and cervical cancers. *Colloids Surfaces B Biointerfaces* **167**, 8–19 (2018).

139. Deng, L. *et al.* Double-layered protein nanoparticles induce broad protection against divergent influenza A viruses. *Nat. Commun.* **9**, (2018).

140. Guo, Z. *et al.* Antitumor effect of gemcitabine-loaded albumin nanoparticle on gemcitabine-resistant pancreatic cancer induced by low hENT1 expression. *Int. J. Nanomedicine* **13**, 4869–4880 (2018).

141. Yu, X. *et al.* Activatable Protein Nanoparticles for Targeted Delivery of Therapeutic Peptides. *Adv. Mater.* **30**, 1705383 (2018).

142. Socinski, M. a *et al.* Weekly nab-paclitaxel in combination with carboplatin versus solvent-based paclitaxel plus carboplatin as first-line therapy in patients with advanced non-small-cell lung cancer: Final results of a phase III trial. *J. Clin. Oncol.* **30**, 2055–2062 (2012).

143. ABRAXANE® for Injectable Suspension (paclitaxel protein-bound particles for injectable suspension) (albumin-bound). *Federal Drug Administartion* (2013). Available at: https://www.accessdata.fda.gov/drugsatfda_docs/label/2013/021660s037lbl.pdf. (Accessed: 8th May 2020)

144. Rahmani, S. & Lahann, J. Recent progress with multicompartmental nanoparticles. *MRS Bull.* **39**, 251–257 (2014).

145. Roh, K. H., Martin, D. C. & Lahann, J. Biphasic Janus particles with nanoscale anisotropy. *Nat. Mater.* **4**, 759–763 (2005).

146. Rahmani, S. *et al.* Chemically orthogonal three-patch microparticles. *Angew. Chemie - Int. Ed.* **53**, 2332–2338 (2014).

147. Rahmani, S. *et al.* Long-circulating Janus nanoparticles made by electrohydrodynamic co-jetting for systemic drug delivery applications. *J. Drug Target.* **23**, 750–758 (2015).

148. Misra, A. C., Luker, K. E., Durmaz, H., Luker, G. D. & Lahann, J. CXCR4-Targeted Nanocarriers for Triple Negative Breast Cancers. *Biomacromolecules* **16**, 2412–2417 (2015).

149. Misra, A. C., Bhaskar, S., Clay, N. & Lahann, J. Multicompartmental particles for combined imaging and siRNA delivery. *Adv. Mater.* **24**, 3850–3856 (2012).

150. Rahmani, S. *et al.* Engineering of nanoparticle size via electrohydrodynamic jetting. *Bioeng. Transl. Med.* **1**, 82–93 (2016).

151. Rahmani, S., Park, T., Frances, A. & Lahann, J. Multimodal delivery of irinotecan from microparticles with two distinct compartments. *J. Control. Release* **172**, 239–245 (2013).

152. Rahmani, S. *et al.* Dual Release Carriers for Cochlear Delivery. *Adv. Healthc. Mater.* **5**, 94–100 (2016).

153. Sokolovskaya, E., Rahmani, S., Misra, A. C., Bräse, S. & Lahann, J. Dual-Stimuli-Responsive Microparticles. *ACS Appl. Mater. Interfaces* **7**, 9744–9751 (2015).

154. Greenfield, N. J. Using circular dichroism spectra to estimate protein secondary structure. *Nat. Protoc.* **1**, 2876–2890 (2007).

155. Greenfield, N. J. Using circular dichroism spectra to estimate protein secondary structure. *Nat. Protoc.* **1**, 2876–2890 (2007).

156. James, N. G. & Mason, A. B. Protocol to determine accurate absorption coefficients for iron-containing transferrins. *Anal. Biochem.* **378**, 202–207 (2008).

157. Sreerama, N. & Woody, R. W. Estimation of protein secondary structure from circular dichroism spectra: Comparison of CONTIN, SELCON, and CDSSTR methods with an expanded reference set. *Anal. Biochem.* **287**, 252–260 (2000).

158. Sreerama, N. & Woody, R. W. A Self-Consistent Method for the Analysis of Protein Secondary Structure from Circular Dichroism. *Anal. Biochem.* **209**, 32–44 (1993).

159. Provencher, S. W. & Glöckner, J. Estimation of Globular Protein Secondary Structure from Circular Dichroism. *Biochemistry* **20**, 33–37 (1981).

160. Compton, L. A. & Johnson, W. C. Analysis of protein circular dichroism spectra for secondary structure using a simple matrix multiplication. *Anal. Biochem.* **155**, 155–167 (1986).

161. Whitmore, L. & Wallace, B. A. Protein secondary structure analyses from circular dichroism spectroscopy: Methods and reference databases. *Biopolymers* **89**, 392–400 (2008).

162. Bhaskar, S., Pollock, K. M., Yoshida, M. & Lahann, J. Towards designer microparticles: simultaneous control of anisotropy, shape and size. *Small* **6**, 404–411 (2010).

163. Taylor, G. I. Disintegration of water drops in an electric field. *Proc. R. Soc. London. Ser. A. Math. Phys. Sci.* **280**, 383–397 (1964).

164. Migneault, I., Dartiguenave, C., Bertrand, M. J. & Waldron, K. C. Glutaraldehyde: Behavior in aqueous solution, reaction with proteins, and application to enzyme crosslinking. *BioTechniques* **37**, 790–802 (2004).

165. Ulbrich, K., Hekmatara, T., Herbert, E. & Kreuter, J. Transferrin- and transferrin-receptor-antibody-modified nanoparticles enable drug delivery across the blood-brain barrier (BBB). *Eur. J. Pharm. Biopharm.* **71**, 251–256 (2009).

166. Sharma, G. *et al.* Nanoparticle based insulin delivery system: The next generation efficient therapy for Type 1 diabetes. *J. Nanobiotechnology* **13**, 1–13 (2015).

167. Sakai, H. Overview of Potential Clinical Applications of Hemoglobin Vesicles (HbV) as Artificial Red Cells, Evidenced by Preclinical Studies of the Academic Research Consortium. *J. Funct. Biomater.* **8**, 10 (2017).

168. Hughey, V. L. & Johnson, E. A. Antimicrobial activity of lysozyme against bacteria involved in food spoilage and food-borne disease. *Appl. Environ. Microbiol.* **53**, 2165–2170 (1987).

169. Gregory, J. V *et al.* Systemic Brain Tumor Delivery of Synthetic Protein Nanoparticles for Glioblastoma Therapy. *bioRxiv* 862581 (2019). doi:10.1101/862581

170. Brown, T. D. *et al.* A microfluidic model of human brain (μHuB) for assessment of blood brain barrier. *Bioeng. Transl. Med.* **4**, (2019).

171. Ross, A. M. *et al.* Persistence, distribution, and impact of distinctly segmented microparticles on cochlear health following *in vivo* infusion. *J. Biomed. Mater. Res. Part A* **104**, 1510–1522 (2016).

172. Vellard, M. The enzyme as drug: Application of enzymes as pharmaceuticals. *Current Opinion in Biotechnology* **14**, 444–450 (2003).

173. Torchilin, V. P. Enzymes in Medicine: Advantages and Disadvantages. in *Immobilized Enzymes in Medicine* 3–12 (Springer, Berlin, Heidelberg, 1991). doi:10.1007/978-3-642-75821-8_2

174. Ansari, S. A. & Husain, Q. Potential applications of enzymes immobilized on/in nano materials: A review. *Biotechnol. Adv.* **30**, 512–523 (2012).

175. Stepankova, V. *et al.* Strategies for stabilization of enzymes in organic solvents. *ACS Catalysis* **3**, 2823–2836 (2013).

176. Sheldon, R. A. & van Pelt, S. Enzyme immobilisation in biocatalysis: why, what and how. *Chem. Soc. Rev.* **42**, 6223–6235 (2013).

177. Torchilin, V. Intracellular delivery of protein and peptide therapeutics. *Drug Discovery Today: Technologies* **5**, e95–e103 (2008).

178. Torchilin, V. P. Immobilized Enzymes in Medicine. in (Springer Berlin Heidelberg, 1991). doi:10.1007/978-3-642-75821-8

179. Gu, Z., Biswas, A., Zhao, M. & Tang, Y. Tailoring nanocarriers for intracellular protein delivery. *Chemical Society Reviews* **40**, 3638–3655 (2011).

180. Howard, M., Hood, E. & Muzykantov, V. Nanocarriers for Therapeutic Enzymes. in *Enzyme Nanocarriers* 159–192 (Pan Stanford, 2015). doi:10.1201/b18970-6

181. Gregoriadis, G. Medical Applications of Liposome-Entrapped Enzymes. *Methods Enzymol.* **44**, 698–709 (1976).

182. Campás, M. & Marty, J.-L. Encapsulation of Enzymes Using Polymers and Sol-Gel Techniques. in *Immobilization of Enzymes and Cells, Second Edition* 77–85 (Humana Press, 2006). doi:10.1007/978-1-59745-053-9_7

183. Sassolas, A., Hayat, A. & Marty, J. L. Enzyme immobilization by entrapment within a gel network. in *Immobilization of Enzymes and Cells, Third Edition* **1051**, 229–239 (Humana Press Inc., 2013).

184. Chen, Y. P. *et al.* A new strategy for intracellular delivery of enzyme using mesoporous silica nanoparticles: Superoxide dismutase. *J. Am. Chem. Soc.* **135**, 1516–1523 (2013).

185. Hood, E. D. *et al.* Endothelial targeting of nanocarriers loaded with antioxidant enzymes for protection against vascular oxidative stress and inflammation. *Biomaterials* **35**, 3708–15 (2014).

186. Neupane, S. *et al.* Enhancing Enzyme Immobilization on Carbon Nanotubes via Metal-Organic Frameworks for Large-Substrate Biocatalysis. *ACS Appl. Mater. Interfaces* **11**, 12133–12141 (2019).

187. Yamaguchi, H., Kiyota, Y. & Miyazaki, M. Techniques for preparation of cross-linked enzyme aggregates and their applications in bioconversions. *Catalysts* **8**, 174 (2018).

188. Quevedo, D. F. *et al.* Multifunctional Synthetic Protein Nanoparticles. *TBA* (2020).

189. Rahmani, S. *et al.* Engineering of nanoparticle size via electrohydrodynamic jetting. *Bioeng. Transl. Med.* **1**, 82–93 (2016).

190. Sweitzer, T. D. *et al.* Pecam-directed immunotargeting of catalase: Specific, rapid and transient protection against hydrogen peroxide. *Free Radic. Biol. Med.* **34**, 1035–1046 (2003).

191. Eike, J. H. & Palmer, A. F. Effect of glutaraldehyde concentration on the physical properties of polymerized hemoglobin-based oxygen carriers. *Biotechnol. Prog.* **20**, 1225–1232 (2004).

192. Grau-Monge, C. *et al.* Marrow-isolated adult multilineage inducible cells embedded within a biologically-inspired construct promote recovery in a mouse model of peripheral vascular disease. *Biomed. Mater.* **12**, 015024 (2017).

193. Rahmani, S. *et al.* Engineering of nanoparticle size via electrohydrodynamic jetting. *Bioeng. Transl. Med.* **1**, 82–93 (2016).

194. Glorieux, C. & Calderon, P. B. Catalase, a remarkable enzyme: targeting the oldest antioxidant enzyme to find a new cancer treatment approach. *Biol. Chem.* **398**, 1095–1108 (2017).

195. Zámocký, M. & Koller, F. Understanding the structure and function of catalases: Clues from molecular evolution and in vitro mutagenesis. *Prog. Biophys. Mol. Biol.* **72**, 19–66 (1999).

196. Conner, E. M. & Grisham, M. B. Inflammation, free radicals and antioxidants. *Nutrition* **12**, 274–277 (1996).

197. Wong, C. M., Wong, K. H. & Chen, X. D. Glucose oxidase: Natural occurrence, function, properties and industrial applications. *Appl. Microbiol. Biotechnol.* **78**, 927–938 (2008).

198. Hoarau, M., Badieyan, S. & Marsh, E. N. G. Immobilized enzymes: understanding enzyme – surface interactions at the molecular level. *Org. Biomol. Chem.* **15**, 9539–9551 (2017).

199. Wang, L. B. *et al.* A new nanobiocatalytic system based on allosteric effect with dramatically enhanced enzymatic performance. *J. Am. Chem. Soc.* **135**, 1272–1275 (2013).

200. Kawamura, A., Yoshioka, Y., Harada, A. & Kono, K. Acceleration of enzymatic reaction of trypsin through the formation of water-soluble complexes with poly(ethylene glycol)-block-poly(α,β-aspartic acid). *Biomacromolecules* **6**, 627–631 (2005).

201. Vladimirov, Y. A. *et al.* Cardiolipin activates cytochrome c peroxidase activity since it facilitates H2O2 access to heme. *Biochem.* **71**, 998–1005 (2006).

202. Xu, D., Tonggu, L., Bao, X., Lu, D. & Liu, Z. Activation and stabilization of a lipase nanogel using GMA for acryloylation. *Soft Matter* **8**, 2036–2042 (2012).

203. Zhang, Y., Ge, J. & Liu, Z. Enhanced Activity of Immobilized or Chemically Modified Enzymes. *ACS Catalysis* **5**, 4503–4513 (2015).

204. Greineder, C. F. *et al.* Vascular immunotargeting to endothelial determinant ICAM-1 enables optimal partnering of recombinant scFv-Thrombomodulin fusion with endogenous cofactor. *PLoS One* **8**, (2013).

205. Kilgore, K. S., Shen, J. P., Miller, B. F., Ward, P. A. & Warren, J. S. Enhancement by the complement membrane attack complex of tumor necrosis factor-alpha-induced endothelial cell expression of E-selectin and ICAM-1. *J. Immunol.* **155**, 1434–41 (1995).

206. Rabe, K. S., Müller, J., Skoupi, M. & Niemeyer, C. M. Cascades in Compartments: En Route to Machine-Assisted Biotechnology. *Angewandte Chemie - International Edition* **56**, 13574–13589 (2017).

207. Stark, W. J., Stoessel, P. R., Wohlleben, W. & Hafner, A. Industrial applications of nanoparticles. *Chem. Soc. Rev.* **44**, 5793–5805 (2015).

208. Lin, W. Introduction: Nanoparticles in Medicine. *Chemical Reviews* **115**, 10407–10409 (2015).

209. Herrera Estrada, L. P. & Champion, J. A. Protein nanoparticles for therapeutic protein delivery. *Biomater. Sci.* **3**, 787–799 (2015).

210. Chockalingam, K., Blenner, M. & Banta, S. Design and application of stimulus-responsive peptide systems. *Protein Engineering, Design and Selection* **20**, 155–161 (2007).

211. Arai, R. Hierarchical design of artificial proteins and complexes toward synthetic structural biology. *Biophysical Reviews* **10**, 391–410 (2018).

212. Yeates, T. O., Liu, Y. & Laniado, J. The design of symmetric protein nanomaterials comes of age in theory and practice. *Current Opinion in Structural Biology* **39**, 134–143 (2016).

213. Desai, N. Technology: A Drug Delivery Platform Utilising Endothelial gp60 Receptor-based Transport and Tumour-derived SPARC for Targeting". *Drug Deliv. Rep.* **505**, 1–9 (2010).

214. Habibi, N., Quevedo, D. F., Gregory, J. V. & Lahann, J. Emerging methods in therapeutics using multifunctional nanoparticles. *Wiley Interdiscip. Rev. Nanomedicine Nanobiotechnology* e1625 (2020). doi:10.1002/wnan.1625

215. Lim, S. I., Lukianov, C. I. & Champion, J. A. Self-assembled protein nanocarrier for intracellular delivery of antibody. *J. Control. Release* **249**, 1–10 (2017).

216. Maruyama, T. *et al.* Improved anticancer effects of albumin-bound paclitaxel nanoparticle via augmentation of EPR effect and albumin-protein interactions using S -nitrosated human serum albumin dimer. *Biomaterials* **140**, 162–169 (2017).

217. Whitesides, G. M. The origins and the future of microfluidics. *Nature* **442**, 368–373 (2006).

218. Meighan, M. M., Staton, S. J. R. & Hayes, M. A. Bioanalytical separations using electric field gradient techniques. *Electrophoresis* **30**, 852–865 (2009).

219. Gencoglu, A., Olney, D., Lalonde, A., Koppula, K. S. & Lapizco-Encinas, B. H. Dynamic microparticle manipulation with an electroosmotic flow gradient in low-frequency alternating current dielectrophoresis. *Electrophoresis* **35**, 362–373 (2014).

220. Xuan, X. Recent advances in direct current electrokinetic manipulation of particles for microfluidic applications. *Electrophoresis* **40**, 2484–2513 (2019).

221. Lentz, C. J., Hidalgo-Caballero, S. & Lapizco-Encinas, B. H. Low frequency cyclical potentials for fine tuning insulator-based dielectrophoretic separations. *Biomicrofluidics* **13**, 044114 (2019).

222. Lapizco-Encinas, B. H. On the recent developments of insulator-based dielectrophoresis: A review. *Electrophoresis* **40**, (2019).

223. Shilov, V., Barany, S., Grosse, C. & Shramko, O. Field-induced disturbance of the double layer electro-neutrality and non-linear electrophoresis. *Adv. Colloid Interface Sci.* **104**, 159–173 (2003).

224. Dukhin, S. S. Electrokinetic phenomena of the second kind and their applications. *Adv. Colloid Interface Sci.* **35**, 173–196 (1991).

225. Coll De Peña, A. *et al.* Creation of an electrokinetic characterization library for the detection and identification of biological cells. *Anal. Bioanal. Chem.* **In press.**, (2020).

226. Kim, D., Sonker, M. & Ros, A. Dielectrophoresis: From Molecular to Micrometer-Scale Analytes. *Anal. Chem.* **91**, 277–295 (2019).

227. Rohani, A. *et al.* Frequency-selective electrokinetic enrichment of biomolecules in physiological media based on electrical double-layer polarization. *Nanoscale* **9**, 12124–12131 (2017).

228. Nakano, A., Camacho-Alanis, F. & Ros, A. Insulator-based dielectrophoresis with [small beta]-galactosidase in nanostructured devices. *Analyst* **140**, 860–868 (2015).

229. Lapizco-Encinas, B. H. Microscale electrokinetic assessments of proteins employing insulating structures. *Curr. Opin. Chem. Eng.* **In press**, (2020).

230. Coll De Peña, A. *et al.* Analysis of Bacteriophages with Insulator-Based Dielectrophoresis. *Micromachines* **10**, 450 (2019).

231. Yang, F., Yang, X., Jiang, H. & Wang, G. Cascade and staggered dielectrophoretic cell sorters. *Electrophoresis* **32**, 2377–2384 (2011).

232. Elitas, M. *et al.* Dielectrophoresis as a single cell characterization method for bacteria. *Biomed. Phys. Eng. Express* **3**, 15005 (2017).

233. Su, Y.-H. *et al.* Quantitative dielectrophoretic tracking for characterization and separation of persistent subpopulations of Cryptosporidium parvum. *Analyst* **139**, 66–73 (2014).

234. Cardenas-Benitez, B. *et al.* Direct Current Electrokinetic Particle Trapping in Insulator-based Microfluidics: Theory and Experiments. *Submitted* (2020).

235. Washizu, M., Suzuki, S., Kurosawa, O., Nishizaka, T. & Shinohara, T. Molecular Dielectrophoresis of Biopolymers. *IEEE Trans. Ind. Appl.* **30**, 835–843 (1994).

236. Bakewell, D. J., Hughes, M. P., Milner, J. J. & Morgan, H. Dielectrophoretic manipulation of avidin and DNA. in *20th International Conference of the IEEE in Medicine and Biology Society* **20(2)**, 1079–1082 (1998).

237. Kawabata, T. & Washizu, M. Dielectrophoretic detection of molecular bindings. *IEEE Trans. Ind. Appl.* **37**, 1625–1633 (2001).

238. Sano, H., Kabata, H., Kurosawa, O. & Washizu, M. Dielectrophoretic chromatography with cross-flow injection. in *IEEE International Conference On Micro Electro Mechanical Systems. Proceedings* 11–14 (2002). doi:10.1109/MEMSYS.2002.984043

239. Nakano, A., Chao, T.-C., Camacho-Alanis, F. & Ros, A. Immunoglobulin G and bovine serum albumin streaming dielectrophoresis in a microfluidic device. *Electrophoresis* **32**, 2314–2322 (2011).

240. Camacho-Alanis, F., Gan, L. & Ros, A. Transitioning streaming to trapping in DC insulator-based dielectrophoresis for biomolecules. *Sensors Actuators B Chem.* **173**, 668–675 (2012).

241. Nakano, A., Camacho-Alanis, F., Chao, T.-C. & Ros, A. Tuning direct current streaming dielectrophoresis of proteins. *Biomicrofluidics* **6**, 34108–34113 (2012).

242. Abdallah, B. G. *et al.* Microfluidic sorting of protein nanocrystals by size for X-ray free-electron laser diffraction. *Struct. Dyn.* **2**, 41719 (2015).

243. Abdallah, B. G., Roy-Chowdhury, S., Coe, J., Fromme, P. & Ros, A. High Throughput Protein Nanocrystal Fractionation in a Microfluidic Sorter. *Anal. Chem.* **87**, 4159–4167 (2015).

244. Abdallah, B. G., Chao, T.-C., Kupitz, C., Fromme, P. & Ros, A. Dielectrophoretic Sorting of Membrane Protein Nanocrystals. *ACS Nano* **7**, 9129–9137 (2013).

245. Rohani, A., Varhue, W., Liao, K.-T., Chou, C.-F. & Swami, N. S. Nanoslit design for ion conductivity gradient enhanced dielectrophoresis for ultrafast biomarker enrichment in physiological media. *Biomicrofluidics* **10**, 33109 (2016).

246. Chaurey, V. *et al.* Scaling down constriction-based (electrodeless) dielectrophoresis devices for trapping nanoscale bioparticles in physiological media of high-conductivity. *Electrophoresis* **34**, 1097–1104 (2013).

247. Liao, K. T. & Chou, C. F. Nanoscale Molecular Traps and Dams for Ultrafast Protein Enrichment in High-Conductivity Buffers. *J. Am. Chem. Soc.* **134**, 8742–8745 (2012).

248. Chi-Han, C., Liang-Ju, C. & Ju-Nan, K. Nanoconstriction-based electrodeless dielectrophoresis chip for nanoparticle and protein preconcentration. *Appl. Phys. Express* **8**, 85201 (2015).

249. Lapizco-Encinas, B. H., Ozuna-Chacón, S. & Rito-Palomares, M. Protein manipulation with insulator-based dielectrophoresis and direct current electric fields. *J. Chromatogr. A* **1206**, (2008).

250. Mata-Gomez, M. A. *et al.* Modelling of electrokinetic phenomena for capture of PEGylated ribonuclease A in a microdevice with insulating structures. *Biomicrofluidics* **10**, 33106 (2016).

251. Sokolovskaya, E., Yoon, J., Misra, A. C., Bräse, S. & Lahann, J. Controlled microstructuring of janus particles based on a multifunctional poly(ethylene glycol). *Macromol. Rapid Commun.* **34**, 1554–1559 (2013).

252. Jordahl, J. H. *et al.* 3D Jet Writing: Functional Microtissues Based on Tessellated Scaffold Architectures. *Adv. Mater.* (2018). doi:10.1002/adma.201707196

253. Rahmani, S. *et al.* Engineering of nanoparticle size via electrohydrodynamic jetting. *Bioeng. Transl. Med.* **1**, 82–93 (2016).

254. Lapizco-Encinas, B. H., Simmons, B. A., Cummings, E. B. & Fintschenko, Y. Insulator-based dielectrophoresis for the selective concentration and separation of live bacteria in water. *Electrophoresis* **25**, 1695–1704 (2004).

255. Lapizco-Encinas, B. H. *Personal Communication on Thoughts About Calculating Electrokinetic Microfluidic Phenomena*. (2020).

256. Coll De Peña, A. *et al.* Creation of an electrokinetic characterization library for the detection and identification of biological cells. *Anal. Bioanal. Chem.* **In press.**, 3935–3945 (2020).

257. Hölzel, R. & Pethig, R. Protein Dielectrophoresis: I. Status of Experiments and an Empirical Theory. *Micromachines* **11**, 533 (2020).

258. Hayes, M. A. Dielectrophoresis of proteins: experimental data and evolving theory. *Anal. Bioanal. Chem.* **412**, 3801–3811 (2020).

259. Quevedo, D. F. *et al.* Electrokinetic characterization of anisotropic synthetic protein nanoparticles. *Beilstein J. Nanotechnol.* **Under Revi**, (2020).

260. Saucedo-Espinosa, M. A. & Lapizco-Encinas, B. H. Refinement of current monitoring methodology for electroosmotic flow assessment under low ionic strength conditions. *Biomicrofluidics* **10**, (2016).

261. Park, J. R., Eggert, A. & Caron, H. Neuroblastoma: Biology, Prognosis, and Treatment. *Hematol. Oncol. Clin. North Am.* **24**, 65–86 (2010).

262. Howman-Giles, R., Shaw, P. J., Uren, R. F. & Chung, D. K. V. Neuroblastoma and Other Neuroendocrine Tumors. *Semin. Nucl. Med.* **37**, 286–302 (2007).

263. Vaidyanathan, G. Meta-iodobenzylguanidine and analogues: chemistry and biology. *Q. J. Nucl. Med. Mol. Imaging* **58**, 351–368 (2008).

264. Riad, R. *et al.* Role of 131-I MIBG Therapy in the Treatment of Advanced Neuroblastoma. *J. Egypt. Natl. Canc. Inst.* **21**, 51–8 (2009).

265. Makadia, H. K. & Siegel, S. J. Poly Lactic-co-Glycolic Acid (PLGA) as biodegradable controlled drug delivery carrier. *Polymers (Basel).* **3**, 1377–1397 (2011).

266. Lucero-Acuña, A. & Guzmán, R. Nanoparticle encapsulation and controlled release of a hydrophobic kinase inhibitor: Three stage mathematical modeling and parametric analysis. *Int. J. Pharm.* **494**, 249–257 (2015).

267. Wang, J., Tian, S., Petros, R. A., Napier, M. E. & Desimone, J. M. The complex role of multivalency in nanoparticles targeting the transferrin receptor for cancer therapies. *J. Am. Chem. Soc.* **132**, 11306–11313 (2010).

268. Dalal, C., Saha, A. & Jana, N. R. Nanoparticle Multivalency Directed Shifting of Cellular Uptake Mechanism. *J. Phys. Chem. C* **120**, 6778–6786 (2016).

269. Hennig, R. *et al.* Multivalent nanoparticles bind the retinal and choroidal vasculature. *J. Control. Release* **220**, 265–274 (2015).

270. Hennig, R., Pollinger, K., Veser, A., Breunig, M. & Goepferich, A. Nanoparticle multivalency counterbalances the ligand affinity loss upon PEGylation. *J. Control. Release* **194**, 20–27 (2014).

271. Ahmad Khanbeigi, R. *et al.* The delivered dose: Applying particokinetics to in vitro investigations of nanoparticle internalization by macrophages. *J. Control. Release* **162**, 259–266 (2012).

272. Teeguarden, J. G., Hinderliter, P. M., Orr, G., Thrall, B. D. & Pounds, J. G. Particokinetics in vitro: Dosimetry considerations for in vitro nanoparticle toxicity assessments. *Toxicol. Sci.* **95**, 300–312 (2007).

273. Hinderliter, P. M. *et al.* ISDD : A computational model of particle sedimentation , diffusion and target cell dosimetry for in vitro toxicity studies ISDD : A computational model of particle sedimentation , diffusion and target cell dosimetry for in vitro toxicity studies. *Part. Fibre Toxicol.* **7**, (2010).

274. Guggenheim, E. J. *et al.* Refining in vitro models for nanomaterial exposure to cells and tissues. *NanoImpact* **10**, 121–142 (2018).

275. Oberdorster, G. Nanotoxicology: in Vitro–in Vivo Dosimetry. *Environ. Health Perspect.* **120**, A13 (2012).

276. Han, X. *et al.* Assessing the relevance of in vitro studies in nanotoxicology by examining correlations between in vitro and in vivo data. *Toxicology* **297**, 1–9 (2012).

277. DeLoid, G. M. *et al.* Advanced computational modeling for in vitro nanomaterial dosimetry. *Part. Fibre Toxicol.* **12**, 1–20 (2015).

278. Yamankurt, G. *et al.* Exploration of the nanomedicine-design space with high-throughput screening and machine learning HHS Public Access Author manuscript. *Nat Biomed Eng* **3**, 318–327 (2019).

279. Jan, E. *et al.* High-content screening as a universal tool for fingerprinting of cytotoxicity of nanoparticles. *ACS Nano* **2**, 928–938 (2008).

280. Deloid, G. *et al.* Estimating the effective density of engineered nanomaterials for in vitro dosimetry. *Nat. Commun.* **5**, 1–10 (2014).

281. Habibi, N. *Personal Communication of Cell Uptake of Various Nanoparticles*. (2018).

282. Deloid, G. M., Cohen, J. M., Pyrgiotakis, G. & Demokritou, P. Preparation, characterization, and in vitro dosimetry of dispersed, engineered nanomaterials. *Nat. Protoc.* **12**, 355–371 (2017).

283. Sunshine, J. C., Perica, K., Schneck, J. P. & Green, J. J. Particle shape dependence of CD8þ T cell activation by artificial antigen presenting cells. *Biomaterials* **35**, 269–277 (2014).

284. Zan, X., Garapaty, A. & Champion, J. A. Engineering Polyelectrolyte Capsules with Independently Controlled Size and Shape. *Langmuir* **31**, 7601–7608 (2015).

285. Petros, R. a & DeSimone, J. M. Strategies in the design of nanoparticles for therapeutic applications. *Nat. Rev. Drug Discov.* **9**, 615–627 (2010).

286. Oh, N. & Park, J. H. Endocytosis and exocytosis of nanoparticles in mammalian cells. *Int. J. Nanomedicine* **9**, 51–63 (2014).

287. Cronican, J. J. *et al.* Potent delivery of functional proteins into Mammalian cells in vitro and in vivo using a supercharged Protein. *ACS Chem. Biol.* **5**, 747–52 (2010).

288. Gratton, S. E. A. *et al.* The effect of particle design on cellular internalization pathways. *Proc. Natl. Acad. Sci. U. S. A.* **105**, 11613–11618 (2008).

289. Champion, J. A. & Mitragotri, S. Role of target geometry in phagocytosis. *Proc. Natl. Acad. Sci. U. S. A.* **103**, 4930–4934 (2006).

290. Roh, K. & Lahann, J. Anisotropic encapsulation of superparamagnetic nanocrystals in polymeric biphasic nanocolloids. *Polym. Prepr.* **48**, 209–267 (2007).

291. Buiting, K., Williams, C. & Horsthemke, B. Angelman syndrome-insights into a rare neurogenetic disorder. *Nature Reviews Neurology* **12**, 584–593 (2016).

292. Turcios, N. L. Cystic fibrosis: An overview. *Journal of Clinical Gastroenterology* **39**, 307–317 (2005).

293. Hanauer, A. & Young, I. D. Coffin-Lowry syndrome: Clinical and molecular features. *Journal of Medical Genetics* **39**, 705–713 (2002).

294. McColgan, P. & Tabrizi, S. J. Huntington's disease: a clinical review. *European Journal of Neurology* **25**, 24–34 (2018).

295. Finer, M. & Glorioso, J. A brief account of viral vectors and their promise for gene therapy. *Gene Therapy* **24**, 1–2 (2017).

296. Balazs, D. A. & Godbey, W. T. Liposomes for Use in Gene Delivery. *J. Drug Deliv.* **2011**, 12 (2011).

297. Kandil, R. & Merkel, O. M. Recent progress of polymeric nanogels for gene delivery. *Current Opinion in Colloid and Interface Science* **39**, 11–23 (2019).

298. Kim, Y., Park, E. J. & Na, D. H. Recent progress in dendrimer-based nanomedicine development. *Archives of Pharmacal Research* **41**, 571–582 (2018).

299. Xiang, Y., Oo, N. N. L., Lee, J. P., Li, Z. & Loh, X. J. Recent development of synthetic nonviral systems for sustained gene delivery. *Drug Discovery Today* **22**, 1318–1335 (2017).

300. Mali, P., Esvelt, K. M. & Church, G. M. Cas9 as a versatile tool for engineering biology. *Nature Methods* **10**, 957–963 (2013).

301. Erickson, H. P. Size and shape of protein molecules at the nanometer level determined by sedimentation, gel filtration, and electron microscopy. *Biological Procedures Online* **11**, 32–51 (2009).

302. Weng, L., Liang, S., Zhang, L., Zhang, X. & Xu, J. Transport of glucose and poly(ethylene glycol)s in agarose gels studied by the refractive index method. *Macromolecules* **38**, 5236–5242 (2005).

303. Dinerman, A. A., Cappello, J., Ghandehari, H. & Hoag, S. W. Solute diffusion in genetically engineered silk-elastinlike protein polymer hydrogels. *J. Control. Release* **82**, 277–287 (2002).

304. Szkudlarek, A., Sułkowska, A., MacIązek-Jurczyk, M., Chudzik, M. & Równicka-Zubik, J. Effects of non-enzymatic glycation in human serum albumin. Spectroscopic analysis. *Spectrochim. Acta - Part A Mol. Biomol. Spectrosc.* **152**, 645–653 (2016).

305. Mohamadi-Nejad, A., Moosavi-Movahedi, A. A., Hakimelahi, G. H. & Sheibani, N. Thermodynamic analysis of human serum albumin interactions with glucose: Insights into the diabetic range of glucose concentration. *Int. J. Biochem. Cell Biol.* **34**, 1115–1124 (2002).

306. Wang, Y. *et al.* Structural mechanism of ring-opening reaction of glucose by human serum albumin. *J. Biol. Chem.* **288**, 15980–15987 (2013).

307. Nasiri, R., Bahrami, H., Zahedi, M., Moosavi-Movahedi, A. A. & Sattarahmady, N. A theoretical elucidation of glucose interaction with hsa's domains. *J. Biomol. Struct. Dyn.* **28**, 211–226 (2010).